Ruprecht-Karls-Universität Heidelberg
Gesamtfakultät für Mathematik-, Ingenieur- und Naturwissenschaften

Dissertation

Tailoring Actuation Properties of Thermoresponsive Hydrogels and Implementation into Soft Robotic Applications

Zur Erlangung des akademischen Grades
Doktor der Ingenieurwissenschaften
(Dr.-Ing)

vorgelegt von
Herrn M.Sc. Tobias Spratte
Heidelberg, November 2023

Tailoring Actuation Properties of Thermoresponsive Hydrogels and Implementation into Soft Robotic Applications

Datum der Einreichung: 15. November 2023

1. Gutachterin: Prof. Dr. Christine Selhuber-Unkel
2. Gutachterin: Prof. Dr. Eva Blasco

Abstract

Soft material robotics relies on the development of responsive, soft materials and requires high standards, with respect to the material properties: High responsivity, robust mechanical properties, high cycle times, and fast responses are some examples for these requirements, which are rarely found in such responsive, soft materials, and thus need to be adjusted by material engineering.

This thesis addresses tailoring the properties of thermoresponsive hydrogels and implementing these materials into soft robotic applications. Furthermore, a thorough investigation of material responsivity and mechanical properties is conducted, which are crucial parameters for the development of soft actuators.

First, a template-assisted fabrication method based on sacrificial zinc oxide templates is introduced, which yields microporous and highly thermoresponsive hydrogels. Compared to its conventional bulk counterpart, this material exhibits a large volume transition and generates considerable stroke forces upon stimulation, which are crucial requirements for actuator applications. These changes in thermoresponsive actuation properties result from the increased surface area created by the microporosity of the hydrogel. Actuation capabilities are demonstrated on the basis of a soft, thermally controlled gripper.

Based on the previous findings, two-photon 3D laser printing is used to fabricate responsive hydrogel microactuators with precise control of actuator surface-to-volume ratio and to investigate actuation capabilities as a function of actuator design and fabrication parameters. It turns out that miniaturization of the actuators and especially the surface-to-volume-ratio have a major impact on responsivity. In addition, variation of the processing parameters during fabrication is found to be a facile strategy for tailoring actuator properties, such as stiffness and responsivity. Moreover, the assembly of individual actuators into microactuator systems, enables cooperative functions, such as capturing and releasing cargo in a microfluidic chip upon thermal stimulation.

The micro engineering strategies presented in this work, provide a toolkit for understanding the science of thermo-actuation and tailoring actuation properties of responsive hydrogels. Furthermore, methods for developing soft robotic applications at the microscale using such hydrogels are demonstrated.

Kurzfassung

Das Forschungsgebiet der Material-basierten, weichen Robotik baut auf die Entwicklung responsiver, weicher Materialien auf und stellt hohe Anforderungen an deren Materialeigenschaften: Eine ausgeprägte Reaktionsfähigkeit, robuste mechanische Eigenschaften, hohe Zyklenzahlen und schnelle Reaktionen sind einige Beispiele für diese Anforderungen, die bei herkömmlichen responsiven, weichen Materialien nur selten vorhanden sind und daher durch die Werkstofftechnik angepasst werden müssen.

Diese Arbeit befasst sich mit der Anpassung der Eigenschaften von thermoresponsiven Hydrogelen und der Implementierung dieser Materialien in Anwendungen innerhalb der weichen Robotik. Darüber hinaus wird eine gründliche Untersuchung der Responsivität und der mechanischen Eigenschaften durchgeführt, welche entscheidende Parameter für die Entwicklung weicher Aktoren sind.

Zunächst wird ein Herstellungsverfahren vorgestellt, welches auf der Grundlage von Opfertemplaten aus Zinkoxid beruht und mikroporöse, hoch thermoresponsive Hydrogele hervorbringt. Im Vergleich zum konventionellen, nicht-porösen Gegenstück weist dieses neue Material eine große Volumenänderung und beträchtliche Hubkräfte unter Anregung auf, was entscheidende Voraussetzungen für Aktorik-Anwendungen sind. Diese Veränderungen der thermoresponsiven Eigenschaften ergeben sich aus der vergrößerten Oberfläche, die durch die Mikroporosität des Hydrogels resultiert. Am Beispiel eines weichen, thermisch gesteuerten Greifers wird schließlich die anwendungsorientierte Leistungsfähigkeit demonstriert.

Aufbauend auf diese Ergebnisse, wird Zwei-Photonen-3D-Laserdruck verwendet, um responsive Hydrogel-Mikroaktoren herzustellen, und deren Leistungsfähigkeit in Abhängigkeit vom Aktordesign und den Herstellungsparametern zu untersuchen. Es zeigt sich, dass die Miniaturisierung der Aktoren und insbesondere deren Oberflächen-Volumen-Verhältnis großen Einfluss auf die Responsivität haben. Weiterhin stellt sich heraus, dass die Variation der Herstellungsparameter eine einfache Strategie zur Anpassung der Aktoreigenschaften, wie Steifigkeit und Ansprechverhalten, darstellt. Darüber hinaus sorgt das Zusammenfügen einzelner Aktoren zu Mikroaktorsystemen für kooperative Funktionen, wie z.B. das Einfangen und Freisetzen von mikroskopischer Fracht unter thermischer Anregung in einem mikrofluidischen Chip.

Die in dieser Arbeit vorgestellten mikrotechnischen Methoden bieten eine Grundlage für das wissenschaftliche Verständnis von thermischer Aktorik und die Anpassung der Aktorik-Eigenschaften von responsiven Hydrogelen. Weiterhin werden Strategien für weich-robotische Anwendungen dieser Hydrogele auf der Mikroskala demonstriert.

Contents

1 Introduction

Since the Old Stone Age, also called the Paleolithic, humans have developed and used tools to simplify and upscale their daily work, as well as to make new, useful products.[1] Over the years, these tools have been refined and became more and more complex, causing a gigantic revolution of human life, evolving from an agricultural society to an industrial society. Mechanical tools were modified and combined to form complex machines, and the discovery of electricity finally lead to the development of large factories, in which machines operated day and night. The invention of computers finally enabled the automation of machines and process chains, which constitutes the birth of robotics. Recent progress in connecting machines via networks, facilitated the communication between robots and even factories, culminating in the formation of so called smart factories.[2]

However, in recent years, the field of robotics has done a fundamental transformation: It shifted its focus, from previous conventional concepts of rigid and typically electrically powered materials, to new approaches relying on flexible, compliant, and adaptable materials, powered by their environment. This new field of research is known as soft (material) robotics and is carried out at the intersection of engineering, materials science, and biology. Besides the use of soft materials, algorithms that allow for soft motions of robotic devices are developed in computer science research, which is also considered soft robotics. However, this work focuses on the material-based soft robotics.

While conventional (hard) robotics is a highly successful field, it features fundamental shortcomings, such as low compatibility in collaboration with humans, in chemically harsh or physiological environments, low thermodynamic efficiency, and difficulties with unstructured, dynamic, and unpredictable surroundings.[3] Soft robotics, in turn, aims for bridging the gap between machines and living organisms, and has the potential to overcome these shortcomings. Soft, responsive materials can autonomously adapt to environmental changes by carrying out predefined, characteristic functions, and can demonstrate safe interactions with humans and biological organisms.[4] Many concepts of soft robotics have been inspired by nature and animals, such as octopus arms, sea stars, worms, and biological skin, which served as models for the design of soft grippers, soft walkers, and soft sensors.[5]–[7] Especially in the biomedical field, soft robotics based on the use of stimuli-responsive

hydrogels, responding to changes in temperature, pH, light, electric or magnetic fields, and more, has gained high attention. This is due to the hydrogel's potential to mimic functions of muscles, tendons, and other soft tissues, which could revolutionize healthcare industries and applications in human-robot-interactions.[8]

In the following chapter, a state of the art overview about recent progress in soft actuator developments based on stimuli-responsive hydrogels is portrayed.

1.1 State of the Art: Stimuli-Responsive Hydrogels in Soft Robotics

Recent research trends in the development of stimuli-responsive hydrogels for soft robotic applications focus on the synthesis of multi-functional hydrogels, responding to several environmental stimuli, as well as increasing the sensitivity and responsivity of such hydrogels. In addition, tailoring mechanical resistance and developing high-precision microfabrication methods, which allow for flexibility regarding substrates, material composition, and design complexity, are of high interest. In particular, healthcare, wearable technology, and human-robot interaction scenarios became highly popular fields of application in recent years.

Classical hard actuator materials, such as piezoelectrics, magnetostrictives or shape memory alloys, are firmly established components of industrial devices. Piezoelectric ceramics for instance offer rapid response times (up to ultrasound range; $>$ 20 kHz)[9], high mechanical stress generation (MPa to GPa)[10], and precise position control (nanometer range)[11]. However, they are brittle, and typically require high voltages for powering[12], which makes them incompatible with physiological environments. In addition, robotic devices based on hard materials are usually assemblies, composed of several individual components, which together perform functions, such as sensing, feedback controlling, and responding, but require sophisticated programming.[13] Responsive soft materials, in contrast, typically combine these functions in one and the same material, due to their adaptive nature and direct response to physicochemical signals.[14] Among these materials, stimuli-responsive hydrogels have gained great attention, due to their high water absorptivity, elasticity, flexibility, biodegradability, and biocompatibility, enabling versatile application in the biomedical field.[15] While hydrogel-based actuators in the millimeter range have been developed and studied extensively, hydrogel microactuators remain less researched. Here, the need for highly advanced microfabrication technologies has been a bottleneck in the past and research has progressed only recently. Therefore, the science behind hydrogel microactuation up to now remains rather poor.

Current research focuses on the synthesis of multi-responsive hydrogels, sensitive to several external stimuli, which allows for more effective treatment in biomedical applications or more diverse actuation modes in soft robotic applications. Dual-responsive hydrogels based on copolymerized methylacrylic acid and *N*,*N*'-methylene

diacrylamide have been developed, for site-specific controlled drug release.[16] This hydrogel is capable of slow drug release in low pH environment and fast release under weak alkaline conditions, due to its pH-dependent swelling. In addition, a local increase in temperature can trigger the drug release on demand and independent of the environmental pH, which offers a higher degree of freedom for the treatment. Liu *et al.* developed a multi-responsive hydrogel system, co-assembled from a phenylalanine and azobenzene derivative, which can respond to temperature, pH, host–guest interaction, and photoirradiation.[17] This material is capable of controlling cell proliferation, encapsulation and on-demand release in three-dimensional environments under the various stimuli. In case of local stimulation, light offers high potential, due to its precise spatiotemporal control possibilities and the availability of manifold light sources. Guo *et al.* have developed a photo-responsive composite hydrogel, based on thermoresponsive poly(*N*-isopropylacrylamide) (PNIPAM) and multi-walled carbon nanotubes. Using this material, a biomimetic butterfly soft robot was fabricated, which is steered by visible light, enabling it to achieve periodic wing movements and propulsion under water.[18]

Common limitations of stimuli-responsive hydrogels include low sensitivities, slow response rates, and poor mechanical robustness, which compromise the applicability of these materials in actuator research. Thus, recent developments aim for increasing hydrogel responsivities as well as mechanical properties. Wei *et al.* have fabricated electrospun hydrogel nanofibers coated with polypyrrole, which exhibit rapid speed (1285.71 $^\circ$ s^{-1} of folding) and complex programmable actuation upon light-irradiation. Furthermore, the material was capable of lifting objects 100 times of its self-weight.[19] Other work has focused on highly sensitive hydrogels, such as composites based on silver flakes and PNIPAM, which serve as highly sensitive, wearable detectors for weak vibrations of the human throat during speaking, sensing sweat, and neuromuscular electrical stimulation when used as skin electrodes.[20] With regards to mechanical reinforcements, Cao *et al.* have developed a highly stretchable, electrically sensitive hydrogel based on polyacrylamide, sodium alginate, and gallium filler. Despite a low elastic modulus (30 kPa), the composite material exhibits high-toughness (2.25 MJ m^{-3}), large tensile deformation (1400%), recoverability, and excellent fatigue resistance. The hydrogel was successfully tested for monitoring various human motions, including large-scale joint bending and tiny facial expression, breathing, voice recognition, and handwriting.[21]

State of the art methods for fabricating stimuli-responsive hydrogel actuators have evolved with advancements in processability of heterogeneous materials, shape complexity, substrate flexibility, and fabrication resolution. Some of the most popular methods include 3D/4D printing technologies, soft lithography, and microfluidic-based fabrication. Microfiber-shaped, axially patterned hydrogel actuators have been fabricated by Takeuchi *et al.*, using a valve-controlled microfluidic device. The programmable microfibers were capable of helical deformation and interaction with external objects upon thermal stimulation.[22] Other work has used soft lithogra-

phy approaches to micromold programmable bilayer hydrogel actuators, capable of mimicking movements of biological organisms.[23] Recently, 3D printing of adaptive hydrogels, also known as 4D printing, has evolved as a promising tool to fabricate complex shaped soft actuators with versatile shape-morphing capabilities.[24]

Manifold applications of stimuli-responsive hydrogels in the biomedical field have been developed in recent years, including drug delivery, tissue engineering, biosensors, and soft robots. In drug delivery, hydrogels offer transport and release of incorporated drugs in a sustained manner and at desired targets, due to their high porosity, high surface area, and high water absorption capability.[25] However, clinical translation of such technologies remains challenging with regard to chemical complexity, biological responses, and predictability of externally triggered release vehicles when used *in vivo*.[26] Kim *et al.* demonstrated light-induced, on-demand release of dexamethasone from poly(*N*-isopropylacrylamide-co-vinyl-2-pyrrolidinone) and magnetite nanoparticle composite hydrogels, to achieve localized, sequential, and long-term release from transdermal patches.[27] A stretchable, conductive artificial nerve tissue was developed by Dong *et al.*, by copolymerizing polyaniline (PANI) and polyacrylamide (PAM). The hydrogel was capable of light-triggered promotion of bioelectric signals in injured nerve tissue.[28] A biomimetic hydrogel sensor, with skin-like strain and pressure sensing behavior, was developed by Xia *et al.*, on the basis of an ionic conductive hydrogel and core–shell hybrid latex particles as physical crosslinking centers.[29] In the field of soft robots, Zheng *et al.* have realized a shape-morphing, soft microrobot based on alginate hydrogel, which is capable of targeting, releasing, and sampling under the control of a magnetic field and environmental ionic stimuli. Versatile actuation modes, including locomotion and encapsulation of nanoparticles, allowed for transportation and navigation in *ex vivo* gastrointestinal environment.[30]

Remaining challenges and current work in progress, regarding stimuli-responsive hydrogels for soft robotic applications, include achieving rapid (milliseconds to seconds) and controllable response times, environmental compatibility, altering mechanical toughness, and development of high precision fabrication technologies. Miniaturization of hydrogel actuators with high spatial resolution (sub-micrometer to low micrometer range), flexibility of substrates, and multi-material compositions are still challenging tasks. Future progress might therefore be made in the direction of implementing hydrogel microactuators into lab-on-a-chip devices, where complex tasks could be accomplished at the microscale, by versatile hydrogel microactuator assemblies.

This thesis will focus on strategies to overcome some of the aforementioned challenges, in particular increasing response times and tailoring mechanical properties of thermoresponsive hydrogel actuators. Macro-sized (millimeter range) responsive bulk hydrogels exhibit relatively slow swelling and deswelling kinetics, as compared to hydrogel microstructures. Hence, one goal of this work will be to develop a strategy to increase response times of macro-sized hydrogel actuators by microstructural

modification, such as incorporation of micropores. Furthermore, this thesis aims at developing thermoresponsive hydrogel microactuators (in the low micrometer range) and providing systematic characterization tools for investigating, understanding, and tailoring the actuation capabilities of thermoresponsive hydrogel microstructures. The possibility of combining individual hydrogel microactuators into microactuator systems, to achieve new, cooperative functions will be explored as well. In the following chapter the objectives of this thesis are explained in more detail.

1.2 Objective

The fundamental objective of this doctoral thesis is to explore, how microstructural modifications of thermoresponsive hydrogels within the domain of soft actuators can tailor actuation properties. Within this context, strategies of increasing response times, adjusting mechanical stiffness and stroke force generation, as crucial actuator parameters, are elaborated. In addition to a thorough characterization of these properties, the material's performance in soft actuator applications shall be tested by implementation into soft robots.

This thesis is structured as follows: First, a detailed description of the fundamental concepts, required to comprehend the results discussed in this thesis, is given in **Chapter 2**. Therein, I introduce functional hydrogels as the material of choice for developing soft actuators. Subsequently, several state of the art techniques for fabricating hydrogel microstructures are presented.

Chapter 3 discusses the results and methods of the experimental work of this thesis. In **Section 3.1** a microengineering approach is introduced, which provides a toolkit to tailor the response properties of macro-sized (millimeter scale) thermoresponsive PNIPAM hydrogels, by microstructural modification. In addition, soft actuators made of the microengineered material are characterized systematically and are finally implemented into a soft actuation setup. To investigate the influence of microstructural changes in more detail and to confirm the hypothesis of faster response times due to increased material surface area, thermoresponsive hydrogel microstructures with different surface-to-volume ratios are investigated in **Section 3.2**. Here, two-photon 3D laser printing of miniaturized (micrometer scale) soft hydrogel actuators is done, and followed by a systematic characterization of actuation capabilities as a function of microstructure design and fabrication parameters. Finally, microactuator systems are developed and implementation into a microfluidic chip is presented. A conclusive discussion of the findings, including an evaluation of limitations and comparison to other research, is added in **Section 3.3**. Finally, I summarized the main results of this thesis in **Chapter 4** and give a perspective into further applications based on functional hydrogel microstructures.

2

Fundamentals

In this chapter, I introduce the fundamental concepts, required to understand the strategies presented in this thesis. First, an introduction to soft robotics and soft actuators is given, with a special focus on stimuli-responsive hydrogels. Afterwards, I explain state of the art fabrication techniques for hydrogel microstructures, namely template-assisted and photolithography methods. Particular emphasis is placed on radical (photo)polymerization and two-photon 3D laser printing, which play a crucial role in the scope of this thesis. Throughout the sections, I refer to applications in soft robotics and microfluidics, to set the results of this work into a broader context.

2.1 Soft Robotics and Soft Actuators

While conventional (hard) robotics is a highly successful field, that has been manifested in industrial applications for decades, it still features fundamental shortcomings, such as high complexity, limitations in collaboration, compatibility with chemically harsh or physiological environments, and low thermodynamic efficiency, just to name a few.[3]

Soft robotics, in turn, is still in its early stages and focuses on the use of flexible and compliant materials, which have the potential to overcome such shortcomings.[31] These materials are capable of autonomous adaptation to environmental changes and demonstrate safer interaction with humans and biological organisms in general.[4] Many concepts of soft robotics have been inspired by nature and animals, such as soft grippers that mimic the function of octopus arms or sea stars, soft walkers imitating the movement of worms, or soft sensors mimicking biological skin.[5]–[7] While early developments in soft robotics were often based on pneumatically or hydraulically driven elastomeric structures, that required tethered connections to external pumps, more recent designs focus on fully autonomous, responsive polymeric materials. Examples are electroactive polymers, liquid crystal elastomers, or responsive hydrogels, which can be controlled remotely.[32]–[34] Stimuli-responsive hydrogels are especially interesting for soft robotic applications in liquid environments or at physiological conditions, due to their compatibility with aqueous media and their mechanical similarity to biological tissue.[35]

Even though the boundaries between the terms robot and actuator are continuous, an actuator can be understood as being a basic component of a robot, which in general converts energy into mechanical motion.[36] Soft actuators often combine functions, such as sensing and reacting, in one and the same part, due to the adaptive nature of the materials in use, while hard robotics commonly requires different components for sensing and actuation, that have to communicate with each other.

Recently, advances in microfabrication technologies have fueled the development of micro-sized soft actuators. Münchinger *et al.* have fabricated bi-layered soft microbeams, capable of significant bending motions under thermal stimulation.[37] Miniaturization has therefore led to the emergence of micro soft robotics, which focuses on performing tasks at micro and nano scales. However, in many cases the reduction of actuator dimensions into the micrometer range remains challenging. Among electroactive polymers, dielectric elastomer actuators (DEAs) are highly popular, which are capable of deformation upon electric stimulation.[38] Here, finding microfabrication processes that allow for manufacturing both the dielectric elastomers as well as compliant electrodes at the microscale and even implementation into integrated circuits represent major obstacles.[39] In contrast, responsive hydrogel actuators can be designed from single material structures and recent advances in microfabrication technologies, such as 3D printing, have shown promising potential for the development of soft microactuators.[40] The following chapter thus focuses on explaining fundamental aspects on some functional hydrogels, which have been used in this thesis.

2.2 Functional Hydrogels

Among the various materials for soft actuator development, functional hydrogels represent a promising candidate. Hydrogels are three-dimensional polymeric networks with a high hydrophilicity, that results in water uptake and a high degree of swelling, as well as soft mechanical properties.[41] These materials can be found in nature, such as agarose, alginate, chitosan, collagen, fibrin, and hyaluronan, but also have been synthesized as in the case of poly(ethylene glycol) (PEG), poly(vinyl alcohol) (PVA), or poly(2-hydroxyethyl methacrylate) (PHEMA).[42] In general, it can be distinguished between physically crosslinked hydrogels, consisting of reversible bonds, such as hydrogen bonds or physical entanglements, and chemically crosslinked hydrogels, representing permanent networks made of covalent bonds. Due to their soft nature, compatibility with aqueous environments, and often biocompatible properties, hydrogels are attractive materials for biomedical research, tissue engineering, drug delivery, and more.[43], [44]

Stimuli-responsive hydrogels belong to the class of smart materials and exhibit distinct changes in their chemical and physical properties in response to environmental changes, such as temperature, light, potential of hydrogen (pH), and electric or magnetic fields. Hence, these materials are especially attractive in the fields of biosensors and soft actuators.[45]

Several methods of synthesizing stimuli-responsive hydrogels have been employed, including free radical polymerization, click chemistry, enzyme catalysis, or self-assembly.[15] Furthermore, multi-responsive hydrogels have been developed by copolymerization of several responsive monomers types, such as thermoresponsive *N*-isopropylacrylamide (NIPAM) and pH-sensitive acrylic acid (AAc), or incorporation of photo-active molecules, such as azobenzenes or spiropyran derivatives.[46], [47] The combination of multiple responsive components into a single hydrogel system enables complex motions as well as multi-functional behaviors.[48]

To understand the behavior and performance of responsive hydrogels, it is crucial to characterize their material properties systematically as a function of an external cue. Here, several methods have been employed, including analysis of the swelling characteristics by monitoring changes in sample size and weight, studying changes of the mechanical properties by compression testing, rheology, or microindentation, and morphological investigation by scanning electron microscopy (SEM) and confocal microscopy.[49]–[52]

In recent years, significant advancements have been made regarding novel stimuli-responsive moieties, crosslinking strategies, and fabrication techniques to enhance the performance and expand the range of applications of stimuli-responsive hydrogels.[15] However, recent challenges remain, such as achieving precise control over the stimuli-response, enhancing mechanical properties, improving long-term stability, and miniaturizing hydrogel samples.

In the following, I provide an overview of the functional hydrogels used in this thesis.

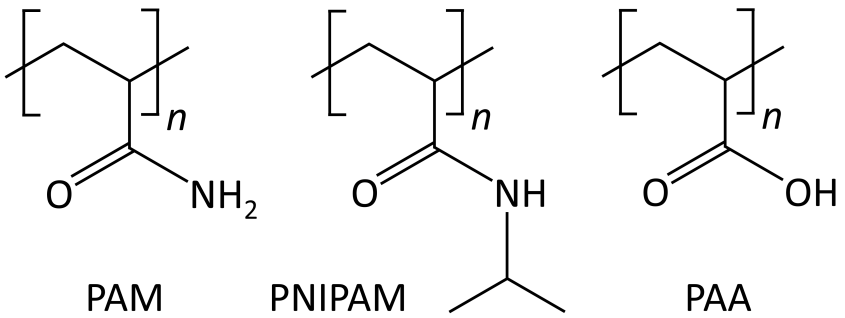

Figure 2.1: Structural formulas of the functional polymers poly(acrylamide) (PAM), poly(*N*-isopropylacrylamide) (PNIPAM), and poly(acrylic acid) (PAA) are depicted.

2.2.1 Polyacrylamide Hydrogels

Poly(acrylamide) (PAM) is a synthetic, linear polymer consisting of acrylamide (AM) monomers and was originally introduced as a support matrix for electrophoresis in 1959.[53] Nowadays, it serves as a versatile biomaterial, with applications ranging from wound healing to biosensors and many more.[54]

Its chemical structure is depicted in **Figure 2.1** and consists of a carbon backbone with hydrophilic amide side groups. Crosslinked PAM hydrogels can be prepared via free radical polymerization, using AM monomers and *N*,*N*'-methylenebis(acrylamide) (BIS) as a crosslinker. Most commonly, APS and TEMED are used as radical initiators, or photoinitiators, such as riboflavin or LAP, in the case of photopolymerization.[55] In contrast to PNIPAM, PAM hydrogels are typically non-thermoresponsive and exhibit consistent swelling behavior across a range of temperatures, which is primarily governed by factors like polymer concentration and crosslinking density.[56] The degree of swelling can vary due to changes in solvent properties, but these changes are not as dramatic as the LCST-driven swelling behavior of PNIPAM.

Poly(acrylamide) hydrogels exhibit biocompatible properties, such as chemical inertness with biological molecules or tissue, low toxicity, and controlled porosity, allowing for cell infiltration and tissue ingrowth. The hydrophilic nature of PAM hydrogels facilitates the diffusion of nutrients and metabolites, resembling to natural tissues in terms of water content. These properties make PAM suitable for tissue engineering scaffolds and controlled release platforms.[57] Moreover, the material can be functionalized or modified using specific bioactive molecules, such as peptides and growth factors, to yield enhanced interactions with cells or tissues.[58] However, proper purification and removal of any residual initiators or monomers are critical, to ensure biocompatibility, and thorough material testing is essential for biomedical applications.

As synthetic biomaterials, PAM hydrogels have been explored for wound healing, contact lenses, drug delivery systems, enzyme immobilization, protein separation, and biosensors.[59]–[61] In addition, PAM is used in water treatment and wastewater purification, due to its high water absorption capacity and capability to absorb pollutants and heavy metal ions.[62] Their widespread use in research suggests that PAM hydrogels exhibit compatibility with a broad range of biological systems.

Recent advancements in PAM hydrogel research include the development of hybrid systems, combining stimuli-responsive moieties with acrylamide monomers, to achieve multi-responsivity and targeted responses. Innovations in fabrication techniques, such as 3D printing and microfluidics, have expanded potential applications to microscale devices. Future research could explore the potential of PAM in fields such as soft robotics and wearable devices.

2.2.2 Thermoresponsive Poly(*N*-isopropylacrylamide)

One of the most popular and most extensively studied thermoresponsive polymers is PNIPAM, which was synthesized for the first time in 1956.[63] The thermoresponsive properties were first investigated systematically in 1968 by Heskins and Guillet.[64] The chemical structure of linear PNIPAM is depicted in **Figure 2.1** and consists of a non-polar backbone with amphiphilic side chains. These side chains are responsible for the thermoresponsive properties, where a thermodynamic balance between hydrophilic interactions from the amide group and hydrophobic interactions from the isopropyl group is established.[65]

The polymer's tendency to form hydrogen bonds between the amide groups and water molecules or to avoid those, can be derived from the Gibbs free energy change ΔG:

$$\Delta G = \Delta H - T \cdot \Delta S \tag{2.1}$$

Here, ΔH denotes a change in enthalpy, T the temperature, and ΔS a change in entropy. In general, a chemical reaction will happen spontaneously if $\Delta G < 0$, whereas it will not happen spontaneously for $\Delta G > 0$, since a reduction in Gibbs energy is thermodynamically favored principally.[66]

In the case of PNIPAM, the formation of hydrogen bonds between amide groups and water molecules corresponds to a decrease in enthalpy ($\Delta H < 0$; favored) and a reduction in entropy ($\Delta S < 0$; not favored), due to an increase in order by a highly structured hydration shell.[67] Both terms are thus competing with each other. Since the entropy term scales with temperature, it dominates for high temperatures, whereas it can be neglected for low temperatures. At a certain temperature, ΔH and $T \cdot \Delta S$ will have the same magnitude and balance out to $\Delta G = 0$. This temperature is called the lower critical solution temperature (LCST) of PNIPAM and denotes the point of phase transition between a hydrophilic and a hydrophobic state of the polymer. Below the LCST, ΔG is < 0 and the polymer chain forms an extended, hydrated coil, while above the LCST, ΔG is > 0 and the polymer chain undergoes a coil-to-globule transition, favoring intrachain interactions rather than binding water molecules. This mechanism is illustrated in **Figure 2.2** Hence, an aqueous solution of PNIPAM below the LCST is transparent, due to the solvated polymer chains, while above the LCST the solution becomes opaque, due to the phase separation of water and dispersed PNIPAM globules. For PNIPAM the LCST is at 32 °C and the phase transition is reversible.[68]

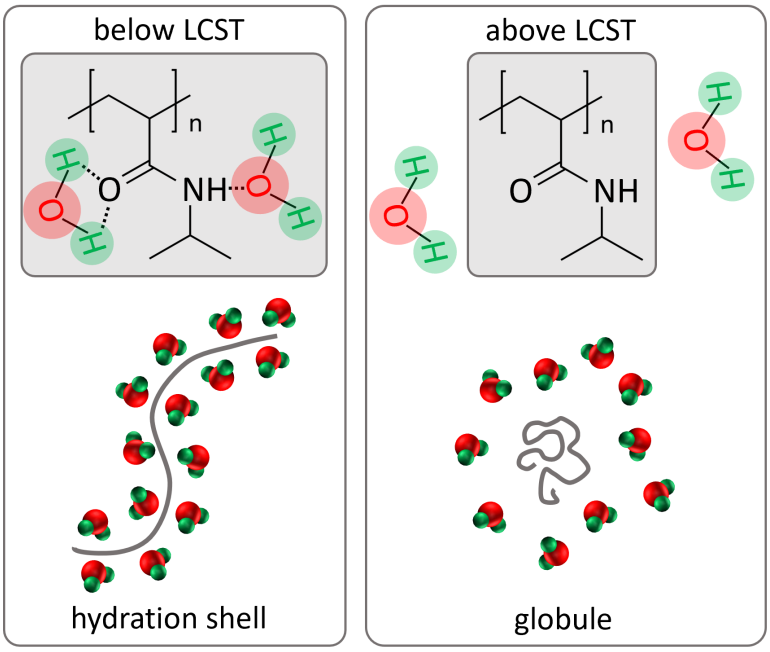

Figure 2.2: The thermoresponsive behavior of a linear PNIPAM chain is illustrated schematically. Below the LCST of 32 °C, the amide groups form hydrogen bonds with water molecules and the polymer remains as a hydrated extended chain. Above the LCST, intramolecular interactions become more favorable, causing the hydrogen bonds to break and the polymer chain to collapse into a globule, by expelling the water.

Crosslinked 3D networks of PNIPAM can be formed by radical polymerization using NIPAM monomers, BIS as a crosslinker and a radical initiator, such as APS and TEMED or LAP. These networks are considered PNIPAM hydrogels and change volume as a response to temperature changes, as depicted in **Figure 2.3**. Below the LCST the hydrogel swells in water, while above the LCST the hydrophobic network collapses and shrinks significantly by expelling the water. The swelling behavior can be tailored by modifying the composition of the hydrogel, such as incorporating additional monomers or varying the crosslinker concentration, to obtain hydrogels with desired swelling properties.[69]

Furthermore, the mechanical properties of PNIPAM hydrogels are often relevant for applications and can be adjusted by the crosslink density and the polymer concentration. In general, these hydrogels are soft and exhibit low mechanical strength. However, the incorporation of crosslinkers or the formation of interpenetrating polymer networks with other polymers can enhance their mechanical properties.[70] This makes the material suitable for applications such as tissue engineering scaffolds or soft actuators, where specific mechanical strength is required. For stimuli-responsive hydrogels, however, the amount of additional (non-responsive) crosslinkers in rela-

tion to (responsive) monomers can strongly affect and suppress their response, if the polymer network becomes too stiff and rigid. Thus, mechanical stability and desired functionality often compete with each other.[71]

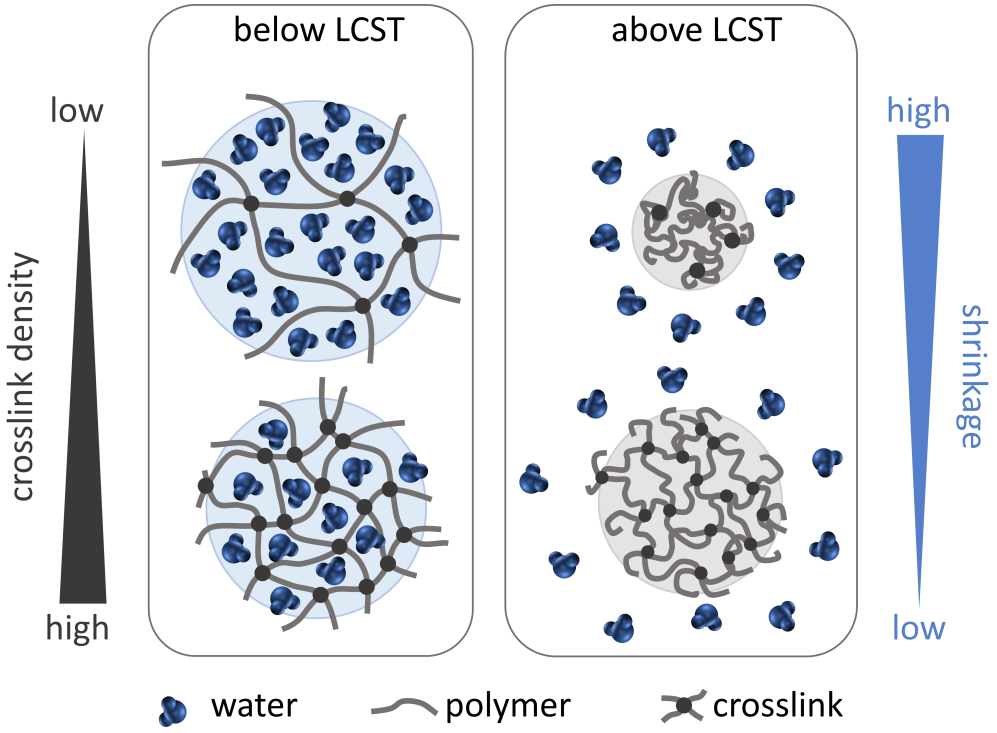

Figure 2.3: The volumetric change of a chemically crosslinked PNIPAM hydrogel as a response to temperature changes is depicted schematically. Below the LCST, the polymer network swells in water and occupies a relatively large volume. Higher crosslink densities result in smaller network pores and make the hydrogel less hydrophilic as compared to lower crosslink densities. Thus, the degree of swelling in less crosslinked PNIPAM hydrogels is higher. Above the LCST, the polymer network becomes less hydrophilic and collapses, by expelling the water and reducing its volume. The magnitude of shrinkage in this process is higher for less crosslinked PNIPAM, as compared to highly crosslinked PNIPAM.

Other synthetic thermoresponsive polymers than PNIPAM have been explored, such as poly(vinyl methyl ether) (PVME), which shows potential application in low fouling coatings and cell harvesting [72], poly(ethylene oxide)-poly(propylene oxide) (PEO-PPO) block copolymers, being studied for drug delivery [73], or poly(*N*-vinylcaprolactam) (PNVCL), showing a promising future in the biomedical field.[74] In addition, some natural polymers demonstrate thermoresponsive properties, such as hydrogel systems based on polysaccharides (cellulose, chitosan and xyloglucan) and proteins (gelatin).[75] However, PNIPAM is by far the most extensively studied

and most frequently used thermoresponsive polymer, due to its facile synthesis, commercial availability, low costs, good biocompatibility, and its phase transition near physiological temperature, which makes it an ideal candidate for various biomedical applications.[76]

In recent years, significant advancements in PNIPAM hydrogel research have been made, including exploration of strategies to increase mechanical stiffness, obtain faster responses, access sensitivities to other stimuli, such as pH or light, and incorporation of bioactive molecules or functional groups for specific applications.[77]–[79] Future research directions involve the development of hybrid hydrogels by combination of PNIPAM with other polymers or formation of composites using nanoparticles, to broaden the material capabilities, increase functionality, and improve overall actuation performance.

2.2.3 pH-Sensitive Polyacrylic Acid

Poly(acrylic acid) (PAA) is a weak anionic polyelectrolyte, meaning that it can be ionized depending on the pH value of the surrounding medium.[80] At low pH (pH < 4.25), the carboxylic acid groups (-COOH) of the polymer chains are protonated, while at high pH (pH > 4.25) these groups deprotonate (-COO^-), resulting in an ionized state of the polymer.[81] Crosslinked hydrogels of PAA thus exhibit pH-dependent swelling characteristics, where electrostatic repulsion in the anionic state results in an extended polymer network and influx of water molecules at elevated pH. The chemical structure of PAA is depicted in **Figure 2.1**.

The responsive nature makes PAA hydrogels interesting materials for application in biosensors, drug delivery, and soft actuators.[82] In **Figure 2.4** a microscope image of 3D laser printed PAA hydrogel microactuators is displayed. The micropillars are responsive to ionic strength and the degree of swelling depends on the chemical composition of the surrounding salt solution. Hence, these actuators could potentially be used for sensing functions. Copolymers containing acrylic acid have also been reported to exhibit thermo-, electro-, and pH-responsive behavior, which increases the range of applications to multiple stimuli.[83], [84]

Future research directions and recent challenges address the long-term stability of PAA hydrogels, increase of drug load efficiency, control of release kinetics, and exploration of 3D printable formulations.

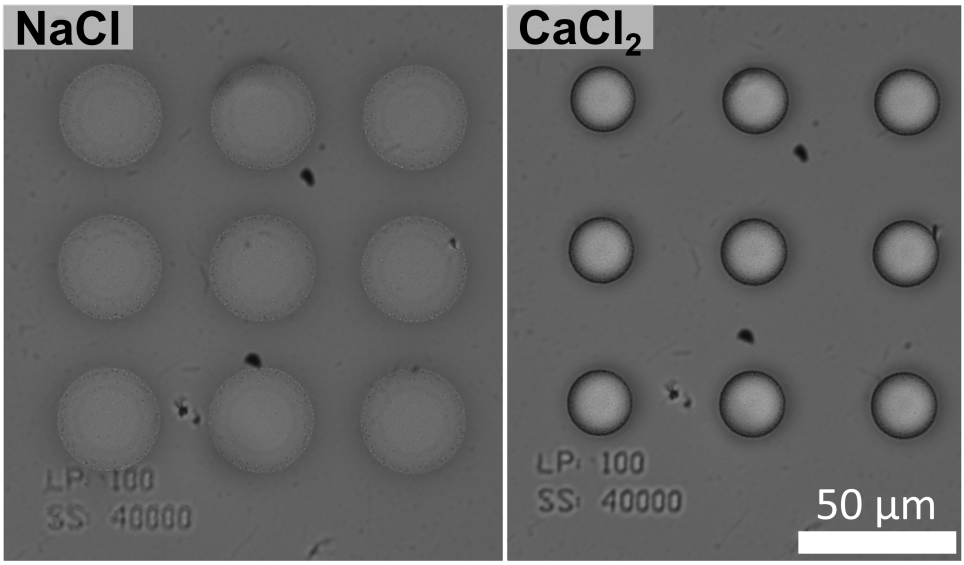

Figure 2.4: Microscope images of poly(acrylic acid) hydrogel micropillars are depicted. In sodium chloride solution the hydrogel swells significantly more, as compared to a calcium chloride solution.

2.3 Fabrication Techniques for Hydrogel Microstructures

The ability to engineer hydrogel microstructures with precise control of size, morphology, and spatial arrangement has opened new avenues for applications ranging from tissue engineering and drug delivery to microfluidics and biosensors.[85] While some fabrication techniques are more suitable for high throughput processing, others are superior in shape complexity and fabrication resolution, or more flexible in changing designs. This chapter deals with the diverse range of fabrication techniques for creating hydrogel microstructures and elaborates their advantages, limitations, and potential applications.

Generating microscale hydrogels requires methods, that can control the crosslinking process with high spatial precision. These techniques can be categorized into photolithography, micromolding, extrusion-based synthesis, template-assisted methods, and emulsification.[86], [87] The following sections focus on template-assisted and photolithographic approaches, which are most relevant in the scope of this thesis.

2.3.1 Template-Assisted Methods

Template-assisted fabrication methods provide versatile and precise approaches for creating hydrogel microstructures with tailored properties and functionalities. These methods are based on using a scaffold material to shape and guide the formation of hydrogel microstructures. Often the hydrogel is polymerized inside or around the scaffold material and if desired, the scaffold can even be removed after polymerization to yield porous microstructures. The template material typically defines the shape and morphology of the final hydrogel microstructure or micropores, while the functionality is pre-determined by the hydrogel precursor composition.[88] However, in advanced template-assisted methods, functionalities can also be included by coating the sacrificial material with another material, such as electrically conductive or magnetic thin films. After removal of the sacrificial scaffold, these coatings remain in the hydrogel microstructure and provide the hydrogel with a new function.[89]

Key aspects of template-assisted fabrication methods include template selection, hydrogel precursor infusion, and template removal strategies. Electrospun fibers, porous membranes, microfluidic devices, and sintered nano- or microparticle scaffolds represent a few examples of template materials.

In wound dressing or tissue mimicking applications, electrospinning can be employed, which uses electrostatic forces to fabricate nanofibrous templates that can be coated with hydrogel precursors.[90] Microfluidic devices can control the flow and crosslinker concentration of hydrogel precursor solutions, to generate hydrogel microstructures with tailored properties. Especially microscale patterns and gradients can be fabricated by this approach and find application in tissue engineering and biosensing.[91] Porous membranes having defined pore sizes and geometries can serve as templates for designing hydrogel microstructures by methods such as membrane casting or freeze-casting. These approaches are useful for cell encapsulation and drug delivery applications.[92] Powders of nano- or microparticles can be molded and sintered to yield highly porous templates, while maintaining a high interconnectivity of the template material. This approach is valuable for applications in neuroscience research or for generating conductive hydrogels.[93]

Despite the various techniques for designing template materials, there are several ways of infusing the hydrogel precursor into the templates. Porous scaffolds can simply be infiltrated, and the hydrogel solution can be polymerized using thermal radical initiators.[89] However, hydrophilic template materials are required for this approach and photoinitiators can only be used, if the template material is transparent for the respective wavelength of light. Thin hydrogel films can be deposited on templates by means of initiated chemical vapor deposition (iCVD), where monomers and initiator in the gaseous phase flow into a vacuum chamber and start a radical polymerization in an adsorption layer on the template surface. The radical initiator is typically excited via resistively heated filaments.[94] Furthermore, hydrogel precursor solutions can be coated onto templates via dip coating or electrospraying. After adhering to the template's surface, the hydrogel is solidified to create the

desired microstructure.[95], [96]

Several template removal strategies have been developed for extracting the hydrogel structures from the templates once they have been formed. Preserving the integrity of the hydrogel microstructures while effectively detaching them from the templates, are essential for a successful removal. The choice of removal strategy depends on factors such as the template material, hydrogel composition, and intended application of the hydrogel microstructures. If the template material is soluble in a specific solvent, it can be dissolved to release the hydrogel microstructure, as for example dissolution of sugar or salt templates in water.[97], [98] Thermal release can be used when the template has a lower melting point than the hydrogel's structural integrity. Here, the template material may soften, melt, or undergo a phase transition, to get separated.[99] If the hydrogel cannot be removed mechanically (for instance by peeling), changing the environmental conditions, such as pH, temperature, or solvent exchange, may facilitate the release. In the case of biodegradable templates, the material itself can degrade over time to release the intact hydrogel microstructure.[100] This method is especially interesting for *in vivo* applications.

Even though some of the aforementioned template-assisted fabrication methods are capable of designing hydrogel structures in the micrometer range, most methods are restricted in miniaturization by the minimum template size, which is often in the millimeter range. Still, such macro-sized hydrogel samples can be used for studying fundamental actuation principles, as in the case of thermoresponsive hydrogel actuators, for instance. For PNIPAM hydrogel bulk samples, it is well known, that thermally-induced shrinkage and swelling is limited by the in- and outflow of water and by formation of a dense skin layer.[101] Hence, template-assisted incorporation of micropores can cause a penetration of the skin layer and promote water flow. By controlling the micropore diameter and pore density, these methods can further be applied to systematically investigate and understand thermoresponsive actuation of hydrogels in general.

2.3.2 Photolithography

Photolithography, within the context of hydrogels, relies on the development of synthetic and natural, photo-crosslinkable pre-polymers, that can form hydrogels upon exposure to light.[102] In this process, typically a small volume of a photosensitive polymer resin is exposed to UV light through a photomask containing the pattern of the final microstructure. As the light reaches the resin through the transparent regions of the mask, it induces a photoreaction that crosslinks the polymer. The residual resin that has not been illuminated by light remains unpolymerized and can be washed away with appropriate solvents, yielding the final hydrogel microstructure. **Figure 2.5** displays the process schematically. In addition, maskless fabrication processes have been developed, such as digital light projection or laser-based stereolithography.[103] Compared to traditional photolithography techniques using

photomasks, these maskless methods offer several advantages, such as enhanced flexibility regarding corrections, modifications, and iterations of the specimen design. Further, production costs and times can be reduced by eliminating the need for expensive photomask fabrication and mask alignment.

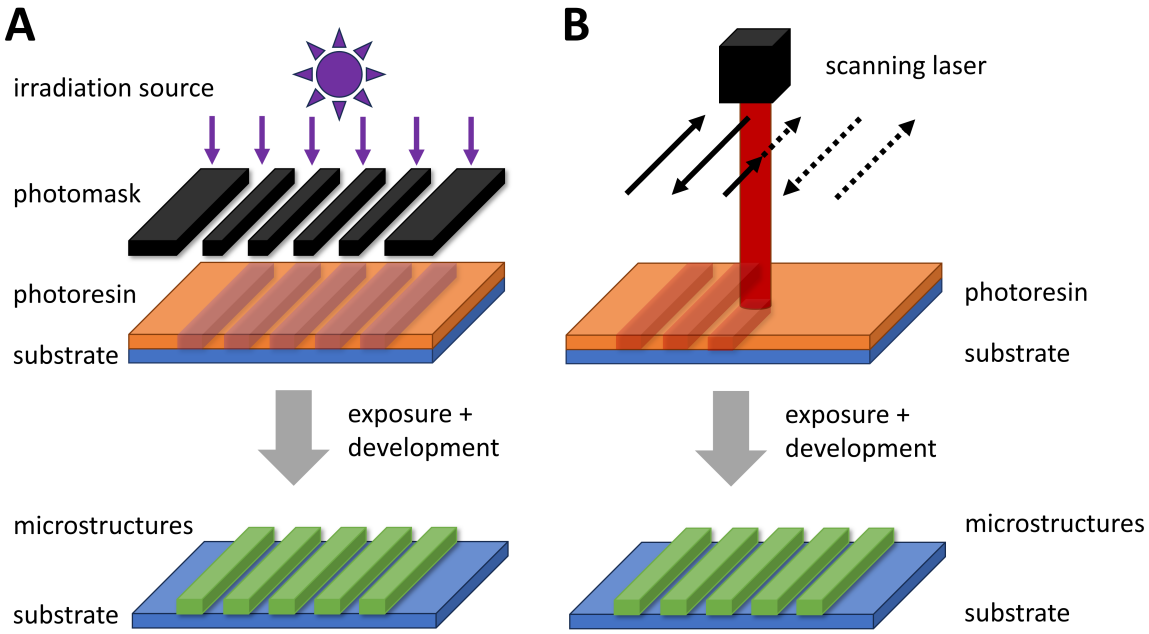

Figure 2.5: The fundamental concept of photolithography is illustrated schematically. (A) In conventional photolithography, a photoresin is exposed to light by use of a photomask, which projects the pattern of choice from a light source into the resin. After development, the solidified part of the resin remains on the substrate, while the soluble part is washed away with a solvent. (B) In maskless photolithography, in contrast, focused light from a laser or LED is typically scanned over the photoresin, transferring the design pattern into the resin.

Photolithography can achieve resolutions that range from sub-micron to millimeter scale, enabling fabrication of hydrogel structures much smaller or much larger than an average cell diameter of approximately 10 microns. This characteristic allows for a spectrum of biological applications, such as tissue engineering. Recently, photolithography-based 3D bioprinting has been used to fabricate implantable bone tissue.[104]

In the context of hydrogel microfabrication, the concepts of radical (photo)polymerization, one- and two-photon absorption, and two-photon polymerization play a fundamental role. Hence, I explain these topics in the following sections.

Radical (Photo)Polymerization

Free radical polymerization (FRP) is a process in chemistry, where individual building blocks (monomers) are successively linking to long chains (polymers) by formation of covalent bonds. This method is widely employed to synthesize a variety of polymers, ranging from common plastics, such as poly(ethylene) (PE), poly(vinyl chloride) (PVC), or poly(methyl methacrylate) (PMMA), to advanced materials exhibiting tailored properties, such as highly stretchable, UV-curable elastomers for digital light processing,[105] or architecturally complex polymers with controlled chain topology and functionality.[106] The process of free radical polymerization can be divided into three steps, namely initiation, propagation, and termination.

During initiation, highly reactive molecules are generated, which are called free radicals and are crucial to start the polymerization. This activation is commonly induced by heat, light irradiation, or redox reactions, and is based on cleavage of a labile bond in the initiator molecule. The free radicals thus possess unpaired electrons and tend to react with monomers to form new radicals. This process starts the propagation, where monomer radicals covalently link to other monomers by forming additional radical monomers. In this way, long polymer chains are formed, which can reach high molecular weights of up to 750 kDa under specific reaction conditions.[107] Finally, the growing polymer chains are terminated via several possible mechanisms, including combination, disproportionation, and chain transfer reactions. **Figure 2.6** illustrates the different steps of a free radical polymerization schematically. Factors influencing the kinetics of free radical polymerization include monomer concentration, initiator concentration, temperature, and properties of the reaction medium.[108]

In the case of photopolymerization, the radical polymerization is initiated by light. Hence, appropriate photoinitiators are required that absorb light at a specific wavelength. Photopolymerization is used in hardening printing inks, dental fillings, coatings of glass fibers and discs, and photoresists.[109] It is particularly relevant in the field of 3D printing, such as in stereolithography (SLA), digital light processing (DLP), and continuous liquid interface production (CLIP). Light-based 3D printing of polymers offers several advantages compared to conventional extrusion-based methods, such as fabrication of complex multi-functional material systems with controllable optical, chemical, and mechanical properties, as well as a higher resolution.[110]–[112]

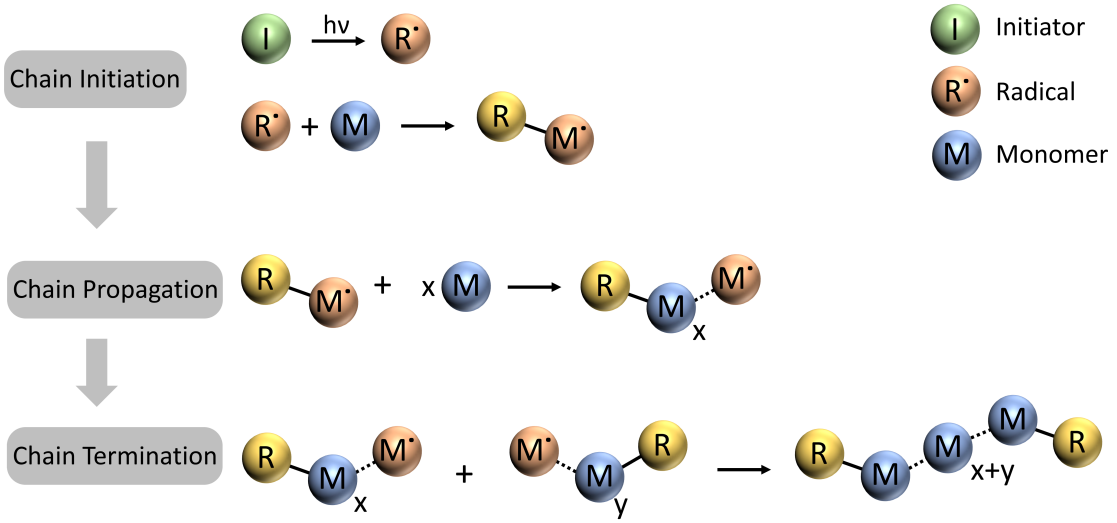

Figure 2.6: The individual steps of a free radical polymerization are illustrated schematically. The growth of a polymer chain is initiated by conversion of an initiator molecule into a free radical, which covalently links to a monomer and turns the monomer into a radical. The excitation of the initiator in this example is induced by light absorption. During chain propagation, more monomers are linked covalently to the growing polymer chain. Termination can happen by combination of two growing chains, as depicted in this example, but also other mechanisms are possible, such as disproportionation or chain transfer reactions.

For the fabrication of responsive hydrogels via light-based 3D printing, a photoresin is required that must be composed at least of three main components mixed in an appropriate solvent: monomers, crosslinkers and photoinitiators. In addition to that, fillers and other functional monomers can be added to tailor mechanical properties as well as multi-responsivity. A reaction schematic of PNIPAM hydrogel formation via chemical crosslinking of NIPAM monomers and BIS crosslinker is depicted in **Figure 2.7**.

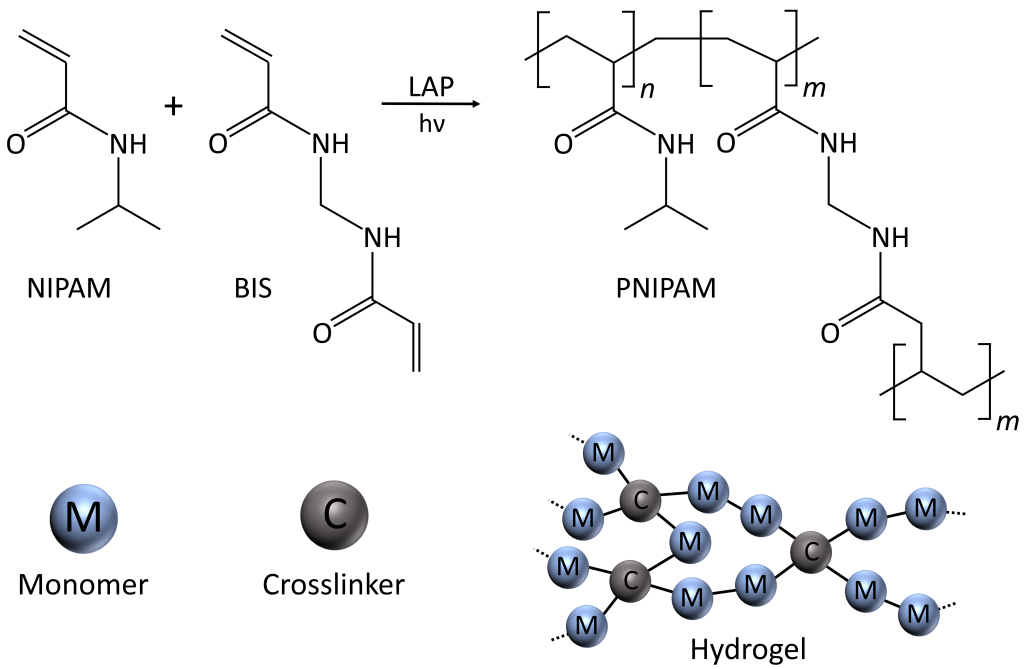

Figure 2.7: Formation of a chemically crosslinked PNIPAM hydrogel is depicted schematically. NIPAM (monomers), BIS (crosslinker), and LAP (photoinitiator) molecules react in a free radical polymerization initiated by light, to form a 3D polymer network. This crosslinked polymer can swell in water to form a PNIPAM hydrogel.

One-Photon and Two-Photon Absorption

In conventional light-based 3D printing techniques, such as SLA, DLP, or CLIP, the photoinitiator is excited by absorption of a single photon. Here, the energy of the photon must match the energy gap between the ground state of the molecule and an excited state, to induce transition of an electron into a higher energy level. This process can be illustrated in a Jabłoński-diagram, as depicted in **Figure 2.8**. The probability for one-photon absorption (OPA) is linearly proportional to the light intensity and typically UV light is required to excite conventional photoinitiators. Printing resolutions in these processes are typically in the low micrometer range, while the print volumes are in the order of cm^3.[113]

Two-photon absorption (TPA), in contrast, is a non-linear process, where the absorption probability is proportional to the square of light intensity. Here, a photoinitiator molecule nearly simultaneously absorbs two lower-energy photons to achieve the same energy transition that would occur in one-photon absorption. Hence, near-infrared light (NIR) is commonly required for excitation. Since this process is only effective in regions of high photon density, tightly focused pulsed laser beams are used. Printing techniques based on two-photon absorption, such as 3D laser nanoprinting, thus can reach much higher resolutions (< 200 nm) compared to one-photon absorption, and print sizes are typically in the order of µm^3 to mm^3.[114]

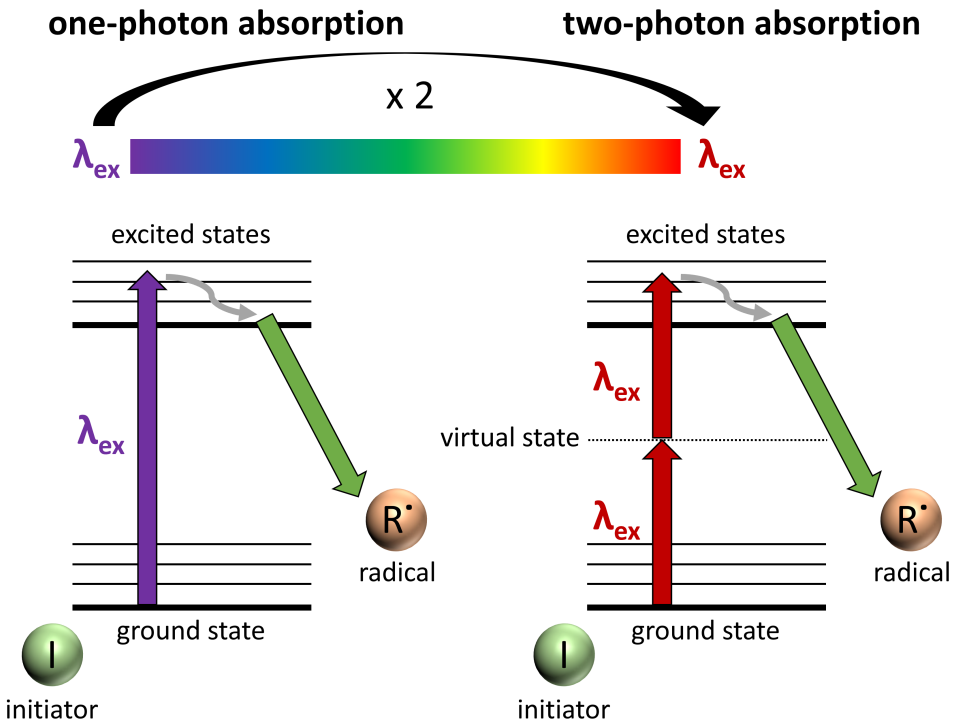

Figure 2.8: Jabłoński-diagrams are presented to illustrate the mechanism of one-photon (left) and two-photon (right) absorption. A photoinitiator molecule is excited by transferring an electron from a ground state into an excited state. The energy required to overcome the gap between these states is provided by light absorption. In the case of one-photon absorption (OPA), a single photon of typically high energy (≈ UV) is absorbed, while in two-photon absorption (TPA), two lower energy photons (≈ NIR) are absorbed nearly simultaneously via a virtual state. Therefore, the photons' wavelength in TPA is twice as much compared to OPA. The excited photoinitiator finally forms a radical, which can initiate a polymerization. [Figure based on: [115]]

Two-Photon Polymerization of Hydrogels

Two-photon polymerization (TPP) has become a widely used method for high precision fabrication of complex and intricate, polymeric 3D microstructures. Especially in the context of hydrogels, this tool has exploited new possibilities in applications such as tissue engineering, drug delivery, and microfluidics.[116]

The method is based on photoinitiated radical polymerization of a hydrogel precursor resin, where the initiator radicals are excited via two-photon absorption. The experimental setup typically includes a highly focused, femtosecond pulsed near-infrared laser ($\lambda \approx 800$ nm), which is stirred by galvo mirrors and focused via an oil immersion objective. A droplet of the photoresin is deposited on a glass substrate and mounted into a piezo-controlled stage. During printing, the focused laser beam is scanned through the droplet in three dimensions, initiating polymerization of the resin, according to a previously generated computer model of the final microstructure. After printing, the sample is developed in appropriate solvents, removing the unpolymerized resin and revealing the final hydrogel microstructure.[117] A schematic of the experimental setup is sketched in **Figure 2.9**.

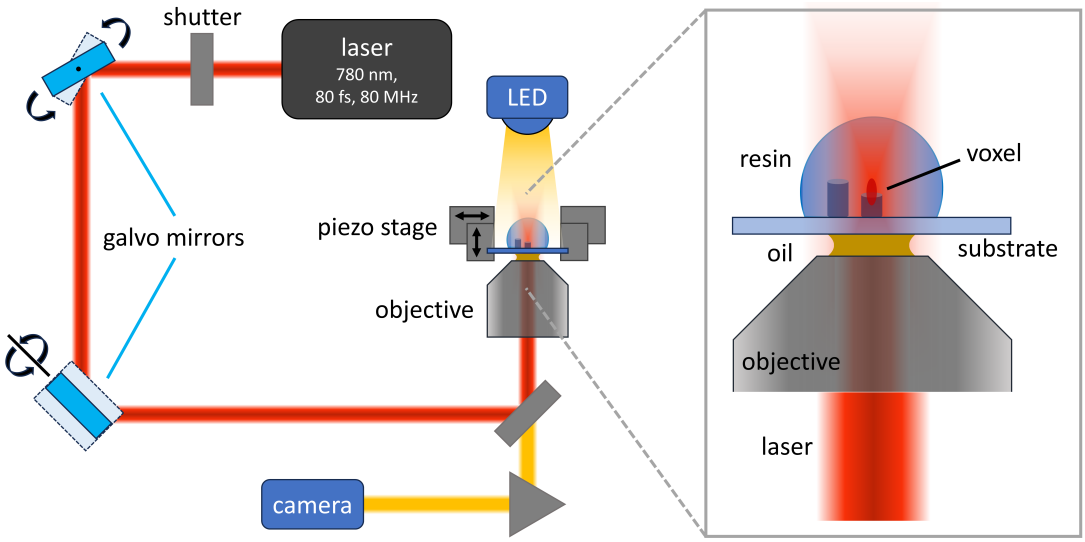

Figure 2.9: The basic setup of a typical two-photon polymerization (TPP) microfabrication device is depicted schematically. This includes a femtosecond pulsed near-infrared laser ($\lambda \approx 800$ nm), which is deflected by galvo mirrors and tightly focused via an oil immersion objective. A glass substrate is loaded with a droplet of photoresin and mounted into a piezo-controlled stage, which can move in x-, y-, and z-direction. Galvo mirrors and piezo-stage allow to scan the focused laser in three dimensions, resulting in polymerization of the photoresin in the regions of the laser focus spot (voxel). A camera is used to visualize the process during 3D printing. [Figure based on:[117]]

The smallest volume element that can be solidified at once is called a volume pixel or voxel, and has an ellipsoidal shape. The main factors influencing the voxel's dimension, and thus the printing resolution, include the optical system of the printer, chemical and optical properties of the photoresin, and printing parameters, such as laser power and scan speed. The implemented galvo mirrors allow for precise and fast steering of the laser beam, resulting in scan speeds of hundreds of millimeters per second. Further, the efficiency of the photoinitiator has a major impact on the resolution. Here, a high probability for two-photon absorption (high two-photon cross-section) is desirable, to efficiently generate radicals. Another requirement in the biomedical field is a low toxicity of the photoinitiator. Promising and frequently used initiators in hydrogel microfabrication include lithium phenyl (2,4,6-trimethylbenzoyl) phosphinate (LAP), bis(2,4,6-trimethylbenzoyl)-phenylphosphine-oxide (TPO), and cyclic benzylidene ketone-based initiators.[118]

In addition to the photoinitiator, the monomer and crosslinker concentrations predetermine the final hydrogel's properties. For stimuli-responsive hydrogels, the type of monomer defines the functionality of the final gel, whereas the crosslink concentration determines the mechanical stability, which usually competes with responsivity. However, the degree of crosslinking practically can be controlled easiest by varying the laser dose and keeping the resin composition constant. A typical resin is composed of about 88% monomers, 10% crosslinker and 2% photoinitiator.[119] Recent advancements of two-photon 3D laser printing include two-photon grayscale lithography and two-step absorption instead of two-photon absorption.

In grayscale lithography, the laser intensity is varied during printing of an object, controlling the local exposure of the resin. Hence, the voxel size is changing according to the laser intensity, which allows for reducing the step sizes of stacked, printed layers at curved surfaces. As a result of increased vertical resolution, curved surface features of an object, such as a lens, become smoother. This is in particular relevant for micro-optics and photonic applications.[120] Moreover, 2D grayscale images can be converted into 3D objects, by relating the brightness of image pixels with the topography of the final object.[121] In hydrogel microactuator fabrication, grayscale lithography can be used to make gradients in crosslink density and achieve anisotropic actuation properties, such as in bending, bi-layered beams.[122]

Two-step absorption has been introduced in 3D laser printing and relies on the use of photoinitiators, which can be excited via a real intermediate state, instead of a virtual intermediate state. These real states have a much longer lifetime compared to the virtual ones. Apart from this, two-step absorption exhibits the same quadratic dependence of exposure dose on light intensity as two-photon absorption, and thus provides the same high precision printing capabilities. However, lasers with much lower optical output power (sub-milliwatt) are sufficient to induce two-step absorption and in turn, reduce the costs and sizes of 3D laser printers significantly.[123]

Comparing two-photon polymerization microfabrication to other additive manufacturing technologies, it outstands with its tremendous printing speed (hundreds

of millimeters per second) with respect to high resolution (sub micrometer), the variety of curable materials and substrates, and a high degree of freedom regarding print shape complexity. Other common microfabrication techniques, such as electron beam or atomic force lithography, are restricted to 2.5D sample geometries and typically exhibit a comparatively low fabrication throughput.[124]

In 3D hydrogel microfabrication, high printing resolution is a key parameter to mimic native 3D environments, in which cells can reside, or to design drug delivery platforms with optimal temporal and spatial release control. Hence, two-photon laser printing is a promising fabrication tool for these kind of applications.[125]

3

Results and Discussion

3.1 Thermoresponsive PNIPAM Hydrogels with Improved Actuation Function for Soft Robotic Applications

Partial results of the presented work have been published in:

- **Spratte, T.**, Arndt, C., Wacker, I., Hauck, M., Adelung, R., Schröder, R.R., Schütt, F., Selhuber-Unkel, C., Thermoresponsive Hydrogels with Improved Actuation Function by Interconnected Microchannels. *Adv. Intell. Syst.* **2022**, 4, 2100081. https://doi.org/10.1002/aisy.202100081

3.1.1 Introduction

In this chapter, I introduce a method for incorporating a microchannel network into thermoresponsive PNIPAM hydrogels using a sacrificial zinc oxide scaffold. This approach leads to a significant increase in thermally induced actuation compared to the conventional bulk material, even though only a small fraction of the hydrogel is replaced by microchannels. Furthermore, the novel material is attractive for soft robotic applications, which is demonstrated in an actuation setup at the end of this chapter.

First, the fabrication process of the microengineered PNIPAM hydrogel is explained in detail (**Section 3.1.2**) and the presence of hollow microchannels is verified by a microstructural examination (**Section 3.1.3**). Subsequently, the temperature-induced shrinking and swelling properties are investigated thoroughly (**Section 3.1.4** and **Section 3.1.5**) and compared with the bulk material, as well as the mechanical material characteristics (**Section 3.1.6**). Finally, the hydrogel's ability to generate stroke forces is studied and verified in an actuation setup (**Section 3.1.7**). For completion, a comparison with other actuation concepts is also included (**Section 3.1.8**).

Thermoresponsive hydrogels are attractive material candidates for soft actuator research due to the possibility of inducing volume changes by simply varying the

environmental temperature.[126] Especially phase transition temperatures close to room temperature and human body temperature are of high interest because the energy input for actuation is comparatively low and could potentially be achieved under physiological conditions.[127] However, compatibility with different environments, adjustable material stiffness, fast response rates, and distinctive volume changes are typical requirements that are difficult to combine and often compete with each other.[128] Bulk thermoresponsive hydrogels, in contrast, are known to exhibit slow response rates and generate comparatively weak stroke forces, limiting the application in soft actuators due to low amplitude deformation.[129] For PNIPAM hydrogels, the formation of a skin layer upon dehydration above the lower critical solution temperature (LCST) is reported, which prevents further shrinkage and reveals another limitation.[130] The microengineered PNIPAM introduced in this work overcomes the limitations of the bulk hydrogel, by showing large shrinkage as well as high stroke forces that can be used to actuate external objects. Furthermore, the material stiffness remains unaffected by the microchannels and can be adjusted by the chemical composition of the hydrogel, while still maintaining a high temperature response. Other established methods of increasing the temperature response of PNIPAM hydrogels are often based on chemical modifications of the polymer network such as copolymerization[131], formation of interpenetrating polymer networks[132], or nanocomposites.[133] These approaches usually are accompanied by undesirable changes in material properties, such as a shift in LCST[134], elasticity[135], or optical transparency.[136] The microengineering approach explained in this work can therefore provide an attractive method of developing highly responsive and chemically unmodified, thermally controlled hydrogel actuators.

3.1.2 Preparation of Bulk and Microengineered PNIPAM Hydrogels

All hydrogel samples were prepared via free radical polymerization, using *N*-isopropylacrylamide (NIPAM) monomers, BIS crosslinker and *N,N,N',N'*-tetramethylethylenediamine (TEMED) in combination with ammonium persulfate (APS) as a radical initiator in an aqueous solution. Three different hydrogel compositions were used with varying crosslinker concentrations according to **Table 3.1** and denoted as *soft*, *medium*, and *hard*. The samples containing microchannels were termed *channel PNIPAM* whereas the ones without channels were termed *bulk PNIPAM*. All chemicals were purchased from Sigma Aldrich (Taufkirchen, Germany) and used without further purification, if not stated otherwise. BIS and TEMED were purchased from BioRad (Hercules, California, USA).

sample composition	NIPAM m / mg	BIS m / mg	APS m / mg	TEMED V / µl	H_2O V / µl
PNIPAM soft	600	**5**	10	23	4600
PNIPAM medium	600	**10**	10	23	4600
PNIPAM hard	600	**15**	10	23	4600

Table 3.1: Compositions of hydrogel precursor solutions with varying crosslinker (BIS) concentration are listed. The different samples used in the experiments are termed *PNIPAM soft, medium*, and *hard*.

In a first step, two aqueous solutions were prepared: one vial containing NIPAM, BIS, and APS and another containing only TEMED. Both vials were sealed with a septum and purged with nitrogen for 10 minutes in an ice bath and under magnetic stirring at 500 rpm, to ensure homogeneous mixing. Afterwards, both solutions were combined and stirred for a few seconds before the hydrogel solution was immediately cast in a mold.

Bulk hydrogel samples were prepared by casting the solution into a poly(tetrafluoroethene) (PTFE) mold. The mold contained cylindrical wells of 8 mm diameter and 12 mm depth, and each well was filled with 750 µl of the hydrogel solution. The filled mold was left at room temperature (22 °C) for 2 hours until the samples were polymerized. After removal from the wells the samples were stored in room temperature MilliQ water. Before using the samples for further experiments, the water was exchanged daily over a period of 5 days to remove any unreacted molecules.

Microengineered PNIPAM hydrogels were prepared according to a previously established method of Dr. Christine Arndt by infiltrating the hydrogel solution into sacrificial, highly porous zinc oxide templates, which were removed after polymerization to yield a microchannel-containing hydrogel.[89] The zinc oxide templates were provided by M. Sc. Margarethe Hauck from the group of Prof. Dr. Rainer Adelung at Kiel University. These sacrificial scaffolds had a cylindrical shape with both diameter and height of 6 mm and consisted of sintered tetrapodal shaped zinc oxide (t-ZnO) microparticles, which were prepared by flame transport synthesis, as described in other studies.[137] The templates were fabricated with densities of 0.2, 0.3, 0.4 and 0.6 g cm^{-3} by compressing the appropriate amount of microparticles into a steel mold, removal of the compressed template and subsequent sintering at 1150 °C for 5 hours. These densities can be calculated into a template porosity P according to **Equation 3.1**, where V_{ZnO} is the volume occupied by zinc oxide microparticles and $V_{template}$ is the total volume of the porous template. The densities of zinc oxide microparticles and template are denoted as ρ_{ZnO} and $\rho_{template}$, respectively.[138] The template porosities used in this work are summarized in **Table 3.2** and are directly related to the final microchannel densities of the hydrogels. After infiltration of the hydrogel solution, the filled templates were left at room

$\rho_{template}$ / g cm^{-3}	ρ_{ZnO} / g cm^{-3}	P / vol%
0.2	5.61	3.6
0.3	5.61	5.3
0.4	5.61	7.1
0.6	5.61	10.7

Table 3.2: Zinc oxide template porosities are listed, based on the various template densities used in the experiments. The porosities were calculated according to equation 3.1.

temperature for 6 hours to polymerize. Subsequently the zinc oxide was dissolved by immersing the samples in 0.5 M hydrochloric acid for at least 24 hours, yielding hydrogels with hollow microchannels. Finally, the acid was removed and replaced with MilliQ water by exchanging the water regularly over 5 days before the samples were used for further experiments.

$$P = \frac{V_{ZnO}}{V_{template}} \cdot 100\% = \frac{\rho_{template}}{\rho_{ZnO}} \cdot 100\% \tag{3.1}$$

3.1.3 Microstructural Analysis by Scanning Electron Microscopy

The presence of hollow microchannels in the prepared microengineered PNIPAM hydrogels was verified by SEM imaging, which was kindly done by Dr. Irene Wacker from the group of Prof. Dr. Rasmus R. Schröder at BioQuant, Heidelberg University. Imaging of highly hydrated materials, such as biological samples or hydrogels, via high-vacuum electron microscopy, requires removal of water and hence special sample preparation before imaging. While conventional methods, such as freeze drying, are prone to induce artifacts, e.g., by large pore formation due to ice crystal growth during the freezing process, alternative approaches need to be used to dry the specimens.[139] Here, small pieces of equilibrated PNIPAM hydrogel were treated with 5 % tannic acid overnight and washed with deionized water. Subsequently incubation in an aqueous solution of osmium tetraoxide (OsO_4) was done for 4 hours to stain the material and combat charging effects from the electron beam. To expose inner surfaces, the pretreated samples were cut open with a scalpel, air dried, and mounted on aluminum sample holders using silver paint. A Crossbeam 540 (Carl Zeiss Microscopy, Oberkochen) was used at 1.5 keV primary energy and 175 pA beam current, to record images of both bulk and microengineered PNIPAM hydrogels.

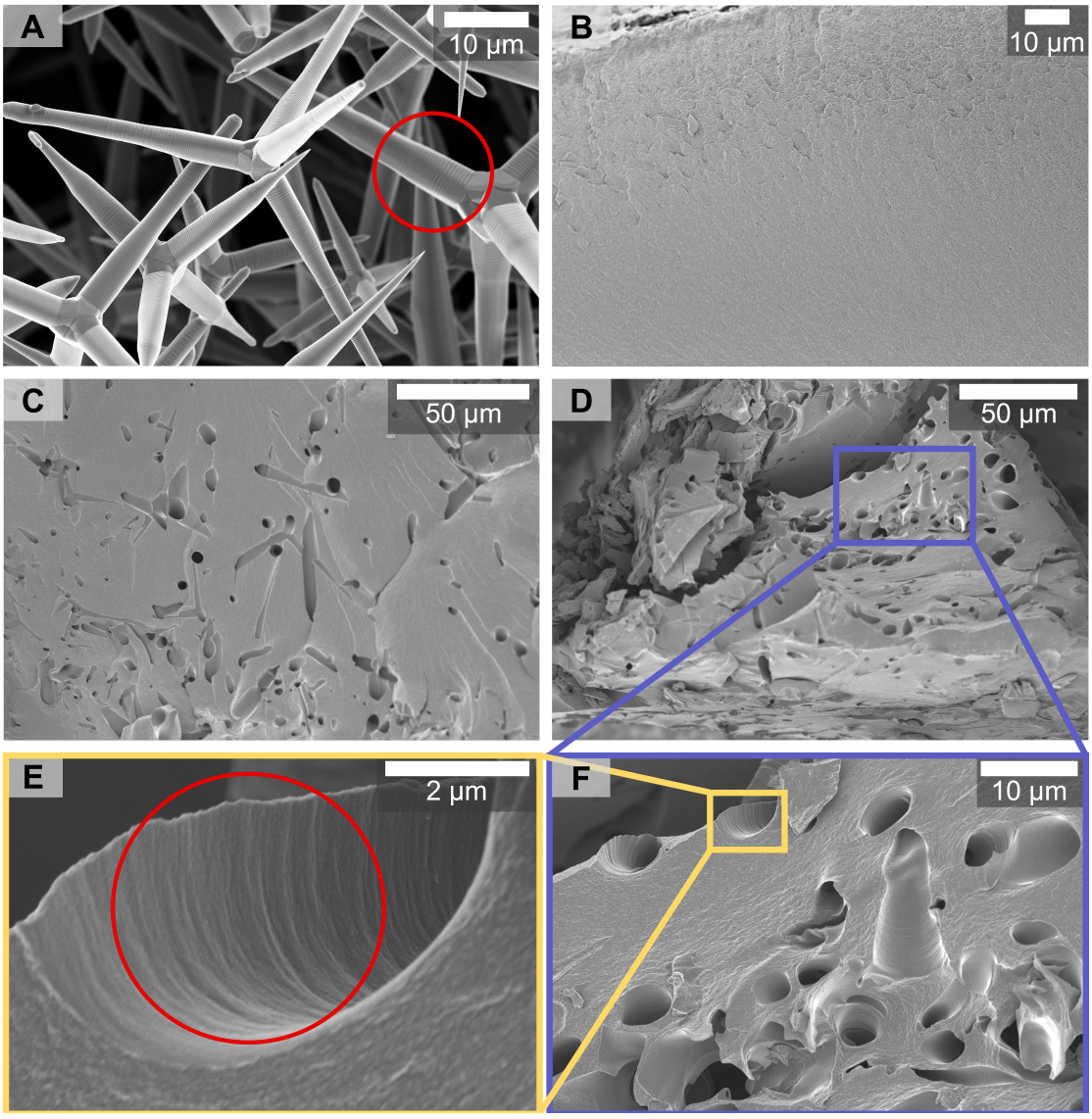

Figure 3.1: Scanning electron microscope images of tetrapodal shaped zinc oxide microparticles (A), bulk PNIPAM (B), and microchannel-containing PNIPAM in various magnifications (C-F) are depicted. The zinc oxide microparticles have a characteristic morphology, which includes four conical shaped legs of 2-3 µm average diameter (A). Inner surfaces of bulk PNIPAM appear featureless and smooth, without any traces of microchannels (B), while microengineered PNIPAM displays hollow cavities, resembling the characteristic shape of dissolved zinc oxide tetrapods (C-F). At high magnification (E), wrinkled features in the microchannel walls become visible, which are replicated from the tetrapod legs (cf. red circles). Reprinted with permission.[140] Copyright 2021, Wiley-VCH GmbH.

The morphology of tetrapodal zinc oxide (t-ZnO) microparticles is depicted in **Figure 3.1 A**, which was kindly provided by Dr. Fabian Schütt from the group of Prof. Dr. Rainer Adelung at Kiel University. These particles have four conical shaped legs with an average leg diameter of 2-3 µm and hexagonal cross-sections.[141] As a reference, the bulk PNIPAM inner surface was imaged (**Figure 3.1 B**) and found to be featureless and smooth without any microchannels. The microengineered PNIPAM surfaces, in contrast, display hollow channels (**Figure 3.1 C-E**), which resemble the characteristic shape of the dissolved zinc oxide tetrapods. At high magnifications (**Figure 3.1 E**), even the typical wrinkled surface features replicated from the tetrapod legs become visible.[142] These results indicate a successful integration of a microchannel network into the hydrogels by the sacrificial template-based method. Due to potential differences in channel diameters of the hydrated hydrogels in comparison to the dried samples, a quantitative analysis of microchannel sizes was not possible. However, the interconnectivity and morphology of these channels in the swollen hydrogel state have been investigated by a former colleague of the group using X-ray microtomography and show high interconnectivity.[89]

3.1.4 Temperature-Induced Shrinking and Swelling Characteristics

The response of the various bulk and channel PNIPAM hydrogel samples to temperature changes was investigated in swell tests above and below the LCST of 32 °C. Each sample was exposed to water at 42 °C for 10 minutes, while the sample weight was recorded for each minute by taking out the sample, removing excess water with a prewetted tissue and weighing the sample on an analytical balance (Kern, $d = 0.1$ mg). Subsequently, the experiment was continued in the same manner in water at 22 °C.

As a hypothesis, the microengineered channel PNIPAM was expected to exhibit enhanced shrinking and swelling characteristics compared to the conventional bulk material. **Figure 3.2** summarizes each material's response to temperature change. In **Figure 3.2 A** individual sample weights are normalized to the initial equilibrated weight at 22 °C and depicted as a function of time and temperature. During the first 10 minutes of exposure to 42 °C all hydrogel samples decrease in weight, whereas subsequent exposure to water at 22 °C causes a weight increase for all samples in the final 10 minutes. The greatest weight change always occurs during the first minutes of exposure. This weight change is attributed to a change of water content in the hydrogels during the thermoresponsive dehydration above the PNIPAM LCST of 32 °C and the swelling below the LCST, as explained in **Chapter 2.2.2**. The change in water content, in turn, is directly related to a volume change as depicted in **Figure 3.2 B**, where a comparison between sample weight and sample volume is depicted. The volume has been calculated from the measured diameter and height of the sample, assuming a cylindrical sample shape.

A significant difference between bulk and channel PNIPAM samples can be observed regarding the weight loss at 42 °C. After 10 minutes exposure, the weight loss of bulk PNIPAM (medium) is 12 % compared to 90 % for channel PNIPAM (medium). The high weight loss of the microengineered hydrogels can be attributed to the hollow microchannel network, which provides interconnected pathways for the water release from the hydrogel matrix. This assumption is supported by the fact that higher channel densities result in faster material shrinkage, as illustrated in **Figure 3.2 C**. In addition, the crosslink density impacts the temperature response of both bulk and microengineered PNIPAM. A clear trend of increased shrinkage for low crosslink concentrations is observed in **Figure 3.2 A**, whereas high crosslink concentrations result in lower shrinkage. This behavior was also observed in other studies and can be explained by the reduced gel hydrophilicity arising from higher crosslinker content and the denser polymer network, as compared to lower crosslink concentrations.[143]

Further, the rate that the gel swells is, in general, slower than the rate the gel shrinks, and the initial sample weight could not be restored after 10 minutes. However, recording the hydration of the shrunken samples over a longer period of time shows complete reswelling, as depicted in **Figure 3.2 D**. The different time scales for shrinking and swelling of the hydrogels and the associated hysteretic behavior are attributed to hydrogen bond formation between side groups of the PNIPAM chains after network collapse above the LCST and subsequent delay in chain dissociation upon reswelling below the LCST.[144]

The experimental results prove that the microengineering approach of incorporating a microchannel network into PNIPAM hydrogels significantly enhances the material's temperature response. In contrast to other methods, which use chemical modifications of the polymer composition to increase the temperature response, this strategy solely alters the hydrogel microstructure without changing chemical properties of the material. Zhang *et al.* have prepared semi-interpenetrating polymer networks of poly(vinyl alcohol) (PVA) and PNIPAM and observed similar shrinkage enhancements of 95 % water retention due to the increased hydrophilicity of PVA. In addition, they observed a comparable retardation upon reswelling. However, compositions of 50/50 w/w of PVA and NIPAM were necessary to achieve this result.[145] The microengineering approach used in this work yielded hydrogels that shrink by 90 %, which is a 7.5-fold increase compared to the bulk material, by only replacing 5 % of bulk sample volume with microchannels. This enhanced actuation during shrinkage makes the channel PNIPAM hydrogels interesting material candidates for soft actuators, where large deformations in short times are desired. A limitation remains the slow swelling speed, which compromises fast actuation and needs further improvements. Presumably, the microchannel network collapses during hydrogel dehydration above the LCST and thus cannot provide an efficient inflow of water during swelling below the LCST, until the channels are slowly restored. It is reported that filler-stabilized pores can be incorporated into nanocomposite PNIPAM

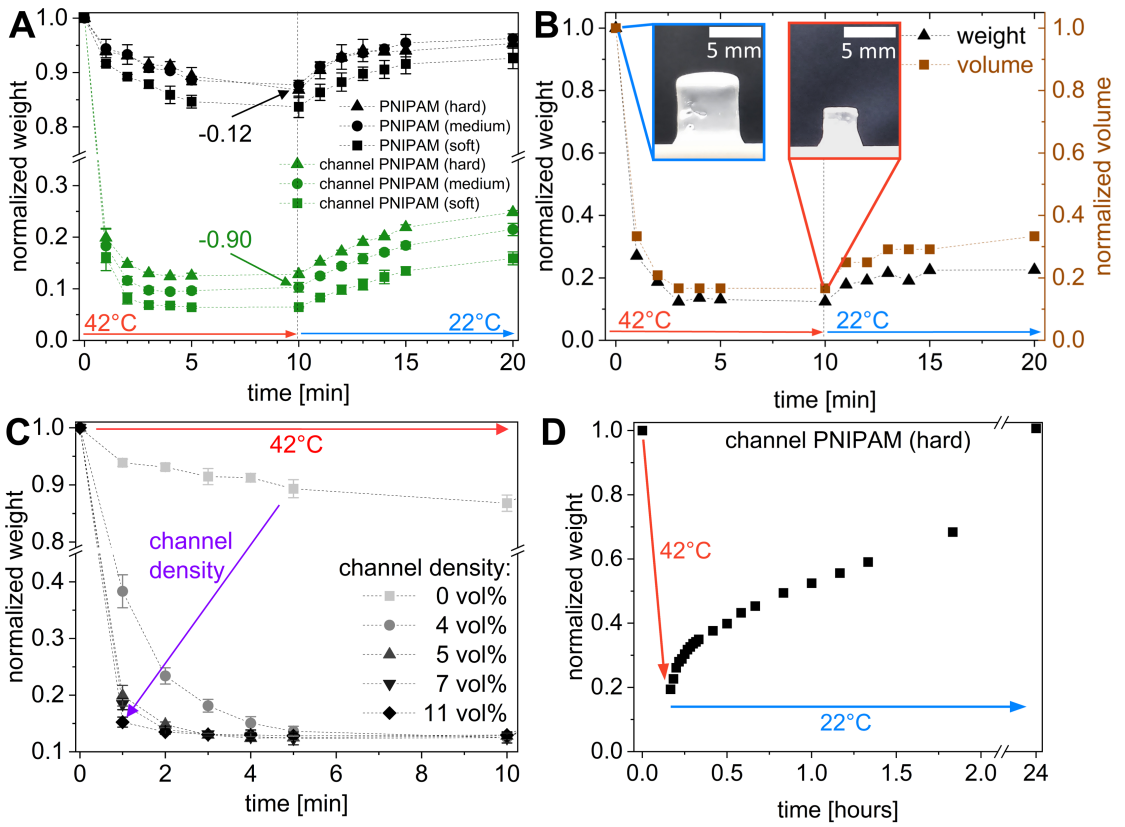

Figure 3.2: Response characteristics of thermally induced shrinking and swelling of both bulk and channel PNIPAM are depicted. Dotted lines serve as a guidance for the eye. (A) Normalized weights (with respect to the initial, equilibrated sample weight at 22 °C) are presented as a function of temperature and time. A significant increase in weight loss and weight reduction speed is observed for the microchannel-containing hydrogels, as compared to the bulk material. Variations in crosslinker concentration induce slight changes in the material's shrinking behavior, where lowly crosslinked gels exhibit higher weight losses as compared to highly crosslinked gels. $N = 3$. (B) Normalized weight and normalized volume of a channel PNIPAM sample are depicted as function of temperature and time. The data shows that both quantities are in consent, and verifies weight measurements as a representative indicator for (volume) shrinkage. Inset images show the measured sample in swollen and shrunken state, respectively. (C) Normalized weights of bulk (0 vol% channels) and channel PNIPAM (4 - 11 vol%) are presented as a function of time during sample exposure to 42 °C. An increase in channel density results in increased shrinkage and shrinking speed. $N = 3$. (D) Reswelling of an initially shrunken channel PNIPAM sample is represented by the plotted normalized sample weight as a function of time. The swelling speed is highest in the first minutes of exposure to 22 °C and decreases as time passes. The initial sample weight is restored withing 24 hours. Reprinted with permission.[140] Copyright 2021, Wiley-VCH GmbH.

hydrogels to mitigate faster reswelling after pore collapse during dehydration.[146] This approach might overcome the previously mentioned limitations.

In addition to a high stimuli response, repeatability is another important property of actuators, which are required to perform in many actuation cycles and with low fatigue. Therefore, the microengineered PNIPAM hydrogel was tested for cyclic shrinking and reswelling. In each cycle, the sample weight was determined after equilibration for 24 hours in water at 22 °C. Subsequently, the material was dehydrated in water at 42 °C for 10 minutes and weighed again. This procedure was repeated for a total of 10 cycles. The results are displayed in **Figure 3.3**, where the normalized sample weight is plotted as a function of temperature and cycle number. For 42 °C the sample weights are about 20 % of the initial weight and show very little deviation, which indicates good repeatability and high reproducibility of thermoresponsive shrinkage. Deviations in the restored initial weights at 22 °C are visible and may be caused by slightly varying temperatures in the lab for each cycle. However, on average, the initial weights were restored within 10 cycles, and there is no significant tendency of fatigue, highlighting the material's potential for repeated actuations.

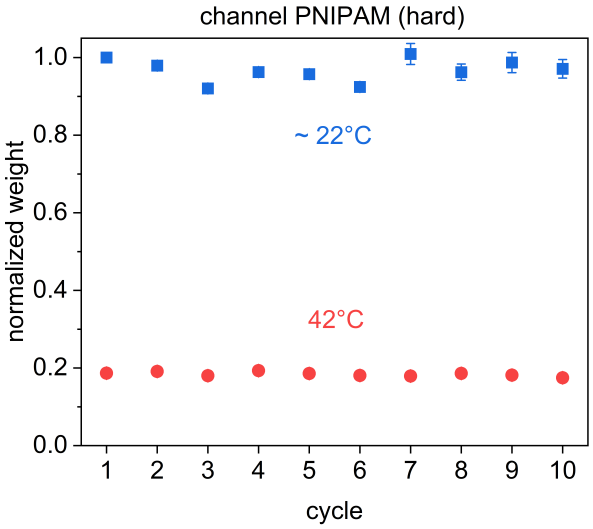

Figure 3.3: Thermally induced shrinking and swelling of channel PNIPAM is depicted for 10 consecutive cycles by means of normalized sample weight. In the shrunken state at 42 °C, small deviations within different cycles indicate a good reproducibility of actuation. In the rehydrated state at 22 °C the deviations of sample weight within the cycles are larger, which is probably due to changing temperatures in the lab at different days. However, the average restored sample weights remain constant over 10 cycles and there is no observation of fatigue within the limits of the experiment. Presented data points are average values of a total of three samples and standard deviations are represented by error bars.

3.1.5 Swelling Ratios of Bulk and Microengineered PNIPAM Hydrogels

The overall capacity of water uptake in a hydrogel can be determined by the swelling ratio SR, which is a unitless number that indicates for a certain temperature how much water is stored in the polymer matrix relative to its dry weight. For hydrogels this number usually is $\gg 1$, which means that the material can store water up to multiples of its dry weight.[147] To compare swelling ratios of bulk and microengineered PNIPAM hydrogels, all samples were placed in water at a certain temperature for 24 hours to reach equilibrium and weighed afterwards on an analytical balance (Kern, $d = 0.1$ mg) after removing excess water with a prewetted tissue. The swelling ratios were calculated according to **Equation 3.2**, where w_{wet} and w_{dry} denote the hydrated sample weight and the dry polymer weight, and are depicted in **Figure 3.4**.

$$SR = \frac{w_{wet} - w_{dry}}{w_{dry}} \tag{3.2}$$

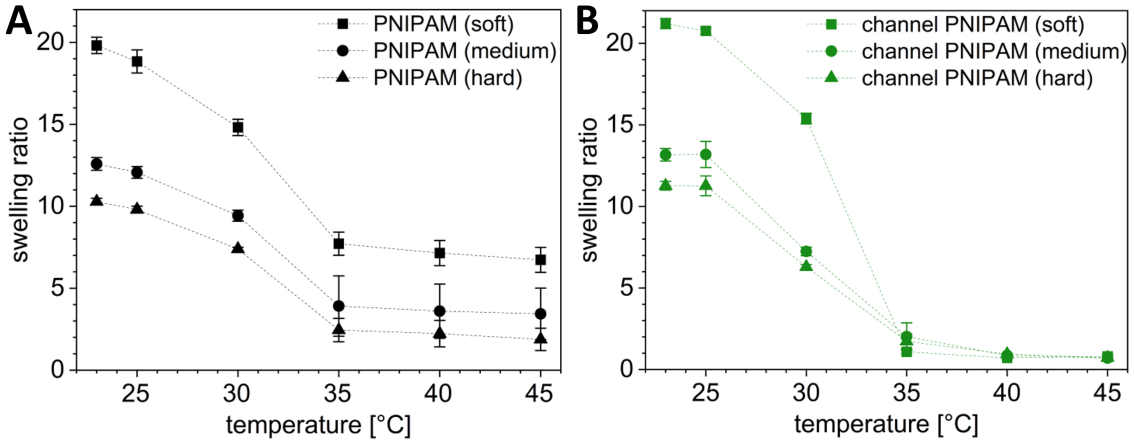

Figure 3.4: Swelling ratios of bulk (A) and channel PNIPAM (B) are presented as a function of temperature and varying crosslinker concentration. All swelling ratios decrease with increasing temperature, where the highest decay is around the LCST of 32 °C for both materials. Channel PNIPAM has slightly higher swelling ratios below 32 °C and lower swelling ratios above 32 °C, as compared to bulk PNIPAM. This indicates a higher overall shrinkage for the microengineered material during thermal stimulation, especially in case of the soft PNIPAM. Both materials show a similar systematic trend of decreasing swelling ratios with increasing crosslinker concentration. $N = 3$. Reprinted with permission.[140] Copyright 2021, Wiley-VCH GmbH.

All swelling ratios decrease with increasing temperature for both bulk and microengineered hydrogels and the highest decay is around the LCST of 32 °C. The reduced water content for higher temperatures is explained by a change of the material's hydrophilic interactions with water molecules below the LCST to hydrophobic interactions above the LCST. When comparing the different materials, slightly higher swelling ratios are observed for the microengineered PNIPAM hydrogels below the LCST, whereas the bulk PNIPAM hydrogel has higher swelling ratios above the LCST. It is assumed that below 32 °C the microchannels are filled with water, resulting in higher swelling ratios compared to the bulk material and that above 32 °C the water release from bulk PNIPAM is restricted due to the absence of microchannels. Other studies have reported that PNIPAM hydrogels form a dense skin layer upon dehydration above the LCST, which limits water release.[130] This effect is mitigated by the microchannel network, which promotes the outflow of water from the microengineered hydrogels, resulting in comparatively low swelling ratios above 32 °C. Both materials show a similar systematic trend of decreasing swelling ratios with increasing crosslinker concentration, which was also observed in the shrinking and swelling experiment discussed in **Section 3.1.4**. High crosslinker concentrations yield hydrogels with smaller pores in the polymer matrix and shorter PNIPAM chains between crosslinks, which in turn have a fewer number of free hydratable NIPAM side chains, as compared to longer chains and larger pores in the case of a low crosslinker concentration.[143] Therefore, lower crosslink concentrations will result in higher swelling ratios. The highest swelling ratio of 21.2 was recorded for the channel PNIPAM soft at 23 °C, which means that the material can store 21.2 times the weight of water compared to the polymer weight. In addition, the same material also exhibits the lowest swelling ratio of 0.8 at 45 °C, which indicates that this hydrogel undergoes the largest volume change during dehydration from 23 °C to 45 °C, thus makes it an interesting candidate for soft actuator applications. The results depicted in **Figure 3.4** are in agreement with other work done by Depa *et al.*, who investigated the swelling ratios of nanocomposite PNIPAM hydrogels.[146]

Concluding the discussed experimental results, the microengineered PNIPAM hydrogels exhibit comparatively high changes in swelling ratio below and above the LCST, which corresponds to distinct volume changes desirable for the design of actuators in soft robotics. In particular, the soft PNIPAM hydrogel displayed the highest change in swelling ratios above and below the LCST as a result of the microchannel network.

3.1.6 Mechanical Material Properties

In addition to the shrinking and swelling characteristics, the mechanical material properties also play an important role for soft actuators applications, since large deformations and high cycle times are required for efficient, long-lasting actuators. Hence, cyclic compression tests were performed using a universal test machine (2.5

kN Zwicki, Zwick/Roell, Ulm) to determine the material's elastic compressive modulus and reversibility of deformation. The machine was set up with a 5 N load cell and a home made cylindrical steel stamp of 15 mm diameter. Prior to testing, the sample dimensions were measured with a caliper ($d = 0.01$ mm). Each sample was compressed to a maximum strain of 10 % and relaxed to an initial load of 10 mN in 10 consecutive cycles at a constant speed of 5 mm s^{-1}. To prevent the hydrogels from drying out, the experiment was performed in a beaker of water, as depicted in **Figure 3.7 A**. The recorded force-displacement curves were calculated into stress-strain curves by using **Equation 3.3** and **3.4** for the engineering stress and strain, respectively, and are depicted in **Figure 3.5 A** and **B**. Here, σ and ϵ denote stress and strain, F the force, A_0 and L_0 the initial sample cross-section area and length and ΔL the change in sample length during the measurement.

$$\sigma_{eng} = \frac{F}{A_0} \tag{3.3}$$

$$\epsilon_{eng} = \frac{\Delta L}{L_0} \tag{3.4}$$

A slight hysteresis can be observed for all material compositions, indicating that the unloading curves differ from the loading curves. This is explained by the viscoelastic nature of the hydrogels.[148] Furthermore, the initial loading curve of each sample differs significantly from the consecutive cycles and a small drift towards lower stress values can be noticed within the 10 cycles. It is assumed that during the compression small amounts of water are squeezed out of the hydrogels reaching an equilibrium after several cycles, which can explain both effects and is most distinct in the first cycle. A clear tendency of decreasing compressive stress is observed for decreasing crosslinker concentrations for both bulk and microengineered PNIPAM hydrogels. To compare the two materials quantitatively, the elastic compressive modulus E of each sample composition was calculated from the slope of each loading curve according to **Equation 3.5**, by a linear fit up to 5 % strain.

$$E = \frac{\sigma(\epsilon)}{\epsilon} \tag{3.5}$$

In **Figure 3.5 C**, these values are depicted for microchannel-containing PNIPAM as a function of cycle number. Neglecting the initial cycle, the compressive elastic modulus remains constant over the residual consecutive cycles, and the average values of cycle 2 to 10 were calculated for each sample composition and shown in **Figure 3.5 D**. It can be observed that for higher crosslinker concentrations the elastic compressive modulus increases from 12.6 kPa for channel PNIPAM soft to 38.1 kPa for channel PNIPAM hard. This is due to a more rigid and denser polymer network as compared to the fewer crosslinks in the soft materials as well as less water in the hard materials, due to the lower hydrophilicity of the crosslinker. However, bulk and microengineered PNIPAM hydrogels exhibit no significant differences regarding the

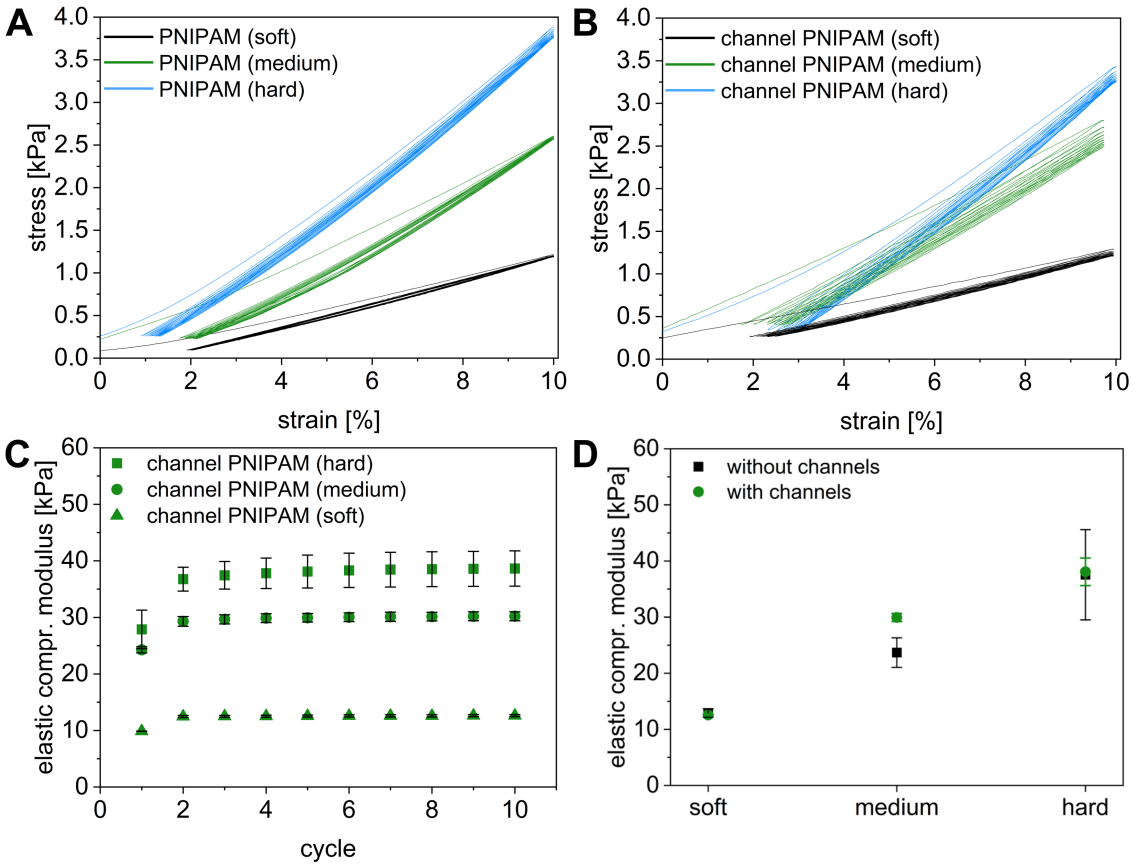

Figure 3.5: Mechanical material properties, including stress-strain curves and elastic modulus are summarized for bulk and channel PNIPAM hydrogels. Representative stress-strain curves up to 10 % compression in ten consecutive cycles are depicted for three different crosslinker concentrations, for bulk (A) and channel PNIPAM (B). Both materials exhibit similar stress-strain-behavior, including a slight hysteresis, which is due to the viscoelastic nature of the hydrogels. A decrease in compressive stress is observed for decreasing crosslinker concentrations. (C) Elastic compressive modulus values of channel PNIPAM as a function of consecutive cycle number are plotted. Neglecting the initial cycle, the elastic modulus remains constant over the residual cycles, which indicates a reproducible deformation. Higher crosslink concentrations result in a higher elastic modulus as compared to lower crosslink concentrations. (D) Comparing bulk and channel PNIPAM, no significant differences in elastic modulus, with respect to the various crosslinker concentrations, are observed. This observation indicates, that the microchannels do not affect the mechanical properties of the hydrogel much. $N = 3$. Reprinted with permission.[140] Copyright 2021, Wiley-VCH GmbH.

compressive elastic modulus and stress-strain-correlation, which indicates that the microchannels do not affect the mechanical properties of the material much. This result is remarkable, since other studies have observed a reduction in mechanical stiffness of porous polymeric materials compared to the bulk materials.[149] The comparably low porosity of 5 vol% microchannels in the microengineered hydrogel as well as the incompressibility of water in the channels are considered the primary reasons for the unchanged mechanical stiffness. The determined range of elastic compressive modulus is in agreement with the work of Haq *et al.*, who found values between 4 kPa and 81 kPa upon reviewing the mechanical properties of native PNIPAM hydrogels.[70]

Further experiments of repeated deformation were carried out over 100 cycles of compression to investigate the fatigue behavior of the microengineered PNIPAM. Here, the same experimental parameters as described above were used. The corresponding stress-strain curve in **Figure 3.6 A** displays reproducible deformation after the drift reaches equilibrium within a few cycles. The calculated elastic compressive modulus is plotted as a function of cycle number in **Figure 3.6 B**. A constant value of about 31.7 ± 0.2 kPa can be determined, neglecting the variations in the first few cycles, which indicates no significant fatigue within the limits of the experiment. This further highlights the suitability of microengineered PNIPAM hydrogel in designing soft actuators with long lasting performance.

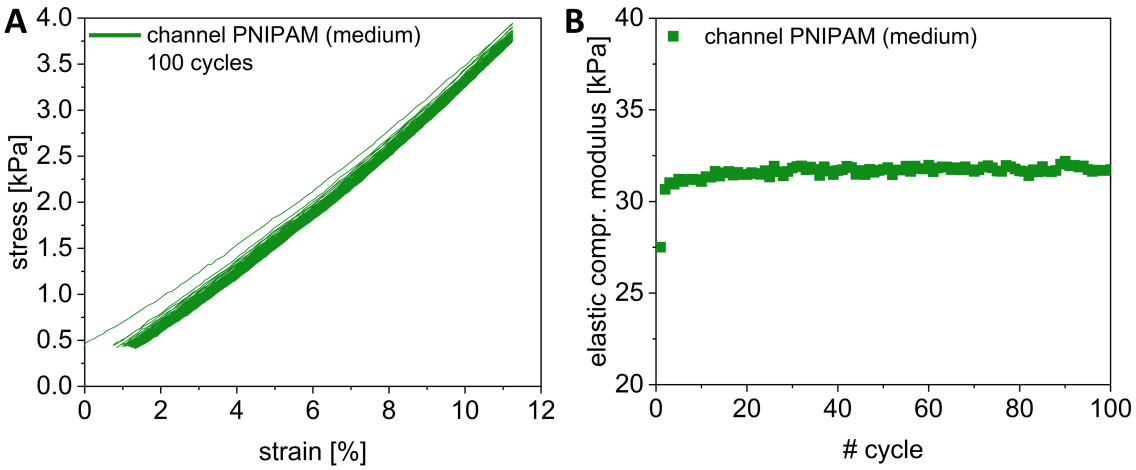

Figure 3.6: Repeated compressive deformation of a channel PNIPAM sample is presented for 100 cycles. (A) After an initial drift, the stress-strain curves approach a steady state within a few cycles, indicating a reproducible cyclic deformation of the microengineered hydrogel. (B) Elastic compressive modulus values are plotted as a function of corresponding deformation cycle. The values remain constant after a few initial cycles, and no significant fatigue is observed within the limits of the experiment, highlighting the material's capability for soft actuation.

3.1.7 Stroke Forces and Application in an Actuation Setup

Another important characteristic of a stimuli-responsive hydrogel in a soft actuator is the ability to generate a stroke force upon swelling, similar to how a piston is moved in a cylinder of a combustion motor by expanding gas. Hence, the compression test procedure was slightly modified to measure the forces exerted by bulk and microengineered hydrogels during swelling. First, the samples were shrunken in water at 42 °C for 10 minutes before they were clamped between the bottom of a glass beaker and the steel stamp with an initial load of 10 mN. Subsequently, the beaker was filled with water at 22 °C and, while the stamp kept its position, the force was recorded as a function of time during hydrogel swelling. The procedure and results are depicted in **Figure 3.7**.

For all sample compositions, an increasing force is generated over time due to the volume increase during swelling. In the first minutes, the force increase is highest and gradually approaches a saturation. However, the channel-containing samples exert significantly higher stroke forces as compared to the bulk material. While after 60 minutes bulk PNIPAM only reaches a negligible maximum force of about 15 mN, PNIPAM containing 4 vol% of microchannels reaches the highest recorded stroke force of 125 mN. This is explained by the enhanced shrinking and swelling characteristics of the microengineered hydrogels compared to the bulk material, as discussed in **Section 3.1.4**. Interestingly, the stroke forces decrease with increasing microchannel density, which is believed to result from a lower resistance to compressive pressure for increased porosities.[150] From this experiment, it can be concluded that integration of only 4 vol% microchannels into PNIPAM hydrogels can increase the stroke force upon swelling by a factor of 8.3, which promises superior performance in an actuation setup compared to conventional bulk PNIPAM hydrogels. To illustrate this capability, a temperature-controlled gripper was developed and tested. Microengineered PNIPAM containing 5 vol% of microchannels, in combination with the highest crosslinker concentration used in this study, was chosen as actuating material due to an optimum trade-off between high stroke forces and mechanical stability, and compared with bulk PNIPAM for reference. The gripper consists of two fingers, which were fabricated from poly(lactic acid) (PLA) using an extrusion based 3D printer (Pro2, Raise 3D, California, USA). The gripper fingers are connected via a freely moving joint and the cylindrical shaped hydrogels were glued to the gripper using two component epoxy resin (UHU Endfest). Upon cyclic exposure to temperatures above and below 32 °C, the hydrogels respond by contraction and expansion and actuate the gripper to close or open, respectively. All experiments were performed in water at 22 °C or 42 °C, and a small piece of sponge was used to be squeezed by the gripper.

The results are summarized in **Figure 3.8**. Due to the comparably small shrinkage and the low stroke forces exerted by bulk PNIPAM, closing the gripper could not be achieved, while the microengineered hydrogel induced a significant contraction and even managed to squeeze the sponge. Repeatable actuation of the gripper

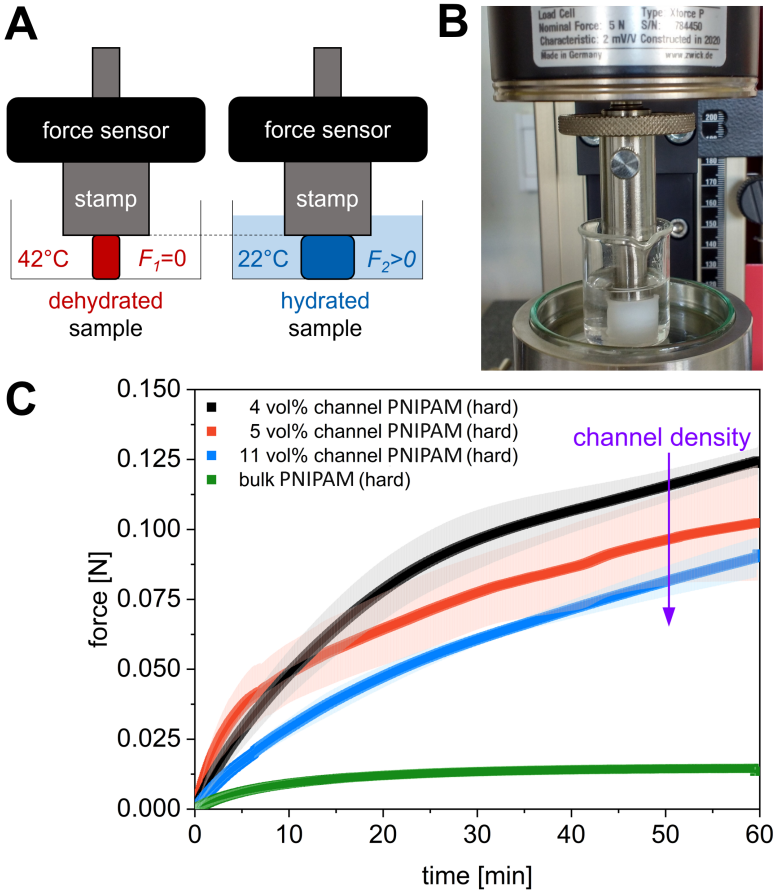

Figure 3.7: The capability of generating stroke forces upon swelling is depicted for bulk and channel PNIPAM hydrogels. A schematic representation (A) and a photograph (B) of the experimental setup are illustrated. (C) Generated stroke forces, resulting from the swelling of hydrogel samples between force sensor and substrate, are plotted as a function of time. Bulk PNIPAM displays comparably low stroke forces, as compared to channel PNIPAM, which generates multiple times higher forces upon swelling. For the range of channel densities tested, a decrease in stroke force generation is observed with increasing channel density. Force curves are averaged from three tested identical samples per material composition and light-colored areas represent error bar ranges. Reprinted with permission.[140] Copyright 2021, Wiley-VCH GmbH.

was demonstrated for 10 cycles without observation of any impairment of the gripper function, which highlights the reversible actuation capabilities of the hydrogel. A limitation remains the slow swelling of the PNIPAM and opening of the gripper, which takes several hours compared to only a few minutes for shrinking and closing. Still, it can be anticipated that such actuators are useful for infrequent

actuations, such as in sensing and monitoring[151][152], or in situations where autonomous recognition of environmental changes is required, such as the warming of an aqueous surrounding.

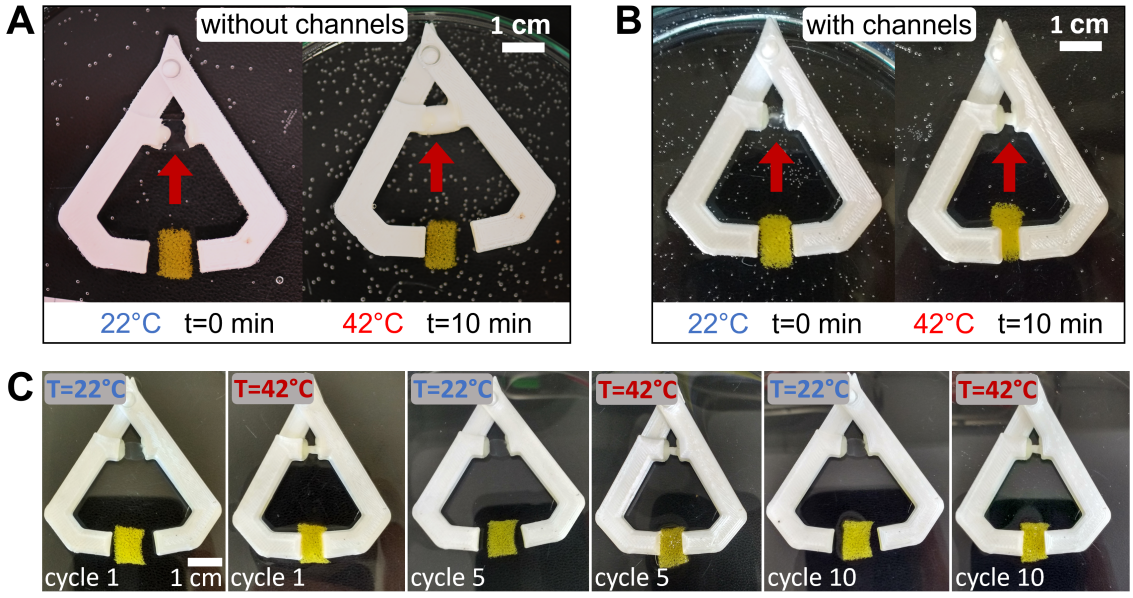

Figure 3.8: Images of a thermally controlled soft gripper are presented, demonstrating the PNIPAM hydrogel's performance in an actuation setup. The location of the actuating hydrogels is indicated by red arrows. (A) Due to its comparatively low shrinkage, bulk PNIPAM is not capable of significantly closing the gripper. (B) In contrast, the microengineered channel PNIPAM causes a closure of the gripper upon thermal stimulation, and a piece of sponge is squeezed eventually. (C) Extracts of a series of ten consecutive actuation cycles of the soft gripper, driven by channel PNIPAM, are illustrated. Reprinted with permission.[140] Copyright 2021, Wiley-VCH GmbH.

3.1.8 PNIPAM Bilayer Soft Robots

While in the previous section actuation resulted from an isotropic deformation of the cylindrical shaped hydrogel, more complex motions, such as hydrogel bending, can be achieved by anisotropic material shrinkage and swelling. Here, the concept of bilayer actuators was exploited, which is based on combining two layers of hydrogels that shrink and swell to a different degree.[153] Upon stimulation, the bilayer structure eventually bends into the direction of the layer with higher shrinkage. By applying this concept, two thermoresponsive soft robots were fabricated, as illustrated in **Figure 3.9**. First, a mold made of PTFE was half filled with PNIPAM hard hydrogel precursor according to the composition listed in **Table 3.1**. After polymerization, a second layer of PNIPAM soft precursor was cast and polymerized onto the first layer by filling the mold completely. Both layers covalently attached to each other, and the bilayer structure could be removed from the mold and washed with deionized water to remove unreacted molecules.

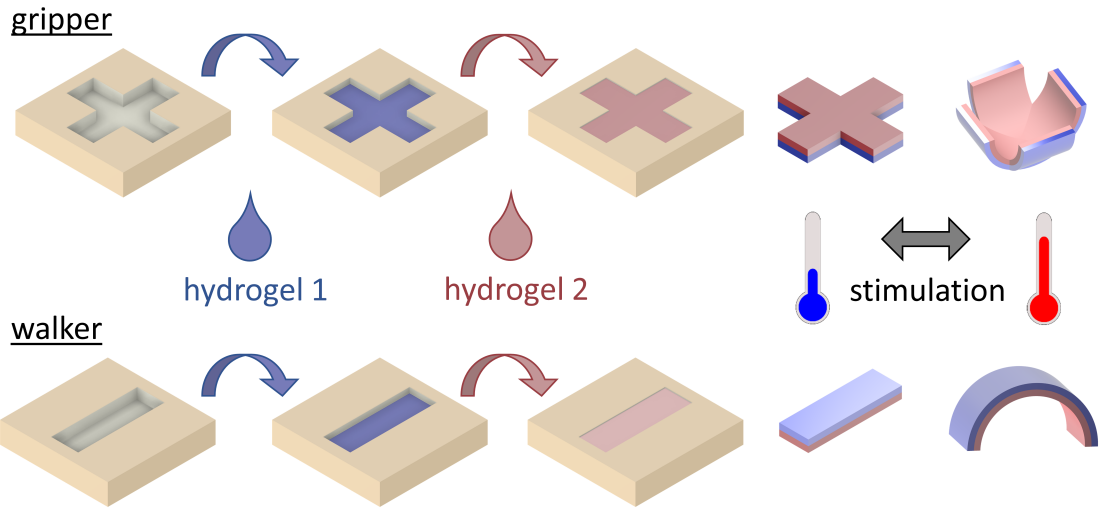

Figure 3.9: Fabrication of soft actuators based on PNIPAM hydrogel bilayers is illustrated schematically. Two hydrogel precursor solutions with different crosslinker concentrations are sequentially filled and polymerized in molds. Depending on the mold geometry, the final hydrogel bilayer performs gripping or crawling functions upon cyclic thermal stimulation.

The performance of the soft gripper was tested by placing it with the soft PNIPAM layer facing upwards into a beaker filled with water. The temperature was controlled by a Peltier-element and a magnetic ball stirrer was placed into the center of the gripper as a test cargo to be captured. A series of pictures was taken with a camera during the actuation cycle and is illustrated in **Figure 3.10**. After 15 minutes of heating, the gripper closes and captures the ball stirrer, which could be lifted without detaching from the gripper. Subsequently, the cargo was released

after 25 minutes of cooling. The anisotropic shape morphing allows for the design of actuators that purely consist of hydrogel in contrast to the previously presented gripper, where the isotropic responsive hydrogel actuated a rigid gripper. For sensitive cargo, such as living organisms, this is especially relevant due to the risk of harming the cargo. Sinatra *et al.* have developed a soft gripper made of a silicone matrix, which is actuated pneumatically, and demonstrated catching and releasing a living jellyfish.[154] However, the pressurized control of this gripper requires attachment to cables and a pump for controlling the flow of air in and out of the system. This attachment restricts the grippers mobility. In contrast, the soft PNIPAM gripper presented in this work can be controlled remotely and even autonomously, when powered by environmental temperature changes. Concepts of introducing light as a stimulus for PNIPAM hydrogels have been employed by several researchers and could further increase the functionality of such PNIPAM grippers.[155] [156]

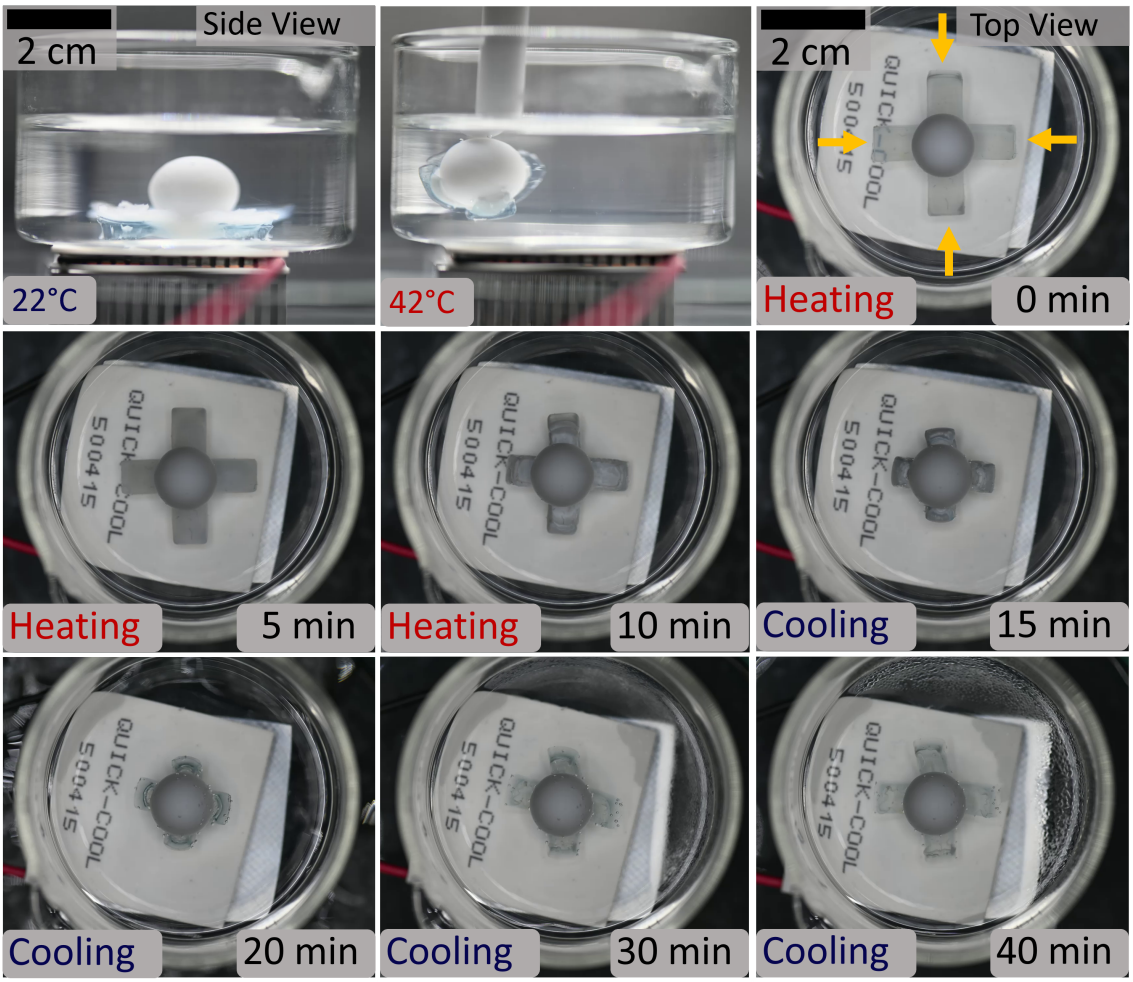

Figure 3.10: A series of sequential images, displaying the performance of a PNIPAM bilayer soft gripper, is depicted. During heating, the gripper closes and captures a PTFE stirring ball, which gets released again after cooling.

Performance of the soft walker was demonstrated by cyclic heating and cooling of the hydrogel bilayer inside a home-built reservoir with a sawtooth shaped aluminum bottom to transfer heat from the Peltier-element into the reservoir and to allow for directional movement of the walker. **Figure 3.11** summarizes the results in a series of pictures taken during actuation.

Upon heating, the less crosslinked PNIPAM bottom layer shrinks more compared to the top PNIPAM layer with higher crosslink concentration, causing the bilayer hydrogel to bend. Upon cooling, the hydrogel layers swell to the initial shape and the walker straightens. Friction between the hydrogel and the aluminum base is different at the front and back end of the hydrogel structure due to the sawtooth patterned surface. This results in unidirectional movement of the soft walker upon cyclic heating and cooling. However, the movement speed of about 50 minutes for a single step

is comparatively low and needs improvement for practical use. Here, microstructural modifications of the material as well as miniaturization of the walker dimensions are believed to increase walking speed. Lee *et al.* exhibited significantly enhanced light-induced volume shrinkage and rapid recovery of comb-type PNIPAM hydrogels and photo-thermal magnetite nanoparticles, where a single step took about 2 minutes.[157] Here, several chemical reaction steps were required, including synthesis of PNIPAM macromonomers, subsequent functionalization to yield vinyl end groups, and crosslinking of the functionalized macromonomers in the presence of magnetite nanoparticles into a composite, graft PNIPAM hydrogel. In contrast to the facile preparation explained in this thesis, the graft PNIPAM hydrogel matrix contains a certain fraction of free mobile chains that promote conformational change upon thermally induced phase transition.

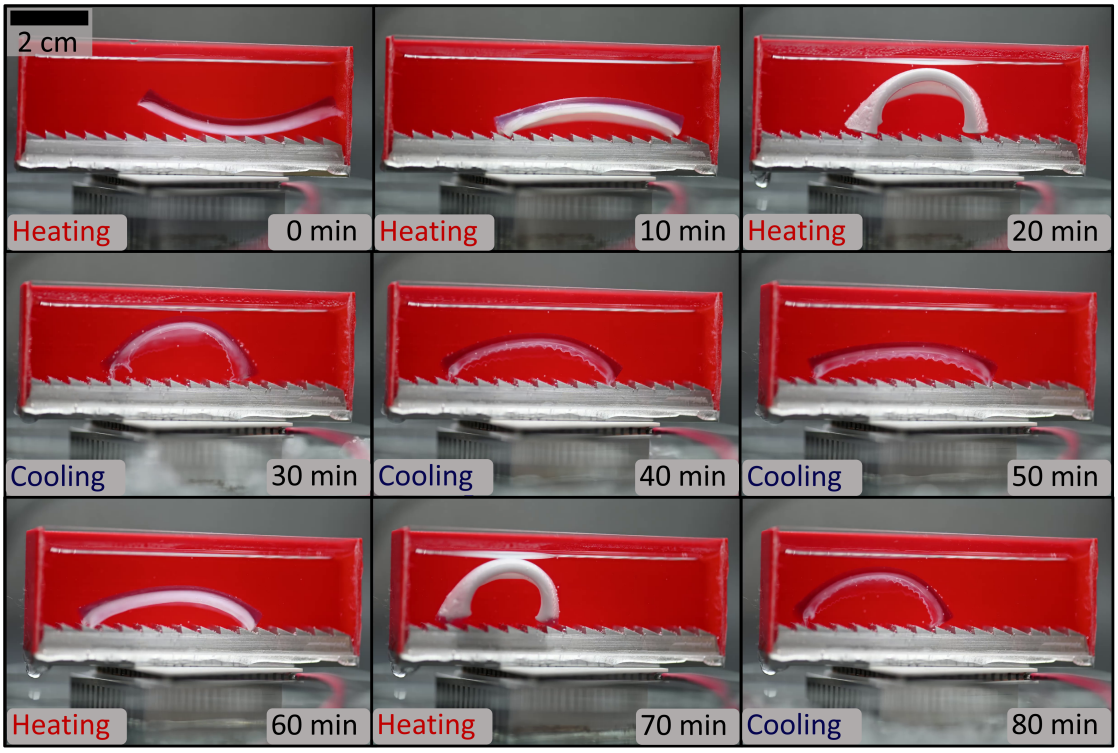

Figure 3.11: A series of sequential images, displaying the performance of a PNIPAM bilayer soft walker, is depicted. During heating, the walker curves and contracts, while upon cooling, it straightens out to its initial shape. A sawtooth shaped subsurface allows for a step-wise directional movement of the walker.

3.1.9 Conclusion and Perspective

In this chapter, a novel microengineering approach was introduced for the fabrication of highly responsive macroscopic PNIPAM hydrogels. Furthermore, a systematic characterization and comparison with conventional bulk PNIPAM hydrogels regarding microstructural morphology, thermoresponsive shrinking and swelling kinetics, mechanical material properties, and implementation into a soft robotic actuation setup was carried out. The microengineered material exhibits superior qualities over the bulk hydrogels, such as a highly increased response to temperature, higher stroke forces and the capability of untethered autonomous actuation controlled by temperature. The facile sample preparation allows for adjusting responsivity by controlling the microchannel density as well as tailoring mechanical properties by regulating the amount of crosslinker during polymerization. Despite this flexibility, the method is purely based on the removal of minor amounts of material rather than chemical modification of the polymer matrix, which is a common approach to achieve similar actuation enhancements.[145] In general, this method can also be applied to other hydrogels as well as for the fabrication of composites by infiltrating the zinc oxide templates with nanoparticles before casting the hydrogel solution.[89]

Taken together, the strategy described in this chapter provides a method for developing macroscopic thermoresponsive soft actuators that can be implemented into a variety of robotic setups in aqueous environments, such as capturing marine objects or sensing and monitoring temperature. Current limitations include the miniaturization of these actuators and realization of complex geometries, due to the restricted sizes and shapes of the sacrificial zinc oxide templates. In general, the method can also be transferred to other sacrificial templates, such as electrospun materials to overcome miniaturization limits. Furthermore, the response times are in the range of several minutes for contraction and hours for the expansion of the actuators. Therefore, the material is not suitable for applications where high speeds are required. As a perspective, future improvements to microchannel stability could possibly avoid the collapse of the channel network during dehydration and thus speed up swelling and expansion of the hydrogel.

Based on the findings in this chapter, stating that structural features, such as microchannels, influence the water transport of hydrogels and thus their responsiveness, the following chapter deals more intensively with the investigation of actuation properties of PNIPAM microstructures.

3.2 Increasing the Efficiency of Thermoresponsive Actuation at the Microscale by Two-Photon Laser Printing of PNIPAM

Partial results of the presented work have been published in:

- **Spratte, T.**, Geiger, S., Colombo, F., Mishra, A., Taale, M., Hsu, L.-Y., Blasco, E., Selhuber-Unkel, C., Increasing the Efficiency of Thermoresponsive Actuation at the Microscale by Direct Laser Writing of PNIPAM. *Adv. Mater. Technol.* **2023**, 8, 2200714. https://doi.org/10.1002/admt.202200714

3.2.1 Introduction

In **Chapter 3.1** the thermally induced shrinkage of microchannel-containing PNIPAM hydrogels was found to be significantly higher and faster compared to bulk hydrogels. One potential explanation is that a high surface area as well as an interconnected network of pathways facilitates water release from the gel upon dehydration above the LCST.[140] Hence, a subsequent hypothesis arose, whether miniaturization of the actuators, and especially varying geometries and surface-to-volume ratios at the microscale, will exhibit similar changes in the shrinking and swelling dynamics. Here, I introduce a two-photon 3D laser printing approach to fabricate thermoresponsive PNIPAM microactuators with high resolution in the low micrometer range and characterize their actuation capabilities.

First, the fabrication process of the PNIPAM microactuators is described in detail (**Section 3.2.2**) and the printing accuracy for different micropillar geometries is analyzed by scanning electron microscopy (**Section 3.2.3**). Subsequently the thermoresponsive hydrogel properties are investigated thoroughly (**Section 3.2.4**) as a function of fabrication parameters and micropillar geometry as well as the material's surface stiffness (**Section 3.2.5**). Finally, the printed PNIPAM microactuators are implemented in a microfluidic application setup (**Section 3.2.6**).

While conventional fabrication methods such as soft lithography or template-assisted approaches often lack sufficient resolution in the low micrometer range as well as limitations to 2.5D geometries, direct laser writing can overcome these restrictions.[158] Specifically, two-photon laser printing enables the manufacturing of microstructures with complex 3D geometries at high resolution in the sub-micrometer range.[159] Furthermore, it is possible to print and combine several materials and to use different types of substrates.[160] Recently this fabrication method was used to develop 4D microstructures, which can be stimulated by temperature and light to change their shape over time.[24]

In the following chapters, I will demonstrate the use of 3D laser printing to tailor the actuation properties of PNIPAM microstructures and provide characterization methods to study the microactuator properties.

3.2.2 Fabrication of PNIPAM Hydrogel Microstructures via Two-Photon Laser Printing

All PNIPAM and PAM hydrogel microstructures were fabricated via two-photon polymerization (2PP) using a nanoscribe PPGT2 (Nanoscribe GmbH & Co. KG, Eggenstein-Leopoldshafen, Germany) two-photon 3D laser printer in a clean room (Class ISO 7) under yellow light conditions. First a hydrogel resin was prepared based on the work of M. Hippler *et al.*, which composition is listed in **Table 3.3**.[119] All chemicals were purchased from Sigma Aldrich (Taufkirchen, Germany) and used without further purification if not stated otherwise. Here, *N*-isopropylacrylamide (≥99 %) and AM (≥99 %) were used as monomers, *N*,*N*′-methylenebis(acrylamide) (>99 %) as a crosslinker, lithium phenyl(2,4,6-trimethylbenzoyl)phosphinate (LAP) (≥95 %) as photoinitiator, and acryloxyethyl thiocarbamoyl Rhodamine B (Polysciences) as a fluorescent dye. All components were weighed on an analytical balance (Kern, $d = 0.1$ mg) and were added into a glass vial covered with aluminum foil, to protect the resin from light. The solvent ethylene glycol (Sigma-Aldrich, ≥99 %) was added by pipetting and the vial was placed into a water bath at 45 °C for about 1 hour while being magnetically stirred at 500 rpm. After all components were dissolved and homogeneously mixed, the resin was passed through a syringe filter (0.2 µm) and transferred into an optically opaque 1.5 ml Eppendorf tube. The hydrogel resin was stored at room temperature and used for 3D printing within a maximum of two weeks of shelf time.

The PNIPAM microstructures were printed on silanized borosilicate glass coverslips (130-160 µm thickness) to facilitate adhesion. In a first step the substrates were cleaned in MilliQ water by sonication for 5 minutes before they were immersed in ethanol (99 %) and sonicated for another 5 minutes. Subsequently the coverslips were dried with a heat gun and functionalized by incubation in 3-(trimethoxysilyl)propyl methacrylate (15 mM in ethanol) overnight while shaking at 240 rpm. Afterwards the substrates were rinsed with MilliQ water and ethanol, dried with a heat gun and placed in an oven at 80 °C for 2 hours. After cooling, the functionalized coverslips were stored in a fridge and used for printing within a maximum of two weeks of shelf time.

3D models of the microstructures to be printed were generated via computer aided design (CAD) using the software *Autodesk Inventor 2019* (Autodesk Inc.) and imported as STL-files (Stereolithography) into the slicing software *Describe* (Nanoscribe GmbH & Co. KG) to prepare the print job. Printing was done in oil immersion configuration using a 25x, $NA = 0.8$ (Zeiss) objective and a near infrared ($\lambda = 780$ nm) femtosecond pulsed laser. If not stated otherwise all microstructures were printed at 100 % laser power (power scaling=1), corresponding to 50 mW power at the backfocal plane, slicing distance of 0.3 µm and hatching distance of 0.2 µm. The scanning speed varied between 10 and 50 mm s^{-1} to fabricate hydrogel microstructures with altering degrees of crosslinking. First a ring shaped PDMS

Material name	PNIPAM		PAM	
	m / mg	V / µl	m / mg	V / µl
NIPAM	400	-	-	-
AM	-	-	250	-
BIS	40	-	40	-
LAP	10	-	10	-
Rhodamine B	4	-	4	-
Ethylene glycol	-	450	-	450

Table 3.3: Compositions of PNIPAM and PAM hydrogel resins are listed. The resins are composed of monomers (NIPAM or AM), crosslinker (BIS), photoinitiator (LAP), fluorescent dye (Rhodamine B), and solvent (ethylene glycol).

spacer was placed into the center of a silanized coverslip and the reservoir was filled with 60 µl of PNIPAM resin. Subsequently the immersion oil was added to the backside of the substrate before it was mounted into the printer. The print jobs were run via the software *Nanowrite* (Nanoscribe GmbH & Co. KG). After printing, the samples were developed in 40 mL of deionized water for 10 minutes followed by 1 minute in a fresh beaker of water before they were stored at 22 °C in deionized water.

3.2.3 Micropillar Shape Analysis

For the various experiments, different micropillar geometries including normal cylinders, hollow cylinders, star-shaped pillars, and cubes were selected and 3D printed via two-photon polymerization. These geometries differ in their surface-to-volume ratios and have distinct surface features, which are assumed to have a major influence on the PNIPAM microactuator properties. To investigate the shape accuracy of the printing process, scanning electron microscope images of the samples were recorded. Since conventional high-vacuum electron imaging techniques require dry samples, the hydrogel microstructures needed to be treated accordingly before imaging. Here, critical point drying (CPD) was chosen, which is a commonly used preparation method in hydrogel drying.[161]

This method relies on gradually exchanging the water in the hydrogel with a solvent, such as ethanol, and subsequent removal of the solvent by evaporation at the critical point. Hereby, the surface tension during evaporation is minimized since the phase boundary of liquid and gas vanishes and the densities become equal in the supercritical state.[162] Thus the fragile micropillars maintain their shapes instead of collapsing due to surface tensions during drying. Finally, the gaseous solvent is exchanged by carbon dioxide gas to prevent condensation at atmospheric conditions,

and the dried samples can be used for sputtering. However, slight changes in the microstructure shapes as well as a certain degree of shrinkage can still occur, which might result in artifacts in the final recorded images.

In this experiment, the printed hydrogel micropillars were directly developed in ethanol (99 %) for ten minutes followed by immersion for one minute in fresh ethanol, to avoid swelling differences during the water-to-ethanol exchange. The samples were then kept in ethanol and treated by critical point drying using a commercial device (EM CPD300, Leica Microsystems). After drying, the samples were sputter coated (Leica EM ACE600, Leica Microsystems) immediately with a 11 nm layer of 80 % gold and 20 % palladium at a rate of 0.03 nm s^{-1}. Finally, scanning electron microscope images were recorded using a Zeiss Leo 1530 SEM at an accelerating voltage of 2 kV and a working distance of 5.2 mm.

For the PNIPAM micropillars displayed in **Figure 3.12** a significant shrinkage is observed, which is most noticeable at the base, where the hydrogel is attached to the glass substrate. In addition, the surface of the dried polymer contains holes of various sizes. Both phenomena might be related to the volume phase transition of the PNIPAM hydrogel induced during temperature changes in the drying process. For this reason, non-thermoresponsive PAM micropillars of identical geometry were fabricated in the same manner and imaged by SEM. These micropillars are believed to have a similar shape as the PNIPAM actuators, but are less affected from the temperature profile of the drying process. The images as well as the computer-designed models are displayed in **Figure 3.13**.

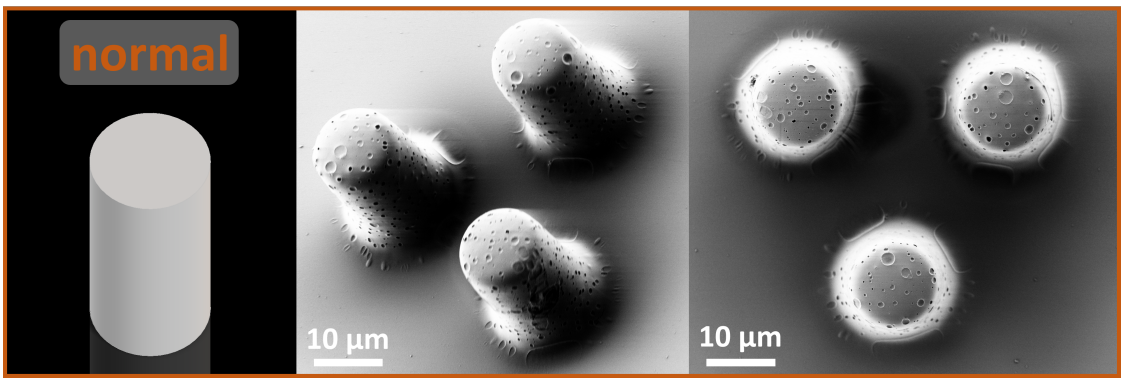

Figure 3.12: Scanning electron microscope images of 3D laser printed PNIPAM micropillars are displayed. The ideal micropillar geometry of a cylinder with aspect ratio 2:1 (height:diameter) is sketched (left). Images of the hydrogel micropillars were recorded in tilted (center) and top view (right). The micropillar surfaces display holes, which are believed to result from sample preparation during critical point drying.

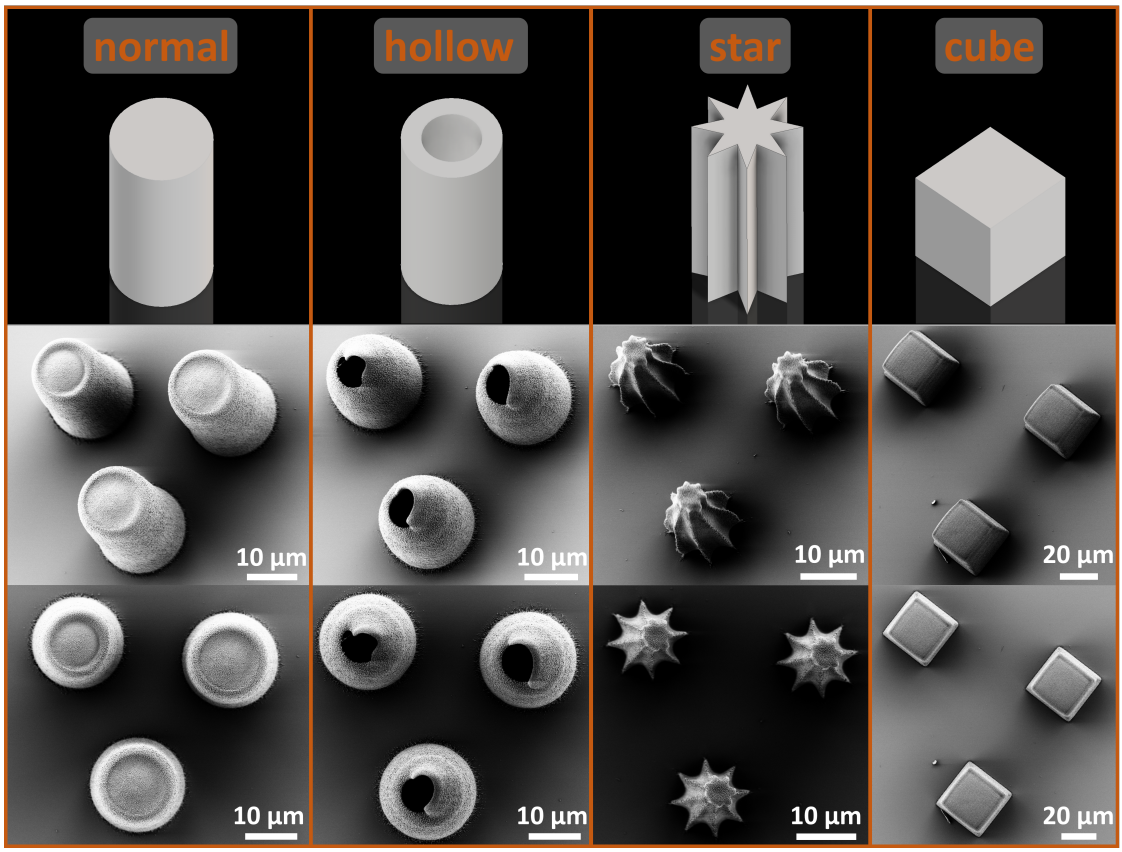

Figure 3.13: Scanning electron microscope images of 3D laser printed PAM micropillars are displayed. Ideal micropillar designs are sketched, including normal, hollow, and star-shaped cylinders, as well as cubes (top row). The recorded images of the hydrogel micropillars were recorded in tilted (center row) and top view (bottom row). While for the simple geometries (normal cylinders, cubes) the printed structures match the ideal design shape well, deviations are observed for more complex geometries (hollow and star-shaped cylinders).

For the cylindrical and cube shaped micropillars, a good conformity of the dried PAM samples and the computer models is observed, while the hollow cylinders and star-shaped pillars display some deviations from the models in the top region of the pillars. Nevertheless, the characteristic features such as a hollow interior and star-like lamellae are clearly visible and match the shape of the models well at the bottom of the pillars. As previously mentioned, these shape deviations might be induced by shrinkage from dehydration during critical point drying and seem to be more prevalent in delicate structures such as thin walls or lamellae. Presumably, shrinkage of the micropillars at the bottom is restricted by adhesion to the glass substrate and induces internal mechanical stresses, which gradually relax towards

the top of the pillars by shrinkage.

Overall, the recorded images confirm the feasibility of two-photon laser printing to fabricate hydrogel micropillars in the low micrometer range and with defined shapes of various surface-to-volume ratios.

3.2.4 Thermoresponsive Shrinking and Swelling Properties as a Function of Microarchitecture

To investigate the influence of surface-to-volume ratio of PNIPAM hydrogel microstructures on the shrinking and swelling dynamics, confocal 3D images of the various hydrogels were recorded at 22 °C and 45 °C and compared. The images were taken with a laser scanning fluorescent microscope (Nikon A1R, Nikon Imaging Center Heidelberg) using a Nikon Plan Fluor 40x objective ($NA = 1.3$) and a temperature-controlled chamber (Tokai Hit chamber). The coverslips were mounted to a home-built observation reservoir, which was filled with water to prevent drying of the hydrogels. First, all microstructures were imaged at room temperature (22 °C) by recording Z-stacks of 0.8 µm distance between each slice and excitation of the fluorescent dye by a 561 nm excitation laser. Subsequently the temperature-controlled chamber was heated to 45 °C and the samples were equilibrated for 15 minutes before further Z-stack images were recorded with the same settings as for 22 °C.

The recorded images were analyzed with *ImageJ*. To evaluate the hydrogel shrinkage both a 2D and a 3D comparison of the micropillar cross-sections and volumes, respectively, was done for both 22 °C and 45 °C. Initially an intensity threshold was chosen and applied to all raw images to yield binary images. Using the binary operations *Erode*, *Dilate*, *Open* and *Close* these images were processed for further analysis. For the 2D comparison slices in the center of each Z-stack were chosen for determining the micropillar cross-section areas and perimeters using the *measure particle* function. For the 3D comparison the *ImageJ* Plugin *3D objects counter* was used to determine the surface area and volumes of the Z-stacks. Finally, percent shrinkage of the micropillars was calculated according to **Equation 3.6** for the 2D comparison and **Equation 3.7** for the 3D comparison, where A and V refer to the cross-section areas and volumes of the microstructures for a given temperature.

$$Shrinkage_{2D} = (1 - \frac{A_{45°C}}{A_{22°C}}) \cdot 100\% \tag{3.6}$$

$$Shrinkage_{3D} = (1 - \frac{V_{45°C}}{V_{22°C}}) \cdot 100\% \tag{3.7}$$

The processed images as well as the calculated percent shrinkages are depicted in **Figure 3.14** and **Figure 3.15**, where **Figure 3.14 A** shows a comparison of the thermally induced shrinkage of cylindrical micropillars having different diameters, namely 50 µm, 20 µm, and 10 µm. In addition, micropillars with the same diameter

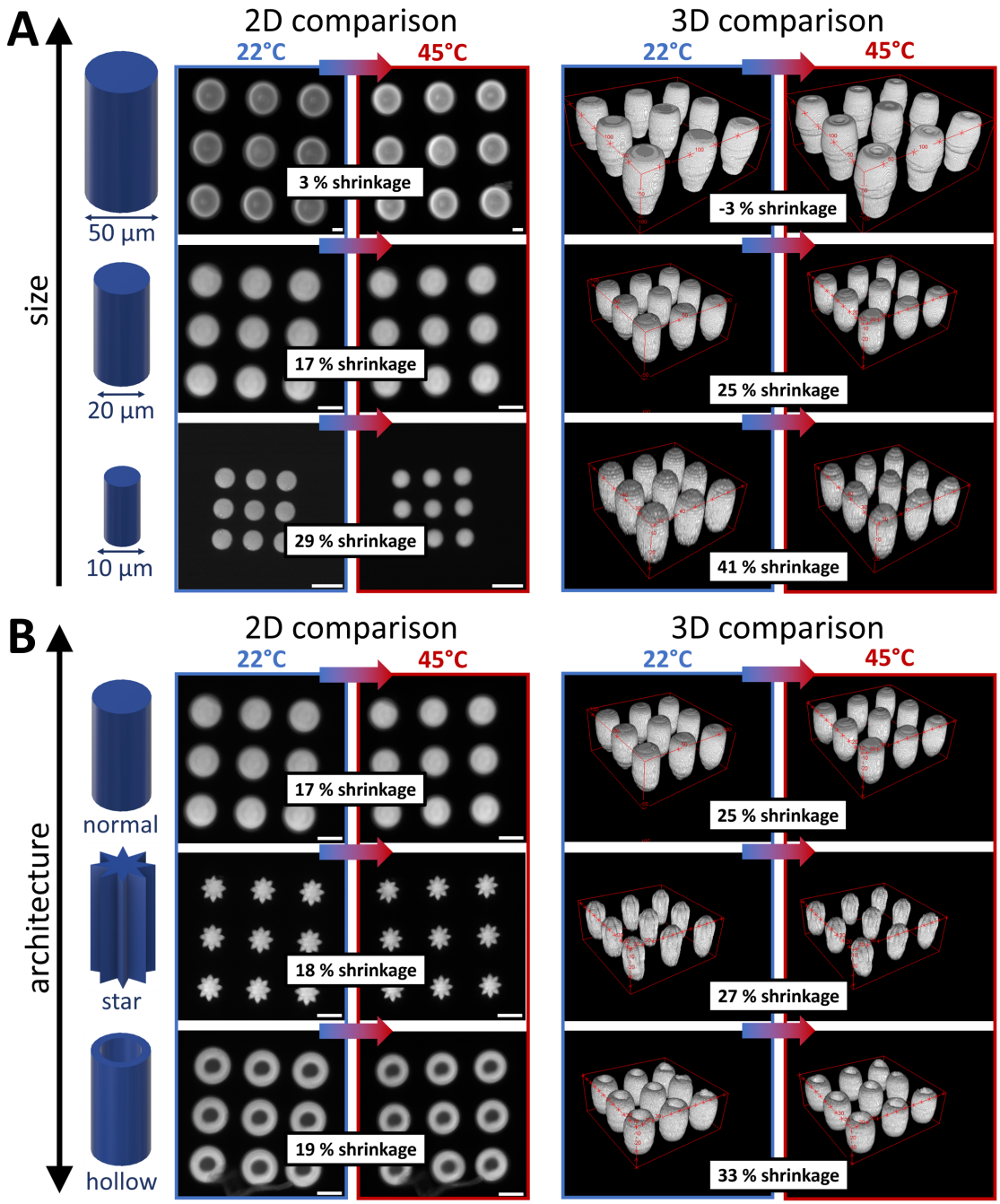

Figure 3.14: A comparison of thermoresponsive shrinkage of various PNIPAM microactuator geometries is displayed, based on confocal fluorescence images. The shrinkage is calculated in a 2D analysis of micropillar cross-sections (left) and in a 3D analysis of reconstructed image stacks (right), before and after thermally induced shrinkage. (A) compares different sizes of cylindrical micropillars having the same aspect ratio, while (B) compares various pillar architectures having the same outer dimensions. Scale bars are 20 µm. Reprinted with permission.[163] Copyright 2022, Wiley-VCH GmbH.

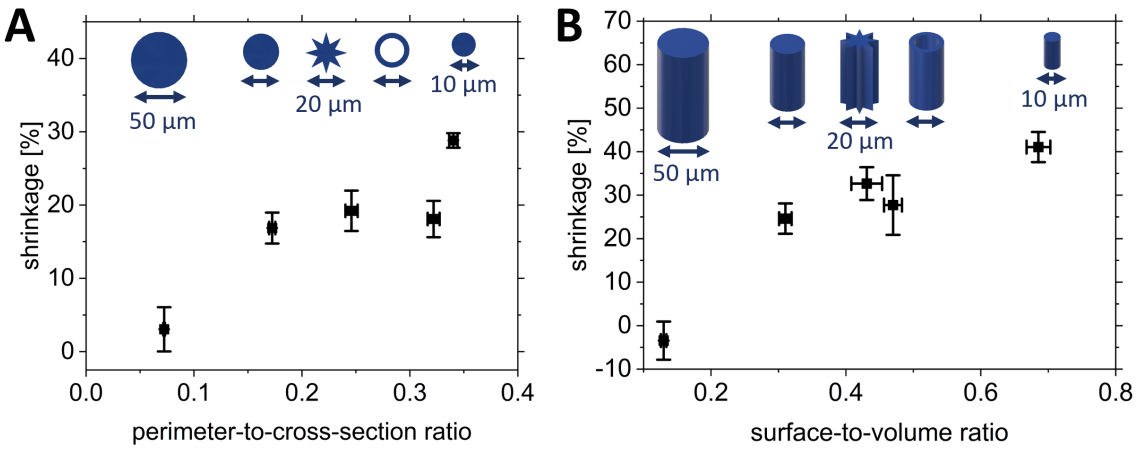

Figure 3.15: A comparison of thermoresponsive shrinkage of various PNIPAM microactuator geometries is displayed. The percentual shrinkage is plotted as a function of perimeter-to-cross-section ratio (A) and surface-to-volume ratio (B), respectively. The shrinkage increases in both cases with increasing ratios. Error bars are standard deviations calculated from nine tested samples each. Reprinted with permission.[163] Copyright 2022, Wiley-VCH GmbH.

of 20 µm but different shapes, including normal, hollow, and star-shaped cylinders, are compared in **Figure 3.14 B**. All micropillars have the same aspect ratio of 2:1 (height:diameter). A clear tendency of increased shrinkage for micropillars having a higher perimeter to cross-section ratio (2D comparison) or surface-to-volume ratio (3D comparison) can be observed in the graphs in **Figure 3.15 A** and **B**, respectively. While only very little shrinkage occurs for the 50 µm pillar, the 10 µm pillar having the highest surface-to-volume ratio reduces its volume by 41 ± 3 %. This finding supports the previously stated hypothesis that miniaturization and sample geometry can drastically increase the hydrogel shrinkage. A higher surface-to-volume ratio facilitates the outflow of water, which means that thinner sample dimensions result in higher shrinkage.[164] Hence, high resolution fabrication processes, such as two-photon laser printing, are highly attractive for adjusting the responsivity of hydrogel microactuators and improving their actuation capabilities. Furthermore, the results highlight the potential of hydrogel actuators at the micro scale, where actuation capabilities are significantly increased compared to macro scale soft actuators.

To investigate reversibility and the reswelling properties of the shrunken hydrogel, the micropillars were imaged again at 22 °C after cooling down from 45 °C and the corresponding cross-section areas and volumes were evaluated. The results are shown in **Figure 3.16** and indicate that there is no significant difference between the initial swollen state and the reswollen state after the heating and cooling cycle. This implies that the 3D printed PNIPAM microactuators can be stimulated reversibly to switch

between a high and low volume state. Wang *et al.* have fabricated microstructures of a composite PNIPAM hydrogel and demonstrated highly reversible switching for at least 100 cycles without significant fatigue.[165] Furthermore, shrinking and swelling times of PNIPAM microstructures on the order of milliseconds have been reported, which means that miniaturization drastically increases the response rates compared to macro sized samples in the millimeter range observed in **Chapter 3.1.4**, where the response times were in the range of minutes to hours.[119] [166]

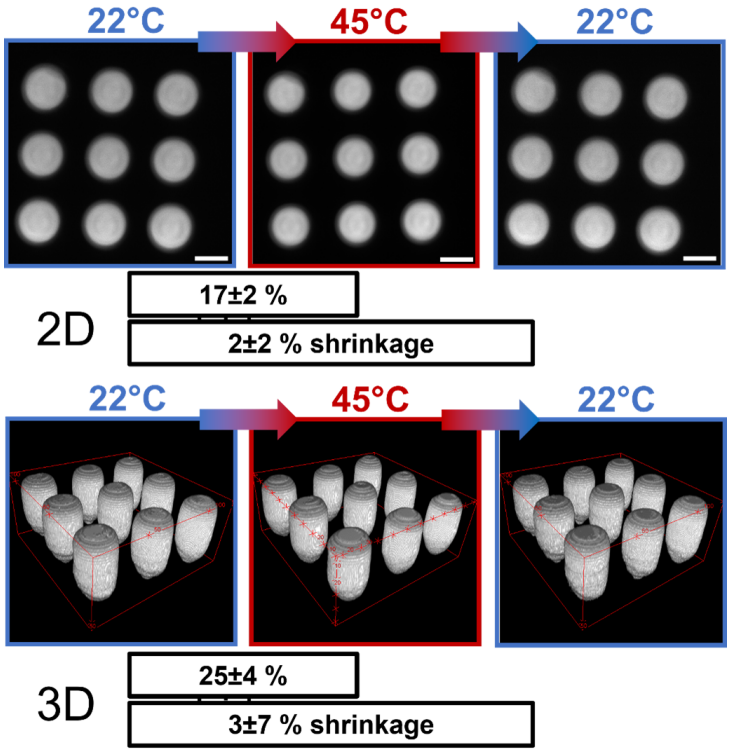

Figure 3.16: Reversibility of thermally induced shrinkage of cylindrical pNIPAM microactuators is depicted by means of confocal 2D (top) and 3D (bottom) images. After cooling down, the initially shrunken hydrogels swell back to their original volume, without any significant permanent shrinkage. This result indicates reversibility of cyclic actuation. Scale bars are 20 µm.

While the previously described experiment solely investigated the effect of micropillar size and shape on the shrinking properties keeping the processing parameters equal for all samples, the following experiment evaluates the influence of changing the laser dose during printing on hydrogel shrinkage. Here, cube shaped test structures of 50 µm side length were printed with varying laser scanning speeds of 10 to 50 mm s^{-1} while keeping the laser power constant at 100 % (50 mW at the back-focal plane). Slower laser scanning speeds locally result in a higher dose of photons

provided for the polymerization of the hydrogel resin and in turn will yield more densely crosslinked polymer networks compared to high laser scan speeds. Since crosslinking degree and shrinkage are correlated, it is expected that the microactuator response can be adjusted by the laser dose. **Figure 3.17 A** compares bright field microscopic images of the printed PNIPAM cubes at 22 °C and 45 °C for the different laser scan speeds. The shrinkage was determined relative to the diagonal of the square cross-section. A systematic trend of increasing shrinkage is observed for increased scan speeds, which is also visible in **Figure 3.17 B**. The decrease in crosslink density for higher laser scan speeds also becomes visible in the materials' transparency, where the PNIPAM cubes printed at 50 mm s^{-1} are more transparent compared to the ones printed at 10 mm s^{-1}. However, the exact crosslinking degree in the final microstructures remains unknown. These findings are in agreement with Contreras-Cáceres *et al.*, who observed an increase in shrinking ratio of hollow PNIPAM hydrogel microparticles for decreased crosslinker concentrations.[167]

It can be concluded from both experiments that controlling both the crosslinking degree as well as the size and shape of the PNIPAM microactuators by the fabrication process, allows for precise tailoring of the responsivity. Especially combining high surface-to-volume ratio geometries with a low crosslinking degree yields highly responsive microactuators that exhibit large volume phase transitions.

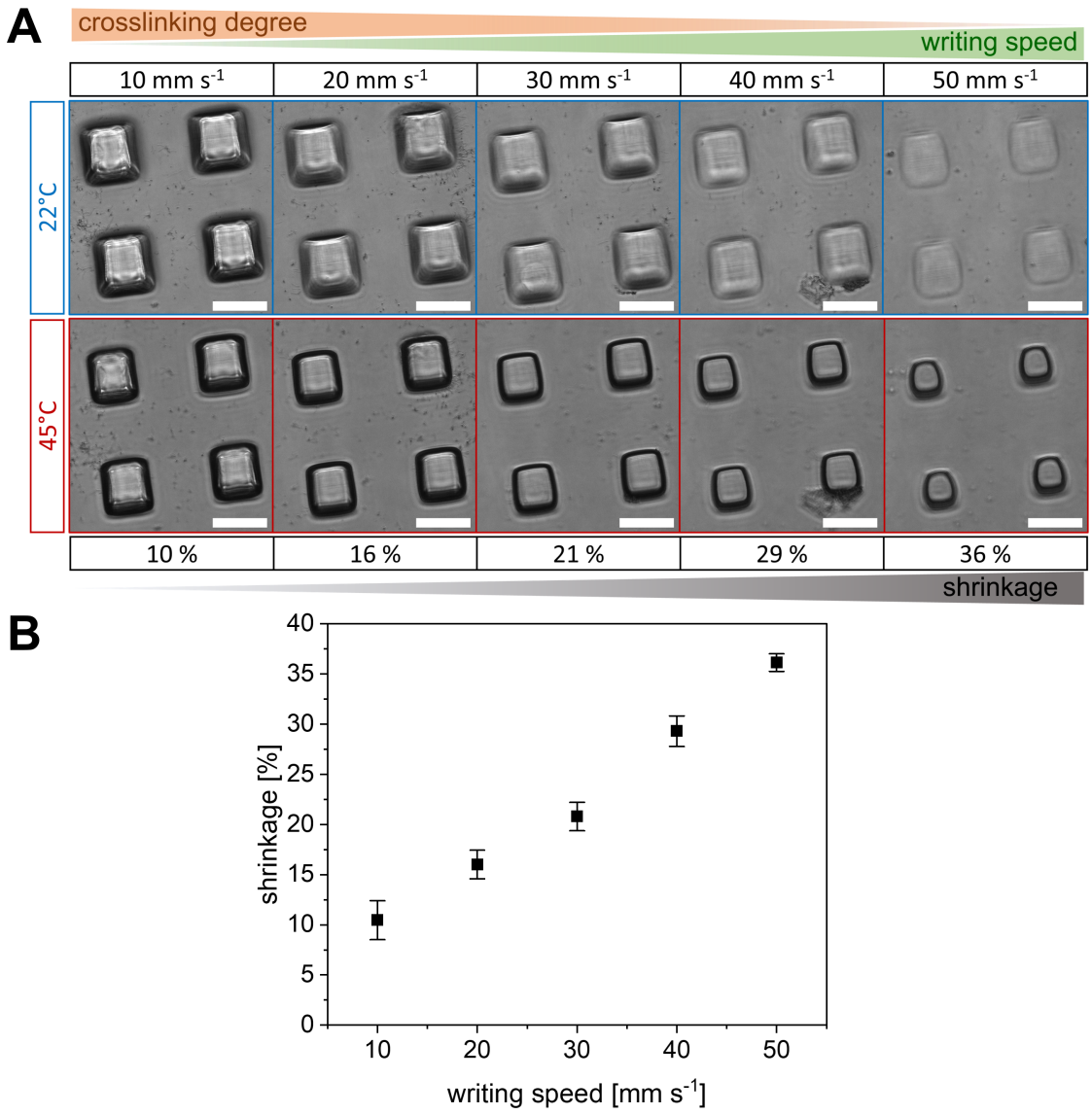

Figure 3.17: Correlation of laser writing speed, crosslinking degree, and thermally induced shrinkage of PNIPAM microactuators is illustrated. (A) Microscope images showing PNIPAM microcubes in swollen (top row) and shrunken (bottom row) state are displayed for various laser writing speeds. The shrinkage increases for higher writing speeds, which is due to the reciprocal correlation of writing speed and crosslinking degree. Scale bars are 50 µm. (B) The percentual shrinkage is plotted as a function of writing speed and shows a linear correlation in the range of 10 to 50 mm s^{-1}. $N = 7$.

3.2.5 Characterization of Surface Stiffness via Nanoindentation

The water content of PNIPAM hydrogels strongly depends on the temperature as well as the crosslinking degree of the polymer network and has a major influence on the mechanical material properties.[168] Hence, the surface stiffness of the hydrogel microactuators was investigated in detail by nanoindentation experiments. Here a commercial nanoindenter (Pavone, Optics11Life, Netherlands) was used to analyze arrays of PNIPAM microcubes, printed at various laser scan speeds ranging from 10 to 50 mm s^{-1}. The nanoindenter was equipped with a precalibrated probe consisting of a silicon cantilever with a spring constant of $k = 0.23$ N m^{-1} and a spherical glass tip of 3 µm radius. For each microcube a square matrix of 3 x 3 indentation points with lateral distance of 2 µm between each point was investigated in the center of the cubes. At each position a single indentation up to 500 nm at a constant indentation speed of 1 µm s^{-1} was performed followed by a holding time of 0.5 s and retraction at the same speed. All samples were equilibrated in deionized water for at least 24 hours before the measurement and immersed in water during indentation.

First the load-indentation curves were recorded at 22 °C for all samples and subsequently at 45 °C by using the temperature-controlled chamber of the nanoindenter. A schematic sketch of the indentation process as well as a bright field microscope image of a PNIPAM microcube array during indentation are depicted in **Figure 3.18 A** and **B**. All indentation curves were analyzed using the software *Data Viewer* (V2.5.0, Optics11Life) and by applying the Hertzian contact model. First the contact point of all loading curves was found using the software integrated contact fit function up to 20 % of maximum load. Then, Hertzian fits were applied to each curve ranging from 0 to 300 nm indentation depth for 22 °C or 0 to 150 nm for 45 °C, respectively. The analyzed experimental data is summarized in **Figure 3.19 A** to **D**, where **A** and **B** show representative load-indentation curves of PNIPAM microcubes printed at a medium laser scan speed of 30 mm s^{-1}. At 45 °C much higher load values are recorded compared to 22 °C for the same indentation depth. This is explained by the PNIPAM phase transition above 32 °C, where the hydrogel collapses into a denser and stiffer polymer network compared to the swollen hydrated state below 32 °C.[70] The effective Young's modulus E_{eff} was calculated from the fitted curves according to **Equation 3.8**, where F is the load, R is the indenter tip radius and d_{indent} is the indentation depth.

$$E_{eff} = \frac{3}{4} \cdot F \cdot \frac{1}{\sqrt{R} \cdot d_{indent}^{\frac{3}{2}}} \tag{3.8}$$

For the PNIPAM microcubes printed at a medium laser scan speed of 30 mm s^{-1} an increase in effective Young's modulus from 19 ± 5 kPa at 22 °C to 475 ± 74 kPa at 45 °C is observed, which is again explained by the lower water content and denser polymer network in the shrunken hydrogel state. Mean values of Young's

modulus for each microcube array were plotted as a function of laser scan speed for both temperatures and are depicted in **Figure 3.19 C** and **D**. A direct correlation between laser scan speed and surface stiffness can be observed, where an increase in scan speed results in a lower stiffness. This is due to a local decrease in photon dose for higher laser scan speeds, which provides less energy to initiate polymerization of the hydrogel resin during the two-photon printing process and finally yields less crosslinked polymer networks compared to lower scan speeds. Schmidt *et al.* have investigated the mechanical properties of PNIPAM microgel films and observed similar results, where the elastic modulus changed from less than 100 kPa at 25 °C to above 600 kPa at 47 °C during the hydrogel phase transition.[169]

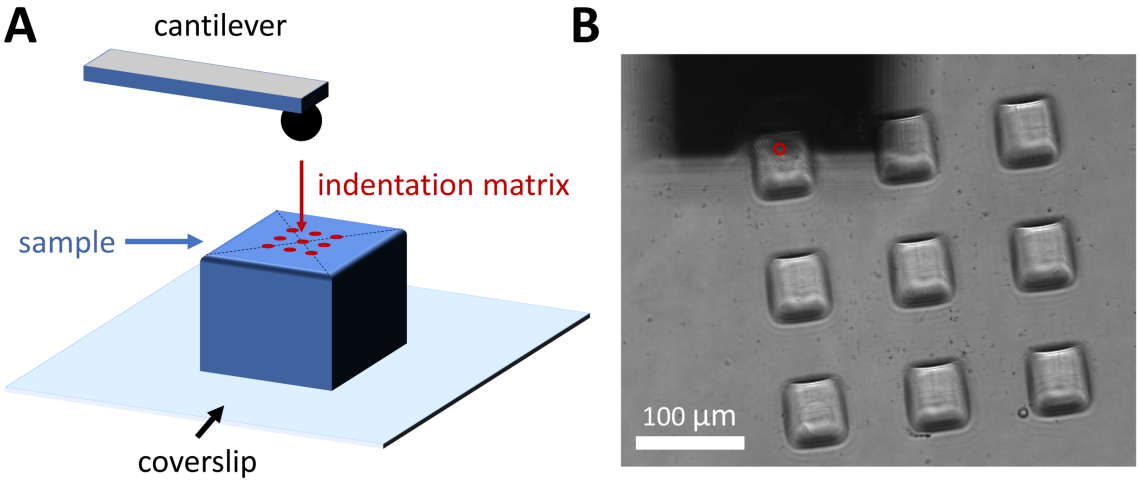

Figure 3.18: Surface stiffness characterization of PNIPAM microactuators via nanoindentation is displayed. (A) The experimental setup is illustrated, including a cantilever, which indents in a matrix manner into the sample surface. (B) A representative microscope image during indentation is depicted, where the cantilever tip position is marked with a red circle. Reprinted with permission.[163] Copyright 2022, Wiley-VCH GmbH.

In conclusion, the nanoindentation experiments proved that surface stiffness of the PNIPAM microactuators changes drastically as a function of hydrogel water content, which in turn depends on external temperature. In addition, a direct correlation between laser scan speed in the 3D printing process and hydrogel surface stiffness was found, which allows to precisely tailor the mechanical properties of the microactuators during fabrication. However, other process parameters such as hatching distance, slicing distance, laser power and even the hydrogel resin composition can also change these material properties. Taking these factors together, the two-photon printing process offers many degrees of freedom to adjust the thermoresponse as well as the mechanical properties of the PNIPAM microactuators, while providing sufficient resolution to control the shape of the microstructures.

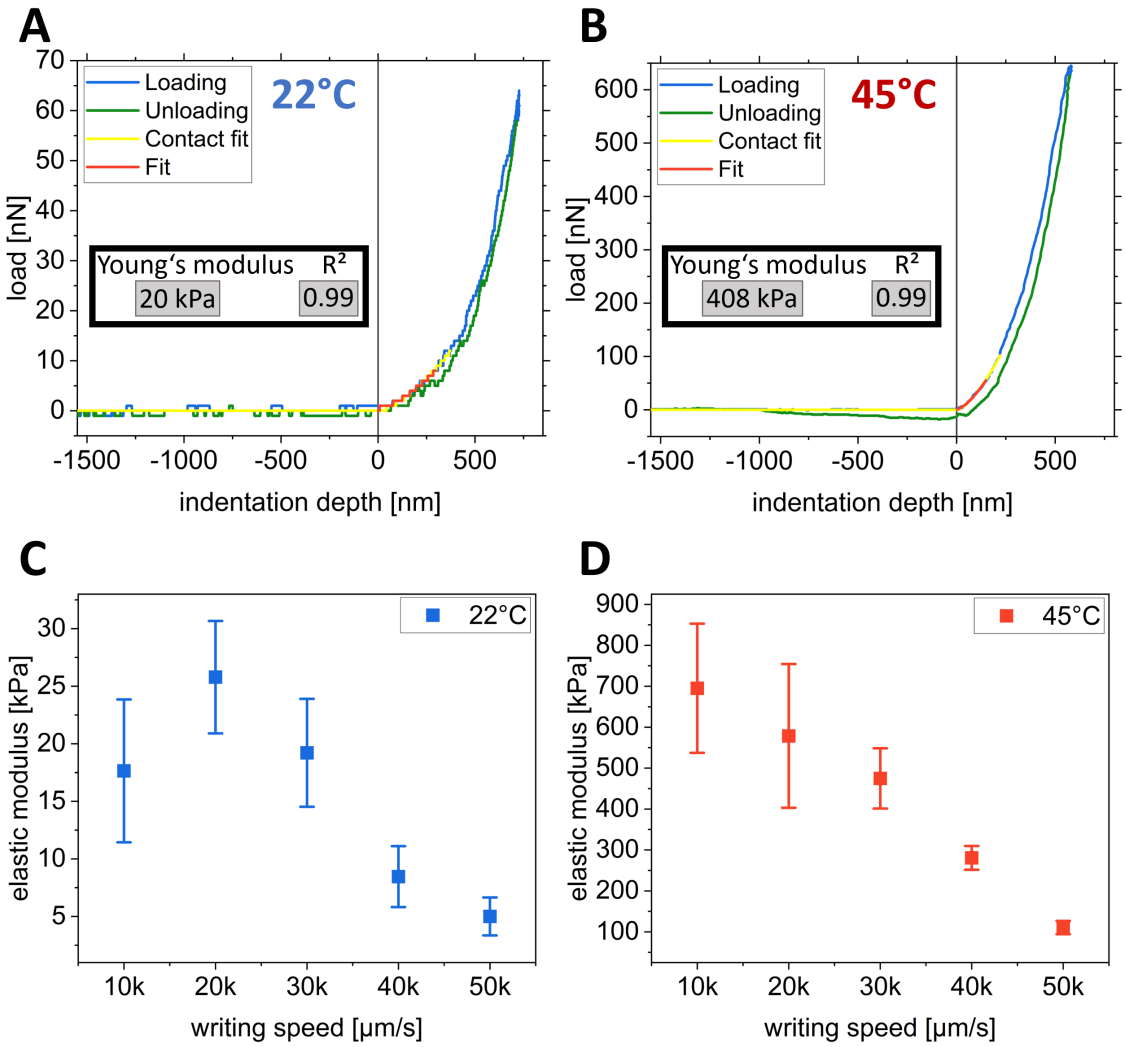

Figure 3.19: Results of surface stiffness characterization of various PNIPAM microactuators via nanoindentation are summarized. Representative force-indentation curves are displayed for a PNIPAM microactuator in the swollen (A) and shrunken state (B). Hertz fits are shown in red and corresponding Young's modulus values are displayed in inset boxes. The modulus increases significantly during shrinkage. For comparison, the elastic modulus of PNIPAM hydrogel microactuators, printed at various writing speeds, is plotted for both swollen (C) and shrunken (D) state. In both temperature regimes, a decreasing trend of elastic modulus is observed with increasing writing speeds. Error bars represent standard deviations calculated from 27 indentations each. Reprinted with permission.[163] Copyright 2022, Wiley-VCH GmbH.

3.2.6 Application in Microfluidics

To investigate the applicability of the PNIPAM micropillars in an actuation setting, several arrays of micropillars were designed and implemented into a microfluidic application setup. Here, different strategies to manipulate microobjects in flow were examined, including the possibility of thermal and photo-thermal stimulation of the PNIPAM microactuators.

In a first experiment, a dense array of PNIPAM micropillars was printed into a channel of a homemade microfluidic PDMS chip to investigate the potential of catching and releasing polystyrene microbeads.

For the fabrication of the PDMS chip, which was kindly provided by Dr. Sadaf Pashapour, a silicon wafer (MicroChemicals, Prime CZ-Si wafer, 2 inch) was spin coated with SU8 Photoresist (microresist, SU8 3050) for 30 seconds at 3000 rpm to gain a thin film of approximately 40 µm height. Subsequently, the photoresist layer was exposed to UV light (365 nm, 350 cm^2 mJ^{-1}) via a maskless aligner (µMLA, Heidelberg Instruments), which projected the pattern of the microfluidic channel design onto the wafer. The photoresist was then developed with mr-dev 600 (microresist) for 10 minutes and washed with isopropanol. The wafer was then placed into a petri dish and a layer of PDMS (Sylgard 184, 9:1 ratio) was poured onto it, degassed and cured at 65 °C for two hours. Finally, a block containing the microstructure was cut off from the wafer and inlet holes for tubing were punched into the ends of the hollow channel, before the PDMS chip together with a glass coverslip was activated by oxygen plasma (30 s, 200 mW, 0.5 mbar) and bonded to each other at 65 °C overnight. A sketch of the microfluidic chip is illustrated in **Figure 3.20**.

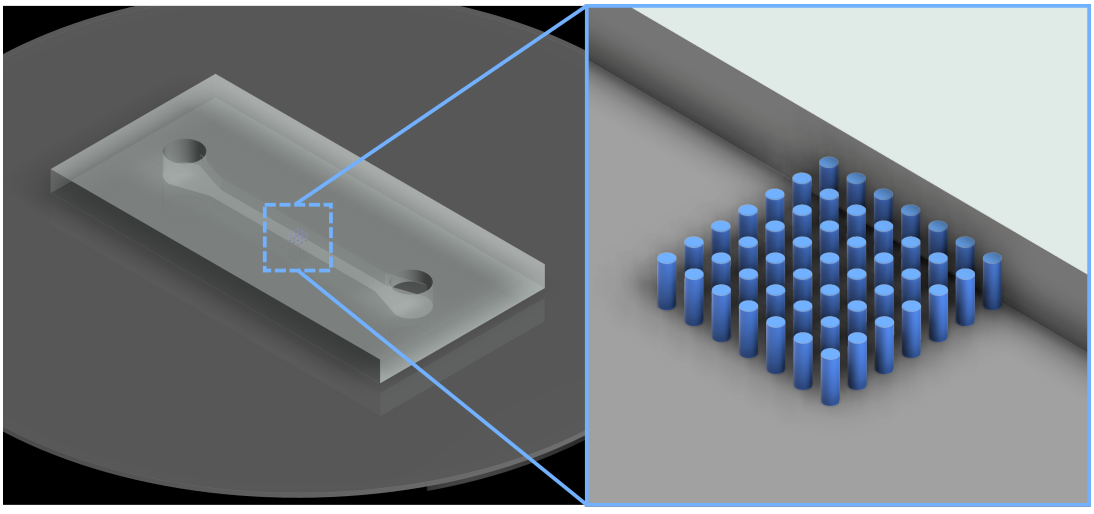

Figure 3.20: A sketch of the microfluidic PDMS chip, containing a 3D laser printed PNIPAM microactuator array, is illustrated. The chip is bonded to a coverslip and can be attached to tubes, for infusing liquids.

The sealed channel of this substrate was then filled with PNIPAM resin by injection and used for two-photon laser printing as described in **Section 3.2.2**. A medium laser scan speed of 30 mm s^{-1} was chosen to obtain both a distinct shrinkage while maintaining sufficient mechanical stability. After printing, the non-polymerized resin was washed out by infusing deionized water.

For the microfluidic experiment, tubes were attached to the inlet and outlet of the chip and a syringe pump was infusing an aqueous suspension of 2 x 10^6 ml^{-1} polystyrene beads (Thermo Fischer, F13838, 15 µm diameter) at a constant flow rate of 100 µl hr^{-1}. To avoid adhesion between the microbeads and the PNIPAM micropillars, 1 vol% of Tween-20 surfactant was added to the suspension prior to infusion. A Peltier-element was used to heat and cool the microfluidic chip and was controlled by a power supply (I = 1.5 A). Movies of the microbeads in flow were recorded with a highspeed camera using an AxioVert A1 Zeiss microscope.

In **Figure 3.21** single images of the videos are depicted in a time series to illustrate the performance of the PNIPAM microactuator array for capturing and releasing the polystyrene beads. At room temperature the gaps between the swollen hydrogel pillars are small enough to trap the beads, causing them to pile up inside the micropillar array (see yellow box). Upon heating above 32 °C the microactuators shrink, and the microbeads start flowing through the array again (see colored circles and arrows). Even though higher flow rates up to 800 µl hr^{-1} and the moving polystyrene beads did not damage the hydrogel micropillars, air bubbles caused damage and need to be avoided during mounting of the tubing. This is a possible explanation why the bottom rows of the pillars are incomplete and misaligned.

The experiment demonstrated the ability of PNIPAM microactuators implemented in a microfluidic chip to capture and release solid cargo on demand from a suspension under flow using temperature control. In addition, the two-photon laser printing approach offers great flexibility regarding the microfluidic chip design and can be easily applied to other channel geometries. This concept could find utilization in lab-on-a-chip applications, where several chips having different functions could even be combined in series or parallel.[170] [171] The fabrication of hydrogel microbeads for drug release applications, for instance, usually involves microfluidic droplet generation and screening of various crosslink concentrations or drug loads.[172] [173] In combination with the PNIPAM array presented in this work, these hydrogel beads could potentially be captured after polymerization and evaluated optically to quickly adjust the fabrication on the same chip.

Limitations such as the narrow size range of particles that can be captured by the array, which is pre-defined by the overall shrinkage of the PNIPAM pillars, and the array design before printing still remain. On the other hand, the two-photon laser printing process offers many degrees of freedom regarding the geometry of the array as well as the number and arrangement of the individual microactuators. Other studies have used similar pillar arrays made from PDMS in fully elastic microfluidic chips and stretched these to change gap sizes and sort microobjects by deterministic

lateral displacement.[174] Here, the implementation into conventional, rigid lab-on-a-chip platforms remains challenging.

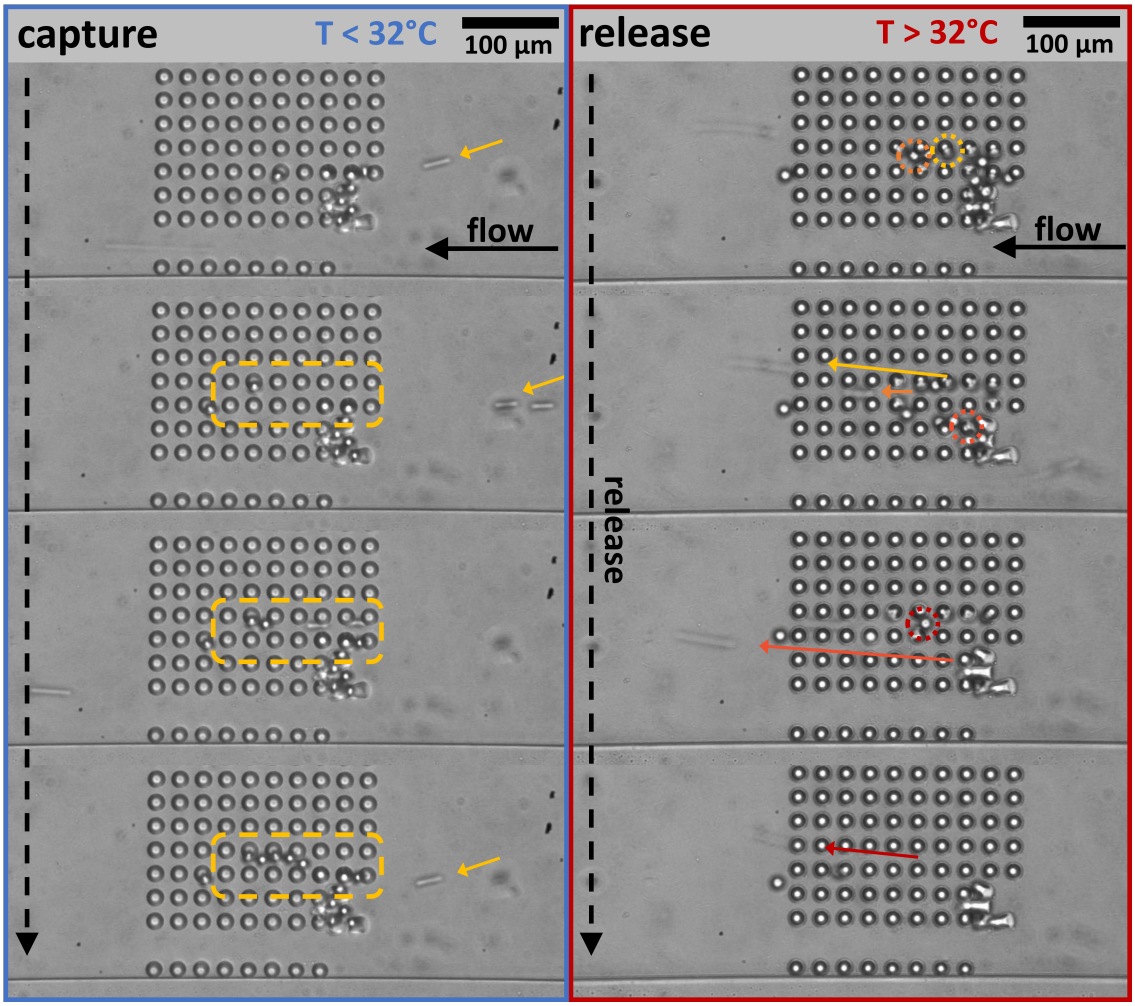

Figure 3.21: Performance of a 3D laser printed PNIPAM microactuator array inside a microfluidic chip is illustrated, by a series of microscope images. Below 32 °C (left), the hydrogel remains swollen and the gaps between neighboring actuators are small enough to capture (yellow box) polystyrene beads in flow (yellow arrows). Above 32 °C (right), the hydrogel actuators shrink and release the captured beads. Colors are assigned to different beads, which get released (arrows) from their trapping positions (circles).

From the findings obtained by the previously discussed experiment, a more advanced idea of manipulating, and possibly sorting, the microbeads was developed. In this experiment, multi-material printing of non-thermoresponsive PAM and thermoresponsive PNIPAM micropillars in the same array was explored, to investigate

whether a single channel can be generated on demand by heating the micropillar array.

In a first step, a micropillar array model containing one empty row of pillars taking two rectangular turns was designed and fabricated by two-photon laser printing of PAM. After this printing step, the residual PAM resin was carefully removed with a pipette and exchanged by adding PNIPAM resin. Then, the empty row was filled with PNIPAM micropillars during the second printing step. Finally, the microstructure was developed and the performance of the micropillar array was investigated using light microscopy. A sketch of the multi-material model as well as the experimental results are summarized in **Figure 3.22**.

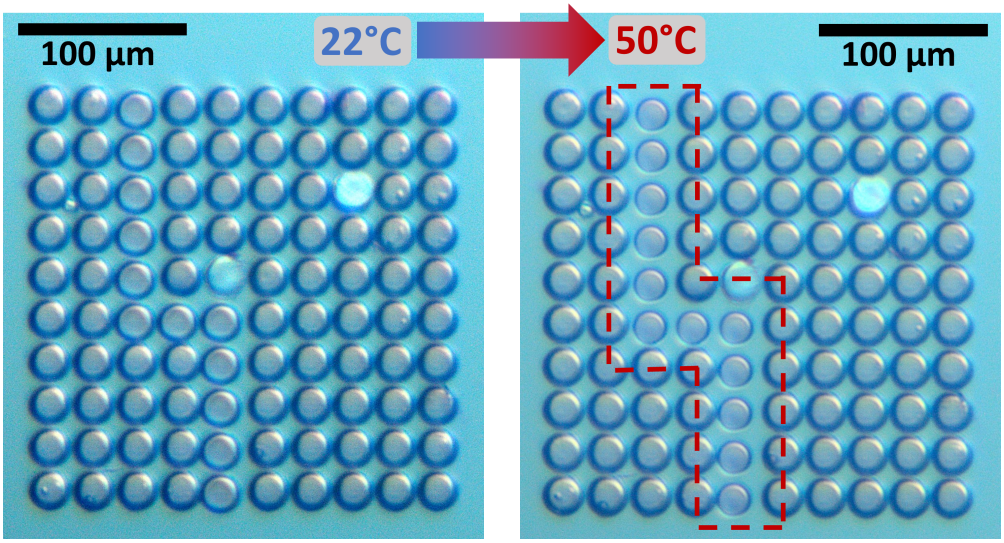

Figure 3.22: A multi-material hydrogel microactuator array is depicted, capable of forming a pre-defined channel upon thermal stimulation. One row of the array consists of thermoresponsive PNIPAM actuators, which are printed in a pre-defined channel geometry, while the surrounding actuators are made of non-thermoresponsive PAM. At 22 °C, the PNIPAM hydrogel is swollen and remains in a similar shape as the PAM micropillars. Upon global heating of the array, only the PNIPAM pillars shrink and thus form the pre-defined channel (red box).

At 22 °C both the PAM and the PNIPAM micropillars have similar shapes and there is no channel in place, while after heating at 45 °C the PNIPAM pillars shrink and thus form the pre-defined channel. Since the PNIPAM phase transition is reversible, the channel can be opened and closed by cyclic heating and cooling. Future work could use this principle to sort microobjects by implementing several channels that lead to different outputs of the array and can be activated locally.

Concepts of local actuation of single PNIPAM hydrogel micropillars have been explored by photo-thermal stimulation using a femtosecond pulsed 780 nm near

infrared laser. A substrate containing a square matrix of 3 by 3 micropillars was placed into the two-photon laser printer, and the in-built laser was focused onto a single PNIPAM microactuator. The sample was immersed in deionized water using a homemade PDMS reservoir, to prevent drying of the hydrogel. Switching the laser on and off in cycles of 5 seconds, the microactuators were stimulated. **Figure 3.23** displays microscopic images of the hydrogel pillars before and after illumination with the laser. The micropillar in focus of the laser is highlighted by a continuous blue circle. Comparing all micropillars, the ones most distant from the stimulated one display no visible shrinkage, while the direct neighbors shrink visibly (blue dotted circle). The highest shrinkage occurs for the micropillar in focus of the laser.

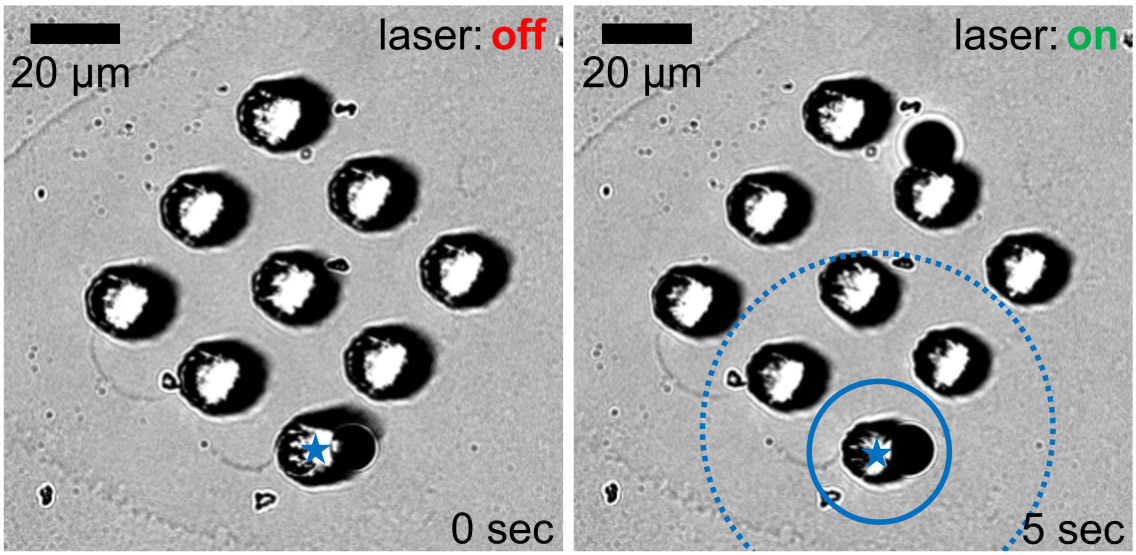

Figure 3.23: Local, photothermal stimulation of PNIPAM microactuators via focused laser light is illustrated. A blue star marks the focus spot of a NIR laser in the center of a micropillar. After switching on the laser, the microactuator shrinks significantly within 5 seconds (blue continuous circle). Due to heat dissipation, PNIPAM pillars in close proximity (blue dotted circle) also shrink to a certain degree.

The experiment demonstrates that a partial stimulation of a PNIPAM micropillar array using laser light is possible to a certain extent. However, spatiotemporal control of a single micropillar could not be achieved within the limits of the experimental setup. For the example described here, a radius of stimulation of about 110 µm was determined. A possible explanation for the extended volume of stimulation is dissipation and transport of heat via water. This limits the range of applications where precise local control of single actuators in the low micrometer range is required. In this scenario, a microfluidic setup designed for dynamic photothermal control of individual channels, would be restricted in the channel width, and in turn in the size of the objects of interest in flow.

Improvements regarding the local stimulation could arise from using a different laser, which has a larger focal spot. In this way, a lower laser dose would be required to heat an entire micropillar, resulting in a smaller heat gradient and lower heat transport. In addition, the hydrogel's light absorbance could be increased by adding photoactive nanoparticles or molecules, that absorb efficiently at the wavelength of the laser.

Hippler *et al.* designed microarrays of beam-shaped PNIPAM heterostructures with a distance of 100 µm from each other, and achieved local photothermal actuation of a single beam. Moreover, the response times were in the order of 100 milliseconds, which highlights the potential of PNIPAM microstructures for fast actuation applications.[119] Such precise control mechanisms of single PNIPAM microactuators unfold the full potential of microactuator systems, like the one presented in this thesis. In this way, dynamic switching between different channel configurations can be achieved and might be used in filtering applications.

In conclusion, first concepts of implementing PNIPAM microactuators in a microfluidic setup were introduced and their capacity to capture and release polystyrene microbeads under flow was demonstrated. Moreover, strategies of global thermal and local photothermal actuation were encompassed, envisioning diverse fields of applications, ranging from collective operation of microactuator arrays to selective control of single microactuators. In this context, two-photon laser printing endows remarkable flexibility regarding the geometrical design of both actuators and arrangement of the arrays. Considering the high resolution of fabrication and the possibility of multi-material printing on various substrates, the framework introduced in this work holds great potential for the domain of lab-on-a-chip applications. Challenges remain the reduction of spatially controlled volume upon stimulation, limiting precise local actuation, and need to be addressed in future improvements.

3.2.7 Conclusion and Perspective

In this chapter it was demonstrated that geometrical modifications at the microscale can significantly enhance the responsivity and actuation capabilities of PNIPAM hydrogel microactuators fabricated via two-photon 3D laser printing. The evaluation of thermally induced shrinkage of the microstructures emphasizes that higher surface-to-volume ratios result in an increased shrinkage. Furthermore, the 3D printing approach offers the possibility to tailor both the actuation efficiency as well as the mechanical properties of the material, by varying the laser dose during the fabrication process. Here, a higher laser dose yields mechanically more stable but less responsive hydrogel microstructures as compared to a lower laser dose. The presented results of this chapter provide a toolkit for precisely adjusting the functionality of thermoresponsive microactuators based on PNIPAM hydrogels.

In addition, it was demonstrated that systems of PNIPAM microactuators can be fabricated and implemented into lab-on-a-chip devices for microfluidic applications, such as capturing and releasing microobjects in flow on demand. Here, the two-photon 3D laser printing technology allows for a versatile selection of chip geometries and even printing inside closed channels. First results of multi-material printing and local photo-thermal stimulation emphasized that even more advanced microactuator systems could be developed by the 3D printing approach, which fulfill more complex functions, such as sorting and directing microobjects in flow selectively.

Future work should focus on integrating other functional monomers to the PNIPAM hydrogel in order to obtain multi-responsivity, such as temperature, light, and pH, to enable a broader range of applications, such as autonomous cell-culture on a chip. Here, the perfusion of various media containing nutrients and drugs could be autonomously controlled depending on the metabolism and functionality of the cells and respective pH.

In addition, local stimulation possibilities would further improve the function of the microactuator systems. Incorporation of photo-active molecules such as azobenzenes or gold nanoparticles have demonstrated promising results in other works.[175] [176] Another interesting approach could be to shift the PNIPAM LCST to human body temperature at 37 °C, which could unlock applications under physiological conditions in biomedical fields, such as drug delivery.[177] [178] In general, the strategy described in this chapter can also be applied to microactuator systems based on other responsive hydrogels, and modifications of PNIPAM, and thus might provide a platform for future developments in soft robotic lab-on-a-chip applications.

3.3 Discussion of Microstructural Modification Strategies to Increase PNIPAM Hydrogel Responsiveness

Thermoresponsive hydrogels have emerged as practical materials for soft actuator research, primarily due to their capacity to induce volumetric transitions via ambient temperature modulation. However, the performance of bulk hydrogels in this context is constrained by their slow response rates, low amplitude deformation, and relatively weak stroke force generation. These attributes impede the material's suitability for soft actuator applications and are part of current research. Addressing these limitations, two approaches of microstructuring PNIPAM hydrogels at the micrometer scale were introduced in this work, and have proven efficacious, yielding pronounced thermoresponsive actuation and increased stroke forces compared to the conventional bulk material. These approaches foster the applicability in actuation scenarios aimed at manipulating external objects, especially in microfluidics.

The first approach, discussed in **Chapter 3.1**, is based on the incorporation of an interconnected 3D network of microchannels in the PNIPAM hydrogel matrix, which provides intricate pathways for the water transport in and out of the material. Consequently, the thermally induced shrinkage occurs faster, and the volume change is increased as compared to bulk PNIPAM. Further, the empirical data presented in this work demonstrates good reproducibility in repeated thermoresponsive contraction and expansion, as well as relatively high changes in swelling ratios below and above the LCST, which is beneficial for designing soft robotic actuators. Importantly, this method, unlike alternative avenues reliant on chemical modifications of the polymer composition, exclusively alters the hydrogel's microstructure, preserving its chemical properties. Apart from the swelling and shrinking dynamics, mechanical material properties are substantial factors to be considered in soft actuators. Achieving substantial deformations and enduring cyclic performance is an inevitable requirement. The cyclic deformation experiments conducted in this work demonstrate long-lasting actuation with no notable signs of fatigue within the parameters of the study. Additionally, the ability to generate stroke forces upon swelling, which is a critical attribute for a stimuli-responsive hydrogels within the context of soft actuators, was experimentally validated. Integration of a minor amount of 4 vol% microchannels into PNIPAM hydrogels leads to an 8.3-fold increase in stroke force upon swelling, promising superior actuation capabilities when contrasted with conventional bulk PNIPAM hydrogels. Overall, the enhanced temperature responsivity makes microchannel-containing PNIPAM hydrogels promising materials for soft robotic applications. Considering the microengineering approach's restriction in sample miniaturization, this method provides an attractive way to design efficient, thermally controlled soft actuators in the millimeter to centimeter range.

In parallel, two-photon 3D laser printing was introduced to fabricate thermoresponsive PNIPAM microactuators, enabling high-resolution manufacturing within the low micrometer range. Like their microchannel-containing counterparts, these miniaturized actuators also exhibit a high responsivity. The experimental findings discussed in **Chapter 3.2** highlight that microactuator geometry and printing parameters exert substantial influence on actuator performance, and thus represent critical factors to consider in PNIPAM-based microactuator development. In particular, it was found that high surface-to-volume ratios expedite water in- and outflow in the hydrogel microstructures, indicating that thinner sample dimensions yield increased actuator contractions. Consequently, high-resolution fabrication techniques such as two-photon laser printing hold considerable potential for tailoring hydrogel microactuator responsivity and enhancing their actuation capabilities. In addition, printing parameters, such as laser power, laser scan speed, slicing distance, and hatching distance, can be used to control the degree of polymer crosslinking, which in turn adjust the hydrogel's mechanical properties. The 3D printed PNIPAM microactuators introduced in this work, display thermally induced, reversible switching between high and low volume states, with shrinking and swelling durations in the order of seconds. Moreover, application in microfluidic experiments demonstrated the feasibility of the introduced concepts, to develop PNIPAM microactuators for soft robotic scenarios.

In conclusion, the integration of microchannel networks and two-photon laser printing stand as potent strategies for designing efficiently performing, thermoresponsive PNIPAM hydrogel microactuators, with wide-ranging implications for microfluidics and lab-on-a-chip technologies. While the first approach is limited to fabricate millimeter and centimeter scale structures, the second strategy provides high resolution to control specific shapes of microstructures, while simultaneously offering multiple avenues to tailor thermoresponse and mechanical properties of PNIPAM hydrogels. Furthermore, the 3D printing approach permits multi-material printing on diverse substrates, and overcomes restrictions in geometric complexity, which is a common limitation in other methodologies, such as soft lithography. The concepts advanced in this thesis could open avenues toward stimuli-guided microactuation within microfluidic systems or lab-on-a-chip devices.

Compared to other established methods aiming to enhance the thermo-response of PNIPAM hydrogels, the approaches of this work benefit from solely physical material modification, rather than chemical adjustments, and thus avoid undesired changes in material properties. Future work should focus on extending the horizons of potential applications with multi-responsivity, by integration of diverse functional monomers into the PNIPAM hydrogel matrix.

4

Conclusion and Perspective

In this thesis, concepts for tailoring the properties of stimuli-responsive hydrogels and implementation of these materials into soft robotic applications have been elaborated. Conventional bulk hydrogels typically exhibit restricted actuation capabilities, due to weak and slow responses when exposed to external stimuli. These restrictions often limit the range of applications and demand for the development of new methods for tailoring the responsive properties of such hydrogels.

First, highly thermoresponsive PNIPAM hydrogels were developed, by introducing a template-assisted fabrication method based on sacrificial zinc oxide templates. This method generates a specific interconnected network of hollow microchannels inside the hydrogel, thus altering its material properties. Large volume transitions of up to 90 % shrinkage by only incorporating 5 vol% of microchannels, considerable stroke forces (8 times higher compared to the bulk hydrogel), and a significantly faster response make this material superior for soft actuator applications as compared to the bulk hydrogel. Furthermore, the fabrication process allows for tailoring the mechanical properties of the hydrogels by varying crosslinker concentrations, while the enhanced responsivity remains. The material's actuation capabilities were tested in a thermally controlled soft gripper, which demonstrated the applicability in soft robotic scenarios. While other established methods of increasing the temperature response of PNIPAM hydrogels often rely on chemical modifications of the polymer network, such as copolymerization, formation of interpenetrating polymer networks, or nanocomposites, this work exclusively alters the hydrogel's microstructure. Hence, undesired property changes, such as a shift in LCST, elasticity, or optical transparency can be avoided. In general, this template-assisted approach could also be applied to other responsive hydrogels and thus contributes to drive the development of highly responsive hydrogels forward.

To understand the impact of surface-to-volume ratio on actuator performance, two-photon 3D laser printing was then used to fabricate thermoresponsive PNIPAM microactuators with high resolution in the low micrometer range and with precise control of microactuator shape. While conventional fabrication methods often lack sufficient resolution as well as limitations to 2.5D geometries, 3D laser printing can overcome these restrictions and enables the manufacturing of microstructures with complex 3D geometries. Within a comprehensive characterization of PNIPAM

microactuator properties, it turned out, that miniaturization of the actuators and especially the surface-to-volume-ratio have a major impact on the responsivity. The evaluation of thermally induced shrinkage of the microstructures emphasizes that higher surface-to-volume ratios result in an increased shrinkage. Besides the geometric microactuator design, alteration of process parameters of the 3D laser printing method, allows for further tailoring of the hydrogel's performance in thermally stimulated actuation. Moreover, these strategies can also be applied to systems of microactuators. Here, PNIPAM microactuator systems were developed, which display cooperative functions and potential application in microfluidic devices. In this way, capturing and releasing cargo in a microfluidic chip upon thermal stimulation was demonstrated. First results of multi-material printing and local photo-thermal stimulation emphasize, that even more advanced microactuator systems could be developed by the 3D printing approach, which could fulfill more complex functions, such as sorting and directing microobjects in flow selectively. Within the scope of locally confined stimulation of single actuators, the use of pre-structured substrates containing metal-based microheaters has been explored in a cooperation project.[179] The results revealed promising potential for the integration into the microactuator systems presented in this thesis in future works.

The strategies presented in this work, demonstrate that responsivity can be significantly enhanced by miniaturization of bulk hydrogel structures, where both intrinsic and surface engineering modifications can show high impact. Thus, the results presented in this thesis can help to shape the future of soft micro actuator research.

Expanding the fabrication towards other functional hydrogel microstructures, could further broaden the range of applications and possibly enable integration of various hydrogel actuator systems in a lab-on-a-chip device.

Combinations of several such hydrogel microstructures on a single substrate open new avenues for multi-functional platforms, that are capable of performing several tasks in parallel or in series. Certainly, uniting recent advances in interdisciplinary research fields with state of the art microfabrication technologies, will have the potential to revolutionize micro soft robotic applications.

5

Publications

- **Spratte, T.**, Arndt, C., Wacker, I., Hauck, M., Adelung, R., Schröder, R.R., Schütt, F., Selhuber-Unkel, C., Thermoresponsive Hydrogels with Improved Actuation Function by Interconnected Microchannels. *Adv. Intell. Syst.* **2022**, 4, 2100081.

- **Spratte, T.**, Geiger, S., Colombo, F., Mishra, A., Taale, M., Hsu, L.-Y., Blasco, E., Selhuber-Unkel, C., Increasing the Efficiency of Thermoresponsive Actuation at the Microscale by Direct Laser Writing of PNIPAM. *Adv. Mater. Technol.* **2023**, 8, 2200714.

- Hsu, L.-Y., Mainik, P., Münchinger, A., Lindenthal, S., **Spratte, T.**, Welle, A., Zaumseil, J., Selhuber-Unkel, C., Wegener, M., Blasco, E., A Facile Approach for 4D Microprinting of Multi-Photoresponsive Actuators. *Adv. Mater. Technol.* **2023**, 8, 2200801.

- Hussain, N., Scholz, A., **Spratte, T.**, Selhuber-Unkel, C., Hirtz, M., Aghassi-Hagmann, J., Direct Writing of Liquid Metal Microheaters for Microvalve Applications. *2023 IEEE International Conference on Flexible and Printable Sensors and Systems (FLEPS)* **2023**, pp. 1-4.

- Giez, C., Pinkle, D., Giencke, Y., Wittlieb, J., Herbst, E., **Spratte, T.**, Lachnit, T., Klimovich, A., Selhuber-Unkel, C., Bosch, T., Microbes as part of ancestral neuronal circuits: Bacterial produced signals affect neurons controlling eating behavior in Hydra. *Current Biology*, **in press**

Bibliography

[1] D. Christian, C. Brown, C. Benjamin, M. Busbridge, and J. Mautone, *Big history: between nothing and everything*. United States: Mcgraw Hill, 2010.

[2] Z. Shi, Y. Xie, W. Xue, Y. Chen, L. Fu, and X. Xu, "Smart factory in industry 4.0," *Systems Research and Behavioral Science*, vol. 37, no. 4, pp. 607–617, 2020.

[3] G. M. Whitesides, "Soft robotics," *Angewandte Chemie International Edition*, vol. 57, no. 16, pp. 4258–4273, 2018.

[4] C. Laschi and M. Cianchetti, "Soft robotics: New perspectives for robot bodyware and control," *Frontiers in Bioengineering and Biotechnology*, vol. 2, pp. 1–5, 2014.

[5] M. Wu, X. Zheng, R. Liu, N. Hou, W. H. Afridi, R. H. Afridi, X. Guo, J. Wu, C. Wang, and G. Xie, "Glowing sucker octopus (stauroteuthis syrtensis)-inspired soft robotic gripper for underwater self-adaptive grasping and sensing," *Advanced Science*, vol. 9, no. 17, p. 2 104 382, 2022.

[6] M. Yamada, M. Kondo, R. Miyasato, Y. Naka, J.-i. Mamiya, M. Kinoshita, A. Shishido, Y. Yu, C. J. Barrett, and T. Ikeda, "Photomobile polymer materials—various three-dimensional movements," *Journal of Materials Chemistry*, vol. 19, pp. 60–62, 1 2009.

[7] T. G. Thuruthel, B. Shih, C. Laschi, and M. T. Tolley, "Soft robot perception using embedded soft sensors and recurrent neural networks," *Science Robotics*, vol. 4, no. 26, eaav1488, 2019.

[8] C. Appiah, C. Arndt, K. Siemsen, A. Heitmann, A. Staubitz, and C. Selhuber-Unkel, "Living materials herald a new era in soft robotics," *Advanced Materials*, vol. 31, no. 36, p. 1 807 747, 2019.

[9] P. Zhang, "Chapter 3 - sensors and actuators," in *Advanced Industrial Control Technology*, P. Zhang, Ed., Oxford: William Andrew Publishing, 2010, pp. 73–116.

[10] K. G. Webber, D. J. Franzbach, and J. Koruza, "Determination of the true operational range of a piezoelectric actuator," *Journal of the American Ceramic Society*, vol. 97, no. 9, pp. 2842–2849, 2014.

[11] J. Deng, W. Chen, K. Li, L. Wang, and Y. Liu, "A sandwich piezoelectric actuator with long stroke and nanometer resolution by the hybrid of two actuation modes," *Sensors and Actuators A: Physical*, vol. 296, pp. 121–131, 2019.

[12] X. Gao, J. Yang, J. Wu, X. Xin, Z. Li, X. Yuan, X. Shen, and S. Dong, "Piezoelectric actuators and motors: Materials, designs, and applications," *Advanced Materials Technologies*, vol. 5, no. 1, p. 1 900 716, 2020.

[13] D. Kortenkamp, R. Simmons, and D. Brugali, "Robotic systems architectures and programming," in *Springer Handbook of Robotics*, B. Siciliano and O. Khatib, Eds. Cham: Springer International Publishing, 2016, pp. 283–306.

[14] C. Kaspar, B. J. Ravoo, W. G. van der Wiel, S. V. Wegner, and W. H. P. Pernice, "The rise of intelligent matter," *Nature*, vol. 594, pp. 345–355, 7863 2014.

[15] A. Roy, K. Manna, and S. Pal, "Recent advances in various stimuli-responsive hydrogels: From synthetic designs to emerging healthcare applications," *Materials Chemistry Frontiers*, vol. 6, pp. 2338–2385, 17 2022.

[16] K. Yang, S. Wan, B. Chen, W. Gao, J. Chen, M. Liu, B. He, and H. Wu, "Dual ph and temperature responsive hydrogels based on β-cyclodextrin derivatives for atorvastatin delivery," *Carbohydrate Polymers*, vol. 136, pp. 300–306, 2016.

[17] G.-F. Liu, W. Ji, W.-L. Wang, and C.-L. Feng, "Multiresponsive hydrogel coassembled from phenylalanine and azobenzene derivatives as 3d scaffolds for photoguiding cell adhesion and release," *ACS Applied Materials & Interfaces*, vol. 7, no. 1, pp. 301–307, 2015.

[18] Q. Guo, W. Yang, H. Liu, W. Wang, Z. Ge, and Z. Yuan, "An aquatic biomimetic butterfly soft robot driven by deformable photo-responsive hydrogel," *Soft Matter*, vol. 19, no. 38, pp. 7370–7378, 2023.

[19] X. Wei, Y. Xue, Y. Sun, L. Chen, C. Zhang, Q. Wu, S. Peng, C. Ma, Z. Liu, S. Jiang, X. Yang, S. Agarwal, and G. Duan, "A robust anisotropic light-responsive hydrogel for ultrafast and complex biomimetic actuation via poly(pyrrole)-coated electrospun nanofiber," *Chemical Engineering Journal*, vol. 452, p. 139 373, 2023.

[20] H. Liu, X. Jia, R. Liu, K. Chen, Z. Wang, T. Lyu, X. Cui, Y. Zhao, and Y. Tian, "Multifunctional gradient hydrogel with ultrafast thermo-responsive actuation and ultrahigh conductivity," *Journal of Materials Chemistry A*, vol. 10, pp. 21 874–21 883, 41 2022.

[21] Q. Cao, Z. Shu, T. Zhang, W. Ji, J. Chen, and Y. Wei, "Highly elastic, sensitive, stretchable, and skin-inspired conductive sodium alginate/polyacrylamide/gallium composite hydrogel with toughness as a flexible strain sensor," *Biomacromolecules*, vol. 23, no. 6, pp. 2603–2613, 2022.

[22] N. Takeuchi, S. Nakajima, K. Yoshida, R. Kawano, Y. Hori, and H. Onoe, "Microfiber-shaped programmable materials with stimuli-responsive hydrogel," *Soft Robotics*, vol. 9, no. 1, pp. 89–97, 2022.

[23] Y. Dong, J. Wang, X. Guo, S. Yang, M. O. Ozen, P. Chen, X. Liu, W. Du, F. Xiao, U. Demirci, and B.-F. Liu, "Multi-stimuli-responsive programmable biomimetic actuator," *Nature Communications*, vol. 10, no. 1, p. 4087, 2019.

[24] C. A. Spiegel, M. Hippler, A. Münchinger, M. Bastmeyer, C. Barner-Kowollik, M. Wegener, and E. Blasco, "4d printing at the microscale," *Advanced Functional Materials*, vol. 30, no. 26, p. 1 907 615, 2020.

[25] J. Li and D. J. Mooney, "Designing hydrogels for controlled drug delivery," *Nature Reviews Materials*, vol. 1, no. 12, p. 16 071, 2016.

[26] S. S. Said, S. Campbell, and T. Hoare, "Externally addressable smart drug delivery vehicles: Current technologies and future directions," *Chemistry of Materials*, vol. 31, no. 14, pp. 4971–4989, 2019.

[27] H. Kim, H. Lee, K.-Y. Seong, E. Lee, S. Y. Yang, and J. Yoon, "Visible light-triggered on-demand drug release from hybrid hydrogels and its application in transdermal patches," *Advanced Healthcare Materials*, vol. 4, no. 14, pp. 2071–2077, 2015.

[28] M. Dong, B. Shi, D. Liu, J.-H. Liu, D. Zhao, Z.-H. Yu, X.-Q. Shen, J.-M. Gan, B.-l. Shi, Y. Qiu, C.-C. Wang, Z.-Z. Zhu, and Q.-D. Shen, "Conductive hydrogel for a photothermal-responsive stretchable artificial nerve and coalescing with a damaged peripheral nerve," *ACS Nano*, vol. 14, no. 12, pp. 16 565–16 575, 2020.

[29] S. Xia, Q. Zhang, S. Song, L. Duan, and G. Gao, "Bioinspired dynamic cross-linking hydrogel sensors with skin-like strain and pressure sensing behaviors," *Chemistry of Materials*, vol. 31, no. 22, pp. 9522–9531, 2019.

[30] Z. Zheng, H. Wang, L. Dong, Q. Shi, J. Li, T. Sun, Q. Huang, and T. Fukuda, "Ionic shape-morphing microrobotic end-effectors for environmentally adaptive targeting, releasing, and sampling," *Nature Communications*, vol. 12, no. 1, p. 411, 2021.

[31] D. Rus and M. T. Tolley, "Design, fabrication and control of soft robots," *Nature*, vol. 521, no. 7553, pp. 467–475, 2015.

[32] G. Gu, H. Shea, S. Seelecke, G. Alici, and G. Rizzello, "Editorial: Soft robotics based on electroactive polymers," *Frontiers in Robotics and AI*, vol. 8, p. 676 406, 2021.

[33] L.-Y. Hsu, P. Mainik, A. Münchinger, S. Lindenthal, T. Spratte, A. Welle, J. Zaumseil, C. Selhuber-Unkel, M. Wegener, and E. Blasco, "A facile approach for 4d microprinting of multi-photoresponsive actuators," *Advanced Materials Technologies*, vol. 8, no. 1, p. 2 200 801, 2023.

[34] Y. Lee, W. Song, and J.-Y. Sun, "Hydrogel soft robotics," *Materials Today Physics*, vol. 15, p. 100 258, 2020.

[35] R. Tognato, A. R. Armiento, V. Bonfrate, R. Levato, J. Malda, M. Alini, D. Eglin, G. Giancane, and T. Serra, "A stimuli-responsive nanocomposite for 3d anisotropic cell-guidance and magnetic soft robotics," *Advanced Functional Materials*, vol. 29, no. 9, p. 1 804 647, 2019.

[36] M. Zupan, M. Ashby, and N. Fleck, "Actuator classification and selection-the development of a database," *Advanced Engineering Materials*, vol. 4, no. 12, pp. 933–940, 2002.

[37] A. Münchinger, V. Hahn, D. Beutel, S. Woska, J. Monti, C. Rockstuhl, E. Blasco, and M. Wegener, "Multi-photon 4d printing of complex liquid crystalline microstructures by in situ alignment using electric fields," *Advanced Materials Technologies*, vol. 7, no. 1, p. 2 100 944, 2022.

[38] C. Keplinger, T. Li, R. Baumgartner, Z. Suo, and S. Bauer, "Harnessing snap-through instability in soft dielectrics to achieve giant voltage-triggered deformation," *Soft Matter*, vol. 8, pp. 285–288, 2 2012.

[39] B. Balakrisnan and E. Smela, "Challenges in the microfabrication of dielectric elastomer actuators," in *Electroactive Polymer Actuators and Devices (EAPAD) 2010*, Y. Bar-Cohen, Ed., International Society for Optics and Photonics, vol. 7642, SPIE, 2010.

[40] J. Li and M. Pumera, "3d printing of functional microrobots," *Chemical Society Reviews*, vol. 50, pp. 2794–2838, 4 2021.

[41] N. A. Peppas and A. S. Hoffman, "1.3.2e - hydrogels," in *Biomaterials Science (Fourth Edition)*, W. R. Wagner, S. E. Sakiyama-Elbert, G. Zhang, and M. J. Yaszemski, Eds., Fourth Edition, Academic Press, 2020, pp. 153–166.

[42] D. A. Gyles, L. D. Castro, J. O. C. Silva, and R. M. Ribeiro-Costa, "A review of the designs and prominent biomedical advances of natural and synthetic hydrogel formulations," *European Polymer Journal*, vol. 88, pp. 373–392, 2017.

[43] M. C. Koetting, J. T. Peters, S. D. Steichen, and N. A. Peppas, "Stimulus-responsive hydrogels: Theory, modern advances, and applications," *Materials Science and Engineering: R: Reports*, vol. 93, pp. 1–49, 2015.

[44] D. Seliktar, "Designing cell-compatible hydrogels for biomedical applications," *Science*, vol. 336, no. 6085, pp. 1124–1128, 2012.

[45] M. A. C. Stuart, W. T. S. Huck, J. Genzer, M. Müller, C. Ober, M. Stamm, G. B. Sukhorukov, I. Szleifer, V. V. Tsukruk, M. Urban, F. Winnik, S. Zauscher, I. Luzinov, and S. Minko, "Emerging applications of stimuli-responsive polymer materials," *Nature Materials*, vol. 9, no. 2, pp. 101–113, 2010.

[46] S. Q. Wang, Q. L. Liu, and A. M. Zhu, "Preparation of multisensitive poly (n-isopropylacrylamide-co-acrylic acid)/tio2 composites for degradation of methyl orange," *European Polymer Journal*, vol. 47, no. 5, pp. 1168–1175, 2011.

[47] A. Abdollahi, H. Roghani-Mamaqani, B. Razavi, and M. Salami-Kalajahi, "The light-controlling of temperature-responsivity in stimuli-responsive polymers," *Polymer Chemistry*, vol. 10, pp. 5686–5720, 42 2019.

[48] X. Le, W. Lu, J. Zhang, and T. Chen, "Recent progress in biomimetic anisotropic hydrogel actuators," *Advanced Science*, vol. 6, no. 5, p. 1 801 584, 2019.

[49] D. Caccavo, S. Cascone, G. Lamberti, and A. A. Barba, "Hydrogels: Experimental characterization and mathematical modelling of their mechanical and diffusive behaviour," *Chemical Society Reviews*, vol. 47, pp. 2357–2373, 7 2018.

[50] S. Huth, S. Sindt, and C. Selhuber-Unkel, "Automated analysis of soft hydrogel microindentation: Impact of various indentation parameters on the measurement of young's modulus," *PLOS ONE*, vol. 14, no. 8, pp. 1–17, 2019.

[51] S.-H. Kim and C.-C. Chu, "Synthesis and characterization of dextran–methacrylate hydrogels and structural study by sem," *Journal of Biomedical Materials Research*, vol. 49, no. 4, pp. 517–527, 2000.

[52] S. M. Paterson, Y. S. Casadio, D. H. Brown, J. A. Shaw, T. V. Chirila, and M. V. Baker, "Laser scanning confocal microscopy versus scanning electron microscopy for characterization of polymer morphology: Sample preparation drastically distorts morphologies of poly(2-hydroxyethyl methacrylate)-based hydrogels," *Journal of Applied Polymer Science*, vol. 127, no. 6, pp. 4296–4304, 2013.

[53] S. Raymond and L. Weintraub, "Acrylamide gel as a supporting medium for zone electrophoresis," *Science*, vol. 130, no. 3377, pp. 711–711, 1959.

[54] A. Herrmann, R. Haag, and U. Schedler, "Hydrogels and their role in biosensing applications," *Advanced Healthcare Materials*, vol. 10, no. 11, p. 2 100 062, 2021.

[55] P. Menter, "Acrylamide polymerization—a practical approach," *Bio-Rad Tech Note*, vol. 1156, p. 24, 2000.

[56] Y. Cohen, O. Ramon, I. J. Kopelman, and S. Mizrahi, "Characterization of inhomogeneous polyacrylamide hydrogels," *Journal of Polymer Science Part B: Polymer Physics*, vol. 30, no. 9, pp. 1055–1067, 1992.

[57] G. Sennakesavan, M. Mostakhdemin, L. Dkhar, A. Seyfoddin, and S. Fatihhi, "Acrylic acid/acrylamide based hydrogels and its properties - a review," *Polymer Degradation and Stability*, vol. 180, p. 109 308, 2020.

[58] R. Censi, P. Di Martino, T. Vermonden, and W. E. Hennink, "Hydrogels for protein delivery in tissue engineering," *Journal of Controlled Release*, vol. 161, no. 2, pp. 680–692, 2012.

[59] K. Zheng, Y. Tong, S. Zhang, R. He, L. Xiao, Z. Iqbal, Y. Zhang, J. Gao, L. Zhang, L. Jiang, and Y. Li, "Flexible bicolorimetric polyacrylamide/chitosan hydrogels for smart real-time monitoring and promotion of wound healing," *Advanced Functional Materials*, vol. 31, no. 34, p. 2 102 599, 2021.

[60] S. Awasthi, J. K. Gaur, M. S. Bobji, and C. Srivastava, "Nanoparticle-reinforced polyacrylamide hydrogel composites for clinical applications: A review," *Journal of Materials Science*, vol. 57, no. 17, pp. 8041–8063, 2022.

[61] L. Yang, X. Zhang, M. Ye, J. Jiang, R. Yang, T. Fu, Y. Chen, K. Wang, C. Liu, and W. Tan, "Aptamer-conjugated nanomaterials and their applications," *Advanced Drug Delivery Reviews*, vol. 63, no. 14, pp. 1361–1370, 2011.

[62] C. B. Godiya, X. Cheng, D. Li, Z. Chen, and X. Lu, "Carboxymethyl cellulose/polyacrylamide composite hydrogel for cascaded treatment/reuse of heavy metal ions in wastewater," *Journal of Hazardous Materials*, vol. 364, pp. 28–38, 2019.

[63] A. Halperin, M. Kröger, and F. M. Winnik, "Poly(n-isopropylacrylamide) phase diagrams: Fifty years of research," *Angewandte Chemie International Edition*, vol. 54, no. 51, pp. 15 342–15 367, 2015.

[64] M. Heskins and J. E. Guillet, "Solution properties of poly(n-isopropylacrylamide)," *Journal of Macromolecular Science: Part A - Chemistry*, vol. 2, no. 8, pp. 1441–1455, 1968.

[65] D. Dhara and P. R. Chatterji, "Phase transition in linear and cross-linked poly(n-isopropylacrylamide) in water: Effect of various types of additives," *Journal of Macromolecular Science, Part C*, vol. 40, no. 1, pp. 51–68, 2000.

[66] J. G. Marques, A. L. Costa, and C. Pereira, "Gibbs free energy (δg) analysis for the naoh (sodium-oxygen-hydrogen) thermochemical water splitting cycle," *International Journal of Hydrogen Energy*, vol. 44, no. 29, pp. 14 536–14 549, 2019.

[67] K. Mochizuki and D. Ben-Amotz, "Hydration-shell transformation of thermosensitive aqueous polymers," *The Journal of Physical Chemistry Letters*, vol. 8, no. 7, pp. 1360–1364, 2017.

[68] G. Pasparakis and C. Tsitsilianis, "Lcst polymers: Thermoresponsive nanostructured assemblies towards bioapplications," *Polymer*, vol. 211, p. 123 146, 2020.

[69] M. Lehmann, P. Krause, V. Miruchna, and R. von Klitzing, "Tailoring pnipam hydrogels for large temperature-triggered changes in mechanical properties," *Colloid and Polymer Science*, vol. 297, no. 4, pp. 633–640, 2019.

[70] M. A. Haq, Y. Su, and D. Wang, "Mechanical properties of pnipam based hydrogels: A review," *Materials Science and Engineering: C*, vol. 70, pp. 842–855, 2017.

[71] Y. Li, L. Liu, H. Xu, Z. Cheng, J. Yan, and X.-M. Xie, "Biomimetic gradient hydrogel actuators with ultrafast thermo-responsiveness and high strength," *ACS Applied Materials & Interfaces*, vol. 14, no. 28, pp. 32 541–32 550, 2022.

[72] E. Malekzadeh and B.-m. Zhang Newby, "Thermoresponsive poly(vinyl methyl ether) (pvme) retained by 3-aminopropyltriethoxysilane (aptes) network," *ACS Biomaterials Science & Engineering*, vol. 6, no. 12, pp. 7051–7060, 2020.

[73] D. A. Chiappetta and A. Sosnik, "Poly(ethylene oxide)–poly(propylene oxide) block copolymer micelles as drug delivery agents: Improved hydrosolubility, stability and bioavailability of drugs," *European Journal of Pharmaceutics and Biopharmaceutics*, vol. 66, no. 3, pp. 303–317, 2007.

[74] J. Liu, A. Debuigne, C. Detrembleur, and C. Jérôme, "Poly(n-vinylcaprolactam): A thermoresponsive macromolecule with promising future in biomedical field," *Advanced Healthcare Materials*, vol. 3, no. 12, pp. 1941–1968, 2014.

[75] L. Klouda, "Thermoresponsive hydrogels in biomedical applications: A seven-year update," *European Journal of Pharmaceutics and Biopharmaceutics*, vol. 97, pp. 338–349, 2015.

[76] S. Ashraf, H.-K. Park, H. Park, and S.-H. Lee, "Snapshot of phase transition in thermoresponsive hydrogel pnipam: Role in drug delivery and tissue engineering," *Macromolecular Research*, vol. 24, no. 4, pp. 297–304, 2016.

[77] J. Liu, L. Jiang, S. He, J. Zhang, and W. Shao, "Recent progress in pnipam-based multi-responsive actuators: A mini-review," *Chemical Engineering Journal*, vol. 433, p. 133 496, 2022.

[78] E. Zhang, T. Wang, C. Lian, W. Sun, X. Liu, and Z. Tong, "Robust and thermo-response graphene–pnipam hybrid hydrogels reinforced by hectorite clay," *Carbon*, vol. 62, pp. 117–126, 2013.

[79] C. Dionigi, L. Lungaro, V. Goranov, A. Riminucci, Y. Piñeiro-Redondo, M. Bañobre-López, J. Rivas, and V. Dediu, "Smart magnetic poly(n-isopropylacrylamide) to control the release of bio-active molecules," *Journal of Materials Science: Materials in Medicine*, vol. 25, no. 10, pp. 2365–2371, 2014.

[80] R. Chollakup, W. Smitthipong, C. D. Eisenbach, and M. Tirrell, "Phase behavior and coacervation of aqueous poly(acrylic acid)-poly(allylamine) solutions," *Macromolecules*, vol. 43, no. 5, pp. 2518–2528, 2010.

[81] X. Jin and Y.-L. Hsieh, "Ph-responsive swelling behavior of poly(vinyl alcohol)/poly(acrylic acid) bi-component fibrous hydrogel membranes," *Polymer*, vol. 46, no. 14, pp. 5149–5160, 2005.

[82] G. Dalei and S. Das, "Polyacrylic acid-based drug delivery systems: A comprehensive review on the state-of-art," *Journal of Drug Delivery Science and Technology*, vol. 78, p. 103 988, 2022.

[83] A. B. Argade and N. A. Peppas, "Poly(acrylic acid)–poly(vinyl alcohol) copolymers with superabsorbent properties," *Journal of Applied Polymer Science*, vol. 70, no. 4, pp. 817–829, 1998.

[84] J. Kim, M. J. Serpe, and L. A. Lyon, "Hydrogel microparticles as dynamically tunable microlenses," *Journal of the American Chemical Society*, vol. 126, no. 31, pp. 9512–9513, 2004.

[85] K. Yue, G. Trujillo-de Santiago, M. M. Alvarez, A. Tamayol, N. Annabi, and A. Khademhosseini, "Synthesis, properties, and biomedical applications of gelatin methacryloyl (gelma) hydrogels," *Biomaterials*, vol. 73, pp. 254–271, 2015.

[86] A. Khademhosseini and R. Langer, "Microengineered hydrogels for tissue engineering," *Biomaterials*, vol. 28, no. 34, pp. 5087–5092, 2007.

[87] F. Yanagawa, S. Sugiura, and T. Kanamori, "Hydrogel microfabrication technology toward three dimensional tissue engineering," *Regenerative Therapy*, vol. 3, pp. 45–57, 2016.

[88] A. Schulte, Q. F. M. Alhusaini, and H. Schönherr, "Anodic aluminum oxide nanopore template-assisted fabrication of nanostructured poly(vinyl alcohol) hydrogels for cell studies," *ACS Applied Bio Materials*, vol. 3, no. 4, pp. 2419–2427, 2020.

[89] C. Arndt, M. Hauck, I. Wacker, B. Zeller-Plumhoff, F. Rasch, M. Taale, A. S. Nia, X. Feng, R. Adelung, R. R. Schröder, F. Schütt, and C. Selhuber-Unkel, "Microengineered hollow graphene tube systems generate conductive hydrogels with extremely low filler concentration," *Nano Letters*, vol. 21, no. 8, pp. 3690–3697, 2021.

[90] B. M. Baker, A. O. Gee, R. B. Metter, A. S. Nathan, R. A. Marklein, J. A. Burdick, and R. L. Mauck, "The potential to improve cell infiltration in composite fiber-aligned electrospun scaffolds by the selective removal of sacrificial fibers," *Biomaterials*, vol. 29, no. 15, pp. 2348–2358, 2008.

[91] G. C. Le Goff, R. L. Srinivas, W. A. Hill, and P. S. Doyle, "Hydrogel microparticles for biosensing," *European Polymer Journal*, vol. 72, pp. 386–412, 2015.

[92] G. Shao, D. A. H. Hanaor, X. Shen, and A. Gurlo, "Freeze casting: From low-dimensional building blocks to aligned porous structures—a review of novel materials, methods, and applications," *Advanced Materials*, vol. 32, no. 17, p. 1 907 176, 2020.

[93] M. Hauck, L. M. Saure, B. Zeller-Plumhoff, S. Kaps, J. Hammel, C. Mohr, L. Rieck, A. S. Nia, X. Feng, N. M. Pugno, R. Adelung, and F. Schütt, "Overcoming water diffusion limitations in hydrogels via microtubular graphene networks for soft actuators," *Advanced Materials*, vol. 35, no. 41, p. 2 302 816, 2023.

[94] W. Reichstein, L. Sommer, S. Veziroglu, S. Sayin, S. Schröder, Y. K. Mishra, E. İ. Saygili, F. Karayürek, Y. Açil, J. Wiltfang, A. Gülses, F. Faupel, and O. C. Aktas, "Initiated chemical vapor deposition (icvd) functionalized polylactic acid–marine algae composite patch for bone tissue engineering," *Polymers*, vol. 13, no. 2, 2021.

[95] L. Jing, L.-Y. Hsiao, S. Li, H. Yang, P. L. P. Ng, M. Ding, T. V. Truong, S.-P. Gao, K. Li, Y.-X. Guo, P. Valdivia y Alvarado, and P.-Y. Chen, "2d-material-integrated hydrogels as multifunctional protective skins for soft robots," *Materials Horizons*, vol. 8, pp. 2065–2078, 7 2021.

[96] J. Wu and Y. Hong, "Enhancing cell infiltration of electrospun fibrous scaffolds in tissue regeneration," *Bioactive Materials*, vol. 1, no. 1, pp. 56–64, 2016.

[97] K. R. Coogan, P. T. Stone, N. D. Sempertegui, and S. S. Rao, "Fabrication of micro-porous hyaluronic acid hydrogels through salt leaching," *European Polymer Journal*, vol. 135, p. 109 870, 2020.

[98] H. Ko, M. C. Ratri, K. Kim, Y. Jung, G. Tae, and K. Shin, "Formulation of sugar/hydrogel inks for rapid thermal response 4d architectures with sugar-derived macropores," *Scientific Reports*, vol. 10, p. 7527, 2020.

[99] K. J. De France, F. Xu, and T. Hoare, "Structured macroporous hydrogels: Progress, challenges, and opportunities," *Advanced Healthcare Materials*, vol. 7, no. 1, p. 1 700 927, 2018.

[100] S. Li, H.-G. Zhang, D.-D. Li, J.-P. Wu, C.-Y. Sun, and Q.-X. Hu, "Characterization of engineered scaffolds with spatial prevascularized networks for bulk tissue regeneration," *ACS Biomaterials Science & Engineering*, vol. 3, no. 10, pp. 2493–2501, 2017.

[101] K. Depa, A. Strachota, M. Šlouf, and J. Brus, "Poly(n-isopropylacrylamide)-sio2 nanocomposites interpenetrated by starch: Stimuli-responsive hydrogels with attractive tensile properties," *European Polymer Journal*, vol. 88, pp. 349–372, 2017.

[102] N. A. Peppas, J. Z. Hilt, A. Khademhosseini, and R. Langer, "Hydrogels in biology and medicine: From molecular principles to bionanotechnology," *Advanced Materials*, vol. 18, no. 11, pp. 1345–1360, 2006.

[103] S. A. Skoog, P. L. Goering, and R. J. Narayan, "Stereolithography in tissue engineering," *Journal of Materials Science: Materials in Medicine*, vol. 25, no. 3, pp. 845–856, 2014.

[104] J. Gao, X. Liu, J. Cheng, J. Deng, Z. Han, M. Li, X. Wang, J. Liu, and L. Zhang, "Application of photocrosslinkable hydrogels based on photolithography 3D bioprinting technology in bone tissue engineering," *Regenerative Biomaterials*, vol. 10, rbad037, 2023.

[105] D. K. Patel, A. H. Sakhaei, M. Layani, B. Zhang, Q. Ge, and S. Magdassi, "Highly stretchable and uv curable elastomers for digital light processing based 3d printing," *Advanced Materials*, vol. 29, no. 15, p. 1 606 000, 2017.

[106] Y. Gao, D. Zhou, J. Lyu, S. A, Q. Xu, B. Newland, K. Matyjaszewski, H. Tai, and W. Wang, "Complex polymer architectures through free-radical polymerization of multivinyl monomers," *Nature Reviews Chemistry*, vol. 4, no. 4, p. 1 606 000, 2020.

[107] A. K. Ho, I. Iin, P. A. Gurr, M. F. Mills, and G. G. Qiao, "Synthesis and characterization of star-like microgels by one-pot free radical polymerization," *Polymer*, vol. 46, no. 18, pp. 6727–6735, 2005.

[108] C. Barner-Kowollik, P. Vana, and T. P. Davis, "The kinetics of free-radical polymerization," in *Handbook of Radical Polymerization*. John Wiley & Sons, Ltd, 2002, ch. 4, pp. 187–261.

[109] J. Fouassier, X. Allonas, and D. Burget, "Photopolymerization reactions under visible lights: Principle, mechanisms and examples of applications," *Progress in Organic Coatings*, vol. 47, no. 1, pp. 16–36, 2003.

[110] M. Layani, X. Wang, and S. Magdassi, "Novel materials for 3d printing by photopolymerization," *Advanced Materials*, vol. 30, no. 41, p. 1 706 344, 2018.

[111] S. C. Ligon, R. Liska, J. Stampfl, M. Gurr, and R. Mülhaupt, "Polymers for 3d printing and customized additive manufacturing," *Chemical Reviews*, vol. 117, no. 15, pp. 10 212–10 290, 2017.

[112] M. Zarek, M. Layani, I. Cooperstein, E. Sachyani, D. Cohn, and S. Magdassi, "3d printing of shape memory polymers for flexible electronic devices," *Advanced Materials*, vol. 28, no. 22, pp. 4449–4454, 2016.

[113] W. Xu, S. Jambhulkar, Y. Zhu, D. Ravichandran, M. Kakarla, B. Vernon, D. G. Lott, J. L. Cornella, O. Shefi, G. Miquelard-Garnier, Y. Yang, and K. Song, "3d printing for polymer/particle-based processing: A review," *Composites Part B: Engineering*, vol. 223, p. 109 102, 2021.

[114] A. Selimis, V. Mironov, and M. Farsari, "Direct laser writing: Principles and materials for scaffold 3d printing," *Microelectronic Engineering*, vol. 132, pp. 83–89, 2015.

[115] Y. Chen, Y. Bai, Z. Han, W. He, and Z. Guo, "Photoluminescence imaging of zn2+ in living systems," *Chemical Society Reviews*, vol. 44, pp. 4517–4546, 14 2015.

[116] S. O'Halloran, A. Pandit, A. Heise, and A. Kellett, "Two-photon polymerization: Fundamentals, materials, and chemical modification strategies," *Advanced Science*, vol. 10, no. 7, p. 2 204 072, 2023.

[117] A. I. Ciuciu and P. J. Cywiński, "Two-photon polymerization of hydrogels – versatile solutions to fabricate well-defined 3d structures," *RSC Advances*, vol. 4, pp. 45 504–45 516, 85 2014.

[118] J. Song, C. Michas, C. S. Chen, A. E. White, and M. W. Grinstaff, "From simple to architecturally complex hydrogel scaffolds for cell and tissue engineering applications: Opportunities presented by two-photon polymerization," *Advanced Healthcare Materials*, vol. 9, no. 1, p. 1 901 217, 2020.

[119] M. Hippler, E. Blasco, J. Qu, M. Tanaka, C. Barner-Kowollik, M. Wegener, and M. Bastmeyer, "Controlling the shape of 3d microstructures by temperature and light," *Nature Communications*, vol. 10, no. 1, p. 232, 2019.

[120] A. Grushina, "Direct-write grayscale lithography," *Advanced Optical Technologies*, vol. 8, no. 3-4, pp. 163–169, 2019.

[121] J. Loomis, D. Ratnayake, C. McKenna, and K. M. Walsh, "Grayscale lithography—automated mask generation for complex three-dimensional topography," *Journal of Micro/Nanolithography, MEMS, and MOEMS*, vol. 15, no. 1, p. 013 511, 2016.

[122] X. Kuang, J. Wu, K. Chen, Z. Zhao, Z. Ding, F. Hu, D. Fang, and H. J. Qi, "Grayscale digital light processing 3d printing for highly functionally graded materials," *Science Advances*, vol. 5, no. 5, eaav5790, 2019.

[123] V. Hahn, T. Messer, N. M. Bojanowski, E. R. Curticean, I. Wacker, R. R. Schröder, E. Blasco, and M. Wegener, "Two-step absorption instead of two-photon absorption in 3d nanoprinting," *Nature Photonics*, vol. 15, no. 12, pp. 932–938, 2021.

[124] M. Malinauskas, M. Farsari, A. Piskarskas, and S. Juodkazis, "Ultrafast laser nanostructuring of photopolymers: A decade of advances," *Physics Reports*, vol. 533, no. 1, pp. 1–31, 2013.

[125] J.-F. Xing, M.-L. Zheng, and X.-M. Duan, "Two-photon polymerization microfabrication of hydrogels: An advanced 3d printing technology for tissue engineering and drug delivery," *Chemical Society Reviews*, vol. 44, pp. 5031–5039, 15 2015.

[126] O. Erol, A. Pantula, W. Liu, and D. H. Gracias, "Transformer hydrogels: A review," *Advanced Materials Technologies*, vol. 4, no. 4, p. 1 900 043, 2019.

[127] L. Klouda and A. G. Mikos, "Thermoresponsive hydrogels in biomedical applications," *European Journal of Pharmaceutics and Biopharmaceutics*, vol. 68, no. 1, pp. 34–45, 2008.

[128] Z. Shen, F. Chen, X. Zhu, K.-T. Yong, and G. Gu, "Stimuli-responsive functional materials for soft robotics," *Journal of Materials Chemistry B*, vol. 8, pp. 8972–8991, 39 2020.

[129] T. Chung, I. K. Han, J. Han, K. Ahn, and Y. S. Kim, "Fast and large shrinking of thermoresponsive hydrogels with phase-separated structures," *Gels*, vol. 7, no. 1, 2021.

[130] T. G. Park and A. S. Hoffman, "Deswelling characteristics of poly(n-isopropylacrylamide) hydrogel," *Journal of Applied Polymer Science*, vol. 52, no. 1, pp. 85–89, 1994.

[131] S. Lanzalaco and E. Armelin, "Poly(n-isopropylacrylamide) and copolymers: A review on recent progresses in biomedical applications," *Gels*, vol. 3, no. 4, 2017.

[132] S. J. Kim, S. J. Park, and S. I. Kim, "Synthesis and characteristics of interpenetrating polymer network hydrogels composed of poly(vinyl alcohol) and poly(n-isopropylacrylamide)," *Reactive and Functional Polymers*, vol. 55, no. 1, pp. 61–67, 2003.

[133] O. Czakkel, B. Berke, and K. László, "Effect of graphene-derivatives on the responsivity of pnipam-based thermosensitive nanocomposites – a review," *European Polymer Journal*, vol. 116, pp. 106–116, 2019.

[134] R. Liu, M. Fraylich, and B. R. Saunders, "Thermoresponsive copolymers: From fundamental studies to applications," *Colloid and Polymer Science*, vol. 287, pp. 627–643, 2009.

[135] C. Yao, Z. Liu, C. Yang, W. Wang, X.-J. Ju, R. Xie, and L.-Y. Chu, "Poly(n-isopropylacrylamide)-clay nanocomposite hydrogels with responsive bending property as temperature-controlled manipulators," *Advanced Functional Materials*, vol. 25, no. 20, pp. 2980–2991, 2015.

[136] A. Gregg, M. F. L. De Volder, and J. J. Baumberg, "Light-actuated anisotropic microactuators from cnt/hydrogel nanocomposites," *Advanced Optical Materials*, vol. 10, no. 13, p. 2 200 180, 2022.

[137] Y. K. Mishra, G. Modi, V. Cretu, V. Postica, O. Lupan, T. Reimer, I. Paulowicz, V. Hrkac, W. Benecke, L. Kienle, and R. Adelung, "Direct growth of freestanding zno tetrapod networks for multifunctional applications in photocatalysis, uv photodetection, and gas sensing," *ACS Applied Materials & Interfaces*, vol. 7, no. 26, pp. 14 303–14 316, 2015.

[138] X. Kang, R. Floyd, S. Lowum, M. Cabral, E. Dickey, and J.-P. Maria, "Mechanism studies of hydrothermal cold sintering of zinc oxide at near room temperature," *Journal of the American Ceramic Society*, vol. 102, no. 8, pp. 4459–4469, 2019.

[139] Z. Kaberova, E. Karpushkin, M. Nevoralová, M. Vetrík, M. Šlouf, and M. Dušková-Smrčková, "Microscopic structure of swollen hydrogels by scanning electron and light microscopies: Artifacts and reality," *Polymers*, vol. 12, no. 3, 2020.

[140] T. Spratte, C. Arndt, I. Wacker, M. Hauck, R. Adelung, R. R. Schröder, F. Schütt, and C. Selhuber-Unkel, "Thermoresponsive hydrogels with improved actuation function by interconnected microchannels," *Advanced Intelligent Systems*, vol. 4, no. 3, p. 2 100 081, 2022.

[141] F. Schütt, M. Zapf, S. Signetti, J. Strobel, H. Krüger, R. Röder, J. Carstensen, N. Wolff, J. Marx, T. Carey, M. Schweichel, M.-I. Terasa, L. Siebert, H.-K. Hong, S. Kaps, B. Fiedler, Y. K. Mishra, Z. Lee, N. M. Pugno, L. Kienle, A. C. Ferrari, F. Torrisi, C. Ronning, and R. Adelung, "Conversionless efficient and broadband laser light diffusers for high brightness illumination applications," *Nature Communications*, vol. 11, no. 1, p. 1437, 2020.

[142] F. Rasch, F. Schütt, L. M. Saure, S. Kaps, J. Strobel, O. Polonskyi, A. S. Nia, M. R. Lohe, Y. K. Mishra, F. Faupel, L. Kienle, X. Feng, and R. Adelung, "Wet-chemical assembly of 2d nanomaterials into lightweight, microtube-shaped, and macroscopic 3d networks," *ACS Applied Materials & Interfaces*, vol. 11, no. 47, pp. 44 652–44 663, 2019.

[143] S. Thiele, J. Andersson, A. Dahlin, and R. L. N. Hailes, "Tuning the thermoresponsive behavior of surface-attached pnipam networks: Varying the crosslinker content in si-atrp," *Langmuir*, vol. 37, no. 11, pp. 3391–3398, 2021.

[144] H. Cheng, L. Shen, and C. Wu, "Lls and ftir studies on the hysteresis in association and dissociation of poly(n-isopropylacrylamide) chains in water," *Macromolecules*, vol. 39, no. 6, pp. 2325–2329, 2006.

[145] J.-T. Zhang, R. Bhat, and K. D. Jandt, "Temperature-sensitive pva/pnipaam semi-ipn hydrogels with enhanced responsive properties," *Acta Biomaterialia*, vol. 5, no. 1, pp. 488–497, 2009.

[146] K. Depa, A. Strachota, M. Šlouf, and J. Hromádková, "Fast temperature-responsive nanocomposite pnipam hydrogels with controlled pore wall thickness: Force and rate of t-response," *European Polymer Journal*, vol. 48, no. 12, pp. 1997–2007, 2012.

[147] J. Sievers, K. Sperlich, T. Stahnke, C. Kreiner, T. Eickner, H. Martin, R. F. Guthoff, M. Schünemann, S. Bohn, and O. Stachs, "Determination of hydrogel swelling factors by two established and a novel non-contact continuous method," *Journal of Applied Polymer Science*, vol. 138, no. 18, p. 50 326, 2021.

[148] O. Chaudhuri, "Viscoelastic hydrogels for 3d cell culture," *Biomaterials Science*, vol. 5, pp. 1480–1490, 8 2017.

[149] X. Chen, Y. Xiang, and J. J. Vlassak, "Novel technique for measuring the mechanical properties of porous materials by nanoindentation," *Journal of Materials Research*, vol. 21, no. 3, pp. 715–724, 2006.

[150] G. Lu, G. (Max) Lu, and Z. Xiao, "Mechanical properties of porous materials," *Journal of Porous Materials*, vol. 6, no. 4, pp. 359–368, 1999.

[151] S. Wang, Z. Sun, Y. Zhao, and L. Zuo, "A highly stretchable hydrogel sensor for soft robot multi-modal perception," *Sensors and Actuators A: Physical*, vol. 331, p. 113 006, 2021.

[152] M. Cianchetti, C. Laschi, A. Menciassi, and P. Dario, "Biomedical applications of soft robotics," *Nature Reviews Materials*, vol. 3, pp. 143–153, 2018.

[153] B. Xu, H. Jiang, H. Li, G. Zhang, and Q. Zhang, "High strength nanocomposite hydrogel bilayer with bidirectional bending and shape switching behaviors for soft actuators," *RSC Advances*, vol. 5, pp. 13 167–13 170, 17 2015.

[154] N. R. Sinatra, C. B. Teeple, D. M. Vogt, K. K. Parker, D. F. Gruber, and R. J. Wood, "Ultragentle manipulation of delicate structures using a soft robotic gripper," *Science Robotics*, vol. 4, no. 33, eaax5425, 2019.

[155] Q. Shi, H. Xia, P. Li, Y.-S. Wang, L. Wang, S.-X. Li, G. Wang, C. Lv, L.-G. Niu, and H.-B. Sun, "Photothermal surface plasmon resonance and interband transition-enhanced nanocomposite hydrogel actuators with hand-like dynamic manipulation," *Advanced Optical Materials*, vol. 5, no. 22, p. 1 700 442, 2017.

[156] Y. Yang, Y. Tan, X. Wang, W. An, S. Xu, W. Liao, and Y. Wang, "Photothermal nanocomposite hydrogel actuator with electric-field-induced gradient and oriented structure," *ACS Applied Materials & Interfaces*, vol. 10, no. 9, pp. 7688–7692, 2018.

[157] E. Lee, D. Kim, H. Kim, and J. Yoon, "Photothermally driven fast responding photo-actuators fabricated with comb-type hydrogels and magnetite nanoparticles," *Scientific Reports*, vol. 5, no. 1, p. 15 124, 2015.

[158] F. Rajabasadi, L. Schwarz, M. Medina-Sánchez, and O. G. Schmidt, "3d and 4d lithography of untethered microrobots," *Progress in Materials Science*, vol. 120, p. 100 808, 2021.

[159] C. Barner-Kowollik, M. Bastmeyer, E. Blasco, G. Delaittre, P. Müller, B. Richter, and M. Wegener, "3d laser micro- and nanoprinting: Challenges for chemistry," *Angewandte Chemie International Edition*, vol. 56, no. 50, pp. 15 828–15 845, 2017.

[160] T. Gissibl, S. Thiele, A. Herkommer, and H. Giessen, "Two-photon direct laser writing of ultracompact multi-lens objectives," *Nature Photonics*, vol. 10, no. 8, pp. 554–560, 2016.

[161] M. L. McFetridge, K. Kulkarni, V. Hilsenstein, M. P. Del Borgo, M.-I. Aguilar, and S. D. Ricardo, "A comparison of fixation methods for sem analysis of self-assembling peptide hydrogel nanoarchitecture," *Nanoscale*, vol. 15, pp. 1431–1440, 3 2023.

[162] S. O. Colgate, A. Sivaraman, C. Dejsupa, and K. C. McGill, "Acoustic cavity method for phase boundary determinations: The critical temperature of CO2," *Review of Scientific Instruments*, vol. 62, no. 1, pp. 198–202, 1991.

[163] T. Spratte, S. Geiger, F. Colombo, A. Mishra, M. Taale, L.-Y. Hsu, E. Blasco, and C. Selhuber-Unkel, "Increasing the efficiency of thermoresponsive actuation at the microscale by direct laser writing of pnipam," *Advanced Materials Technologies*, vol. 8, no. 1, p. 2 200 714, 2023.

[164] S. Li, W. Wang, W. Li, M. Xie, C. Deng, X. Sun, C. Wang, Y. Liu, G. Shi, Y. Xu, X. Ma, and J. Wang, "Fabrication of thermoresponsive hydrogel scaffolds with engineered microscale vasculatures," *Advanced Functional Materials*, vol. 31, no. 27, p. 2 102 685, 2021.

[165] J. Wang, J. Wang, Z. Chen, S. Fang, Y. Zhu, R. H. Baughman, and L. Jiang, "Tunable, fast, robust hydrogel actuators based on evaporation-programmed heterogeneous structures," *Chemistry of Materials*, vol. 29, no. 22, pp. 9793–9801, 2017.

[166] C. Zheng, F. Jin, Y. Zhao, M. Zheng, J. Liu, X. Dong, Z. Xiong, Y. Xia, and X. Duan, "Light-driven micron-scale 3d hydrogel actuator produced by two-photon polymerization microfabrication," *Sensors and Actuators B: Chemical*, vol. 304, p. 127 345, 2020.

[167] R. Contreras-Cáceres, L. Schellkopf, C. Fernández-López, I. Pastoriza-Santos, J. Pérez-Juste, and M. Stamm, "Effect of the cross-linking density on the thermoresponsive behavior of hollow pnipam microgels," *Langmuir*, vol. 31, no. 3, pp. 1142–1149, 2015.

[168] X.-Z. Zhang, D.-Q. Wu, and C.-C. Chu, "Effect of the crosslinking level on the properties of temperature-sensitive poly(n-isopropylacrylamide) hydrogels," *Journal of Polymer Science Part B: Polymer Physics*, vol. 41, no. 6, pp. 582–593, 2003.

[169] S. Schmidt, M. Zeiser, T. Hellweg, C. Duschl, A. Fery, and H. Möhwald, "Adhesion and mechanical properties of pnipam microgel films and their potential use as switchable cell culture substrates," *Advanced Functional Materials*, vol. 20, no. 19, pp. 3235–3243, 2010.

[170] H. R. Luckarift, B. S. Ku, J. S. Dordick, and J. C. Spain, "Silica-immobilized enzymes for multi-step synthesis in microfluidic devices," *Biotechnology and Bioengineering*, vol. 98, no. 3, pp. 701–705, 2007.

[171] L. Mazutis, J.-C. Baret, P. Treacy, Y. Skhiri, A. F. Araghi, M. Ryckelynck, V. Taly, and A. D. Griffiths, "Multi-step microfluidic droplet processing: Kinetic analysis of an in vitro translated enzyme," *Lab on a Chip*, vol. 9, pp. 2902–2908, 20 2009.

[172] Z. Zhao, Z. Wang, G. Li, Z. Cai, J. Wu, L. Wang, L. Deng, M. Cai, and W. Cui, "Injectable microfluidic hydrogel microspheres for cell and drug delivery," *Advanced Functional Materials*, vol. 31, no. 31, p. 2 103 339, 2021.

[173] Y. Han, J. Yang, W. Zhao, H. Wang, Y. Sun, Y. Chen, J. Luo, L. Deng, X. Xu, W. Cui, and H. Zhang, "Biomimetic injectable hydrogel microspheres with enhanced lubrication and controllable drug release for the treatment of osteoarthritis," *Bioactive Materials*, vol. 6, no. 10, pp. 3596–3607, 2021.

[174] T. S. H. Tran, B. D. Ho, J. P. Beech, and J. O. Tegenfeldt, "Open channel deterministic lateral displacement for particle and cell sorting," *Lab on a Chip*, vol. 17, pp. 3592–3600, 21 2017.

[175] T. Kawano, Y. Niidome, T. Mori, Y. Katayama, and T. Niidome, "Pnipam gel-coated gold nanorods for targeted delivery responding to a near-infrared laser," *Bioconjugate Chemistry*, vol. 20, no. 2, pp. 209–212, 2009.

[176] A. Sutton, T. Shirman, J. V. I. Timonen, G. T. England, P. Kim, M. Kolle, T. Ferrante, L. D. Zarzar, E. Strong, and J. Aizenberg, "Photothermally triggered actuation of hybrid materials as a new platform for in vitro cell manipulation," *Nature Communications*, vol. 8, no. 1, p. 14 700, 2017.

[177] Y.-Z. You, K. K. Kalebaila, S. L. Brock, and D. Oupický, "Temperature-controlled uptake and release in pnipam-modified porous silica nanoparticles," *Chemistry of Materials*, vol. 20, no. 10, pp. 3354–3359, 2008.

[178] G. Huang, J. Gao, Z. Hu, J. V. St. John, B. C. Ponder, and D. Moro, "Controlled drug release from hydrogel nanoparticle networks," *Journal of Controlled Release*, vol. 94, no. 2, pp. 303–311, 2004.

[179] N. Hussain, A. Scholz, T. Spratte, C. Selhuber-Unkel, M. Hirtz, and J. Aghassi-Hagmann, "Direct writing of liquid metal microheaters for microvalve applications," in *2023 IEEE International Conference on Flexible and Printable Sensors and Systems (FLEPS)*, 2023, pp. 1–4.

List of Abbreviations

2PP two-photon polymerization

3D three-dimensional

4D four-dimensional

AAc acrylic acid

AM acrylamide

APS ammonium persulfate

BIS *N*,*N*'-methylenebis(acrylamide)

CAD computer aided design

CLIP continuous liquid interface production

CPD critical point drying

DEAs dielectric elastomer actuators

DLP digital light processing

FRP free radical polymerization

hr hours

iCVD initiated chemical vapor deposition

LAP lithium phenyl(2,4,6-trimethylbenzoyl)phosphinate

LCST lower critical solution temperature

LED light emitting diode

NA numerical aperture

NIPAM *N*-isopropylacrylamide

NIR near-infrared light

OPA one-photon absorption

OsO_4 osmium tetraoxide

PAA poly(acrylic acid)

PAM polyacrylamide

PANI polyaniline

PDMS poly(dimethylsiloxane)

PE poly(ethylene)

PEG poly(ethylene glycol)

PEO-PPO poly(ethylene oxide)-poly(propylene oxide)

pH potential of hydrogen

PHEMA poly(2-hydroxyethyl methacrylate)

PLA poly(lactic acid)

PNIPAM poly(*N*-isopropylacrylamide)

PNVCL poly(*N*-vinylcaprolactam)

PMMA poly(methyl methacrylate)

PTFE poly(tetrafluoroethene)

PVA poly(vinyl alcohol)

PVC poly(vinyl chloride)

PVME poly(vinyl methyl ether)

rpm revolutions per minute

SEM scanning electron microscopy

SLA stereolithography

STL stereolithography

TEMED *N,N,N',N'*-tetramethylethylenediamine

TPA two-photon absorption

TPO bis(2,4,6-trimethylbenzoyl)-phenylphosphineoxide

TPP two-photon polymerization

t-ZnO tetrapodal zinc oxide

UV ultraviolet

List of Symbols

$^\circ$	degree
Δ	delta
ϵ	strain
λ	wavelength
ν	frequency
ρ	density
σ	stress
M	molar
A	area
d	accuracy
d_{indent}	indentation depth
E	Young's Modulus
F	force
G	Gibbs free energy
H	enthalpy
h	Planck constant
I	(electric) current
k	spring constant
L	length

m	mass
N	number
NA	numerical aperture
P	porosity
R	radius
S	entropy
SR	swelling ratio
T	temperature
V	volume
w	weight

Acknowledgments

I would like to take this opportunity to thank all those who have supported me in various ways on my journey to this work and contributed to its success.

First, I thank Prof. Dr. Christine Selhuber-Unkel for being part of her research team at Heidelberg University and for the opportunity to work on this fascinating topic. I am very grateful for your excellent guidance and input, as well as the freedom to develop and realize my own ideas. Thank you for the trust you placed in me!

I would like to express my special thanks to Prof. Dr. Eva Blasco, for reviewing my thesis and for the constructive discussions we shared, and to her group, for the nice collaborations and exchange we had.

For proof reading of my thesis, I am very grateful to Stephen Casale and Dr. Trevor Kalkus.

I would like to thank Dr. Christine Arndt for introducing me into the first steps of my work!

Furthermore, I would like to thank all collaborators for their efforts in our projects: For the work with zinc oxide templates, I would like to thank Prof. Dr. Rainer Adelung, Dr. Fabian Schütt, and Margarethe Hauck from Kiel University. I also want to acknowledge and thank Prof. Dr. Rasmus R. Schröder, Dr. Irene Wacker, and Ernest Ronald Curticean for collaborating with me, taking scanning electron micrographs of my samples, and discussing results. Prof. Dr. Jasmin Aghassi-Hagmann, Dr. Alexander Scholz, and Navid Hussain have supported me in the project of microheaters and local heating. I would like to acknowledge the support of Ankit Mishra in taking SEM images of hydrogel microstructures. For collaborating in the Hydra project, I would like to thank Prof. Dr. Thomas C. B. Bosch, Christoph Giez, and Denis Pinkle.

All my former and present colleagues in the group I would like to thank, for sharing this exciting PhD time with me: Aldo Leal-Egana, Angeles De La Cruz Garcia, Ankit Mishra, Annabelle Sonn, Barbara Schamberger, Chantal Barwig, Christine Arndt, Federico Colombo, Fereydoon Taheri, Florine Sessler, Gaurav Dave, I Chen,

Jonathan Schmidt, Krishna Ramesh, Laith Kadem, Malin Schmidt, Maria Villiou, Mehran Mehrabanian, Miguel Angel Juarez Estrada, Mishal Khan, Mohammadreza Taale, Qiyang Jiang, Sadaf Pashapour, Sandra Sindt, Sebastian Weber, Sophie Geiger, Stephen Casale, Sunil Rajput, Tanisha Gebert, Trevor Kalkus, Viktoria Albert, Yasmin Antonelli, Zeynab Tavasolyzadeh, and Zhe Wang. Thank you for all your support!

I would like to say a big thank you to my students and HiWis: Anton Walte, Frederick Koch, Julien-Maurice Roquette, Karolin Becker, and Patricia Kennedy.

I am very grateful to my office members Malin, Florine, Gaurav, Miguel and Steffi for the best working atmosphere and the many scientific and non-scientific conversations we had.

Furthermore, I am grateful to the staff of the mechanical workshop at the PCI, as well as to the secretaries and administrative staff of the Institute, especially Beni, Steffi, and Corinna.

I thank the German Research Foundation for funding through the project SE 1801/4-1 "Switchable, Bistable Microactuator Systems Based on Stimuli-Responsive Polymers" within the Priority Programme SPP 2206 "KOMMMA". Furthermore, I would like to thank my collaborators in this project: Prof. Dr. Anne Staubitz and Ruchira Colaco.

Additionally, my special thanks goes to my dear friends Ankit, Gaurav, Angeles, and Mishal, for our friendship and the great time we spent together in and outside Heidelberg! Trevor, thank you for giving the best hugs!

In particular, I would like to thank Helge and Cati for accompanying me during all my time inside and outside university and for our friendship.

Above all, I would like to thank my parents, my sister and my friends for always being there for me and supporting me throughout my life, and my girlfriend Meli for sharing life with me and always cheering me up!